

Spring 5-15-2015

## Surface-Engineered Magnetic Nanoparticles for Sample Preparation and Analysis of Proteins and Peptides

Parisa Pirani  
ppirani@uno.edu

Follow this and additional works at: <https://scholarworks.uno.edu/td>

 Part of the [Analytical Chemistry Commons](#)

---

### Recommended Citation

Pirani, Parisa, "Surface-Engineered Magnetic Nanoparticles for Sample Preparation and Analysis of Proteins and Peptides" (2015). *University of New Orleans Theses and Dissertations*. 2012.  
<https://scholarworks.uno.edu/td/2012>

This Dissertation is protected by copyright and/or related rights. It has been brought to you by ScholarWorks@UNO with permission from the rights-holder(s). You are free to use this Dissertation in any way that is permitted by the copyright and related rights legislation that applies to your use. For other uses you need to obtain permission from the rights-holder(s) directly, unless additional rights are indicated by a Creative Commons license in the record and/or on the work itself.

This Dissertation has been accepted for inclusion in University of New Orleans Theses and Dissertations by an authorized administrator of ScholarWorks@UNO. For more information, please contact [scholarworks@uno.edu](mailto:scholarworks@uno.edu).

Surface-Engineered Magnetic Nanoparticles for Sample Preparation and Analysis of Proteins  
and Peptides

A Dissertation

Submitted to the Graduate Faculty of the  
University of New Orleans  
in partial fulfillment of the  
requirements for the degree of

Doctor of Philosophy  
in  
Chemistry

By  
Parisa Pirani

B.Sc., Chemistry, University of Tehran, 2004  
M.Sc., Organic Chemistry, Sharif University of Technology, 2008

May 15, 2015

## Acknowledgements

I would like to express my gratitude and appreciation to my advisor, Professor Matthew A. Tarr for his support and guidance throughout my graduate research. His kindness, patience and encouragement helped me overcome a lot of difficulties I encountered during my graduate studies. His knowledge and experience contributed many of the inspiring ideas to this research and led me to the right way.

I would like to thank my committee members, Prof. Mark L. Trudell, Prof. John Wiley, and Prof. Steven Rick for their time and helpful discussions and suggestions. My appreciation also goes to Dr. Yang Cai for helping me to understand the concept of the mass spectrometry, proteomics and data analysis which was very unknown to me when I started my research in this field. I am appreciative to Prof. Trudell and Tushar Apsunde for their collaboration. My acknowledgements are extended to everyone in the department of chemistry and material research institute for their help and support during my graduate career.

I am grateful to Dr. Casey Grimm for allowing us to use the liquid chromatography and mass spectrometry equipments at USDA. My appreciation is also extended to Ujwal Patil and Angela Elender for their time and help with sample analysis. I am thankful to my research group members who have been helpful throughout the various stages of my research, whether through technical discussions or with helpful perspective. I'm appreciative to my friends Kristen Williams and Donna Peralta for their true friendship and encouragement.

I am truly thankful to my father, mother and brother for their unconditional love, help, and encouragement. My deepest expression of appreciation goes to my wonderful husband, Abouzar Rahmati, for his immense love, patience, and support.

## Table of Contents

List of figures.....	vii
Abstract.....	x
Chapter 1 .....	1
Introduction .....	1
1.1 Magnetic iron oxide nanoparticles-applications, synthesis, functionalization and quantification of surface ligands.....	2
1.2 Cardiovascular diseases (CVD) .....	6
1.3 Low density lipoproteins (LDL) .....	8
1.4 Apolipoprotein B-100 (ApoB-100).....	10
1.5 Mapping protein structure using Amino acid-specific covalent labeling.....	11
1.6 LC-MS/MS based proteomics.....	12
1.7 Database Search .....	14
1.8 Disulfide bonds in proteins .....	15
1.9 Reduction and alkylation of proteins.....	16
References: .....	18
Chapter 2 .....	28
Protein surface labeling reactivity of <i>N</i> -hydroxysuccinimide ester group conjugated to Fe <sub>3</sub> O <sub>4</sub> @SiO <sub>2</sub> magnetic nanoparticles.....	28
2.1 Introduction.....	28
2.2 Experimental procedures .....	31
2.2.1 Materials .....	31
2.2.2 Synthesis of silica coated iron oxide nanoparticles (Fe <sub>3</sub> O <sub>4</sub> @SiO <sub>2</sub> NPs, diameter100 nm).....	32
2.2.3 Synthesis of silica coated iron oxide nanoparticles (Fe <sub>3</sub> O <sub>4</sub> @SiO <sub>2</sub> NPs, 20 nm diameter).....	33
2.2.4 Surface functionalization of Fe <sub>3</sub> O <sub>4</sub> @SiO <sub>2</sub> NPs (100 nm and 20 nm in diameter) with NHS ester groups.....	35
2.2.5 Conjugation of dansylcadaverine to NHS ester modified Fe <sub>3</sub> O <sub>4</sub> @SiO <sub>2</sub> MNPs.....	35
2.2.6 Synthesis of 3-Mercaptopropanamido dansylcadaverine (3-MPA-Dansyl).....	36
2.2.7 Characterization of 3-MPA- Dansyl.....	37
2.2.8 HPLC instrumentation and chromatography conditions .....	37

2.2. 9	Fluorescence microscopy imaging of dansylcadaverine modified Fe <sub>3</sub> O <sub>4</sub> @SiO <sub>2</sub> MNPs.....	38
2.2. 10	Fluorescence intensity calculations using MATLAB.....	38
2.2. 11	Measurement of BSA conjugated to Fe <sub>3</sub> O <sub>4</sub> @SiO <sub>2</sub> nanoparticles .....	39
2.3	Results and discussion .....	40
2.3. 1	NHS ester conjugated Fe <sub>3</sub> O <sub>4</sub> @SiO <sub>2</sub> MNPs .....	41
2.3. 2	Fluorescence-based quantification of active NHS ester groups on the surface of Fe <sub>3</sub> O <sub>4</sub> @SiO <sub>2</sub> MNPs.....	43
2.3. 3	Quantification of NHS ester groups by cleave-analyze approach.....	46
2.3. 4	Semiquantitative fluorescence microscopic characterization of dansylcadaverine modified Fe <sub>3</sub> O <sub>4</sub> @SiO <sub>2</sub> MNPs.....	48
2.3. 5	Labeling efficiencies of exposed lysine residues in native protein by NHS ester conjugated Fe <sub>3</sub> O <sub>4</sub> @SiO <sub>2</sub> MNPs.....	51
2.4	Conclusions.....	55
	References .....	56
	Chapter 3 .....	28
	Solvent exposed lysine residues of native apolipoprotein B-100.....	59
3.1	Introduction.....	59
3.2	Materials and Methods .....	62
3.3	Synthesis of silica coated iron oxide magnetic nanoparticles (Fe <sub>3</sub> O <sub>4</sub> @SiO <sub>2</sub> MNPs) .....	63
3.4	Surface functionalization of Fe <sub>3</sub> O <sub>4</sub> @ SiO <sub>2</sub> MNPs with NHS ester groups .....	63
3.5	Labeling solvent exposed lysine groups of ApoB-100 in native human low density lipoprotein (LDL) using NHS ester functionalized Fe <sub>3</sub> O <sub>4</sub> @SiO <sub>2</sub> MNPs.....	64
3.6	LC-MS/MS and data analysis of ApoB-100 peptides labeled with NHS ester modified Fe <sub>3</sub> O <sub>4</sub> @SiO <sub>2</sub> MNPs.....	65
3.7	Result and discussion.....	66
3.7.1	Synthesis of NHS ester functionalized Fe <sub>3</sub> O <sub>4</sub> @SiO <sub>2</sub> MNPs.....	66
3.7.2	Labeling solvent exposed amine groups of ApoB-100 in native human LDL using NHS ester modified Fe <sub>3</sub> O <sub>4</sub> @ SiO <sub>2</sub> MNPs.....	67
3.8	Conclusion .....	73
	References .....	74
	Chapter 4 .....	77
	Reduction of disulfide bonds in peptides and proteins using TCEP immobilized Fe <sub>3</sub> O <sub>4</sub> @SiO <sub>2</sub> magnetic nanoparticles.....	77

4.1	Introduction.....	77
4.2	Experimental procedures .....	80
4.2.1	Materials .....	80
4.2.2	Preparation of amino-functionalized Fe <sub>3</sub> O <sub>4</sub> @SiO <sub>2</sub> magnetic nanoparticles.....	81
4.2.3	Synthesis of TCEP coated Fe <sub>3</sub> O <sub>4</sub> @SiO <sub>2</sub> magnetic nanoparticles .....	81
4.2.4	Nanoparticle characterization with transmission electron microscopy (TEM) and dynamic light scattering (DLS).....	82
4.2.5	Reduction of disulfide bond in cyclic peptides using TCEP-immobilized Fe <sub>3</sub> O <sub>4</sub> @SiO <sub>2</sub> magnetic nanoparticles .....	82
4.2.6	Reduction of disulfide bonds in bovine pancreas insulin using TCEP-immobilized Fe <sub>3</sub> O <sub>4</sub> @SiO <sub>2</sub> magnetic nanoparticles .....	83
4.2.7	LC-MS/MS and data analysis of reduced/ alkylated peptides .....	83
4.3	Result and discussion.....	84
4.3.1	Surface modification of Fe <sub>3</sub> O <sub>4</sub> @SiO <sub>2</sub> nanoparticles with TCEP .....	84
4.3.2	Reduction and alkylation of cyclic peptides .....	86
4.3.3	Reduction and alkylation of bovine pancreas insulin.....	91
4.4	Conclusion .....	93
	References .....	95
	Chapter 5 .....	97
	Conclusion.....	97
	VITA .....	<b>Error! Bookmark not defined.</b>

## List of figures

Figure 1.1: Global mortality projection by cause.....	7
Figure 1.2: Age adjusted trends in mean plasma LDL-cholesterol for total population and by gender. ....	8
Figure 1.3: Schematic representation of an LDL particles. ....	9
Figure 2.1: Conversion of RGB image (a) to grayscale image (b) in order to calculate the image intensity. .....	39
Figure 2.2: TEM image of a) $\text{Fe}_3\text{O}_4@SiO_2$ nanoparticles (100 nm diameter) and b) $\text{Fe}_3\text{O}_4@SiO_2$ nanoparticles (20 nm diameter). MNPs were uniform in size and shape, and well dispersible in aqueous solvents.....	42
Figure 2.3: Fluorescence spectrum of 3-MPA Dansylcadaverine Excitation: 335 nm and Emission: 530 nm.....	46
Figure 2.4: Chromatogram obtained by HPLC-fluorescence analysis of (a) Control, (b) dansylcadaverine (5 $\mu\text{M}$ ) (c) 3-MPA-Dansyl (20 $\mu\text{M}$ ) and (d) 3-MPA- Dansyl released from 7 mg of $\text{Fe}_3\text{O}_4@SiO_2$ MNPs (100nm in diameter) upon cleaving the disulfide bond. For all samples the injection volume was 100 $\mu\text{L}$ . The isocratic elution with mobile phase of 80% ACN and 20% H <sub>2</sub> O was performed for all samples. The control sample was prepared by reacting thiol coated MNPs (7 mg) with dansylcadaverine.....	47
Figure 2.5: Fluorescence micrographs of $\text{Fe}_3\text{O}_4@SiO_2$ MNPs labeled with dansylcadaverine. a) Micrographs (a1-a6) represent fluorescence images obtained from 5, 10, 20, 40, 80 and 160 $\mu\text{g}$ of dansylcadaverine labeled $\text{Fe}_3\text{O}_4 @SiO_2$ MNPs. The control sample (a7, 20 $\mu\text{g}$ ) was prepared by reacting the hydrolyzed NHS ester coated $\text{Fe}_3\text{O}_4 @SiO_2$ MNPs with dansylcadaverine. The fluorescence intensity on a7 is below detection limit. b) Integrated fluorescence intensities of the images in a were plotted against quantity of MNPs. ....	50
Figure 2.6: Quantitative study of labeling BSA by NHS ester modified $\text{Fe}_3\text{O}_4@SiO_2$ MNPs. The amount of BSA conjugated to the NHS ester coated $\text{Fe}_3\text{O}_4@SiO_2$ MNPs was calculated by subtracting the amount of remaining BSA from the initial amount of BSA. In the series of experiments presented in Fig. 2.6a, the	

amount of NHS ester coated Fe<sub>3</sub>O<sub>4</sub>@SiO<sub>2</sub> MNPs (0.5 mg) was kept constant and amount of BSA was varied (20,40,60,80 and 100 μg). In Fig. 2.6 B, the quantity of BSA (20 μg) conjugated was kept constant, and the quantity of NHS ester modified MNPs was varied (0.05, 0.1, 0.5, 1 and 3 mg)..... 54

Figure 3.1: Labeling surface exposed lysine residues of apoB-100 in intact LDL using NHS ester modified Fe<sub>3</sub>O<sub>4</sub>@SiO<sub>2</sub> MNPs. .... 69

Figure 3.2: MS/MS spectrum of the labeled peptide "VNDESTEGKTSYR" of m/z 843.89 (molecular mass of 1685.76 Da)..... 71

Figure 4.1: (a) Synthesis of TCEP-immobilized Fe<sub>3</sub>O<sub>4</sub>@SiO<sub>2</sub> MNPs and (b) reduction of disulfide bonds in proteins and peptides using TCEP functionalized magnetic nanoparticles..... 85

Figure 4.2: ESI analysis of NGR peptide before (a) and after (b) reduction reaction using TCEP-coated MNPs. a) In this mass spectrum, the peaks at m/z 1079.47 and 540.23 correspond to singly and doubly charged ions , respectively. c) The singly charged ion at m/z 1193.51 and doubly charged ion at m/z 597.26 correspond to reduced NGR with both cysteine residues modified with carbamidomethyl group. b) MS/MS spectra of the doubly charged reduced/alkylated NGR. .... 89

Figure 4.3: ESI analysis of oxytocin peptide before (a) and after (b) reduction reaction using TCEP-coated MNPs. a). In this mass spectrum, the peaks at m/z 1007.7 and 504.85 correspond to singly and doubly charged ions, respectively. c) The singly charged ion at m/z 1121.48 and the doubly charged ion at m/z 561.25 correspond to reduced NGR with both cysteine residues modified with carbamidomethyl group. b) MS/MS spectra of the doubly charged reduced/alkylated oxytocin. .... 90

Figure 4.4:MS/MS spectrum of the reduced/alkylated peptide "ASVCSLYQLENYCN" of m/z 843.89 (molecular mass of 1719.72 Da) ..... 93

## List of Schemes

Scheme 2.1: Synthesis of Fe<sub>3</sub>O<sub>4</sub> MNPs (80 nm in diameter) by hydrothermal method. .... 33

Scheme 2.2: Preparation of Fe<sub>3</sub>O<sub>4</sub>@SiO<sub>2</sub> MNPs (~20 nm in diameter, with a iron oxide core of (~10 nm in diameter) by thermal decomposition plus reverse microemulsion method..... 34

Scheme 2.3: Mixing method for labeling BSAb by NHS ester modified Fe <sub>3</sub> O <sub>4</sub> @SiO <sub>2</sub> MNPs. ....	40
Scheme 2.4: A cleave-analyze approach for quantification of 3-MPA-Dansyl released upon cleaving disulfide bond between nanoparticles and dansylcadaverine. ....	44
Scheme 2.5: Synthesis of 3-Mercaptopropanamido dansylcadaverine (3MPA-Dansyl, a calibration standard for fluorometric measurements) .....	45

## List of Tables

Table 3.1: Solvent gradient used for analysis of tryptic digests of labeled apoB-100. Solvent A: water (100%), formic acid (0.1%). Solvent B: Acetonitrile: water (90:10), formic acid (0.1%). ....	66
Table 3.2: List of apoB-100 peptides with lysine (represented K) residues being labeled with NHS ester coated Fe <sub>3</sub> O <sub>4</sub> @SiO <sub>2</sub> MNPs and detected by LC-MS/MS analysis. ....	70
Table 4.1: Sequences of cyclic peptides used in this study. Each peptide contains two cysteine residues connected by an intramolecular disulfide bond. ....	87
Table 4.2: List of peptides in A and B chains of bovine insulin obtained by LC-MS/MS analysis of reduced/alkylated bovine insulin. All cysteine residues in A and B chains of insulin were modified with carbamidomethyl group. ....	92

## Abstract

Sample preparation as an essential step in mass spectrometry-based analysis, plays a critical role in proteomics studies. Magnetic nanoparticles (MNPs) have been widely used in protein and peptide sample preparation due to their magnetic properties, biocompatibility, easy synthesis and surface functionalization. MNPs loaded with analyte or analyte modification reagent can be easily separated from the reaction medium by an externally applied magnetic field. The small size of MNPs provides high analyte loading and extraction capacity. Additionally, MNP can be decorated with different functional groups to achieve selective modification or extraction of analyte. In this study we have utilized silica coated iron oxide magnetic nanoparticles ( $\text{Fe}_3\text{O}_4@\text{SiO}_2$  MNPs) for protein and peptide sample preparation.

Fluorescence-based methods were utilized for quantitative and qualitative characterization of *N*-hydrosuccinimidyl (NHS) ester groups on the surface of  $\text{Fe}_3\text{O}_4@\text{SiO}_2$  MNPs. Fluorophore Dansylcadaverine was conjugated to NHS ester functional groups. Fluorometric measurement of cleaved dansylcadaveine was employed to determine the number of NHS ester groups per MNPs that was found to be  $2.6 \times 10^2$  and  $3.4 \times 10^3$  for 20 nm and 100 nm  $\text{Fe}_3\text{O}_4@\text{SiO}_2$  MNP respectively. The efficiency of labeling native bovine serum albumin (BSA) by NHS ester coated  $\text{Fe}_3\text{O}_4@\text{SiO}_2$  MNPs was also explored in terms of maximizing the number of MNPs conjugated per BSA molecule or maximizing the number of BSA molecules conjugated per each MNP.

Lysine residues of apolipoprotein B-100 (apoB-100) on the surface of intact human low density lipoprotein (LDL) were labeled by NHS ester modified  $\text{Fe}_3\text{O}_4@\text{SiO}_2$  MNPs in aqueous solvents at room temperature. The MNP labeled apoB-100 was treated by SDS to remove lipids

and then digested using trypsin. Tryptic peptides were eluted from MNPs by cleaving disulfide linkage between labeled peptides and MNPs. LC-MS/MS analysis found 28 peptides containing labeled lysine residues. These lysine residues should be on the solvent exposed surface of LDL since the large size of MNPs prevents contact of the labeling reagent to those lysines embedded inside the structure of LDL.

TCEP- immobilized  $\text{Fe}_3\text{O}_4@\text{SiO}_2$  MNPs were fabricated and utilized for reduction of disulfide bonds in bovine pancreas insulin and two different cyclic peptides. Disulfide bonds were efficiently cleaved at room temperature in both organic and aqueous solvents confirmed by LC-MS/MS analysis of reduced/alkylated protein and peptides. Disulfide reduction and alkylation reactions was performed in one step and the reducing agent was simply separated from peptide and protein solution by magnetic separation.

Keywords: Silica coated iron oxide magnetic nanoparticles ( $\text{Fe}_3\text{O}_4@\text{SiO}_2$  MNPs), *N*-hydrosuccinimidyl (NHS) ester, fluorometric quantification, protein labeling efficiency, apolipoprotein B-100 (apoB-100), low density lipoprotein (LDL), surface exposed lysines, disulfide bond, TCEP- immobilized  $\text{Fe}_3\text{O}_4@\text{SiO}_2$  MNPs, LC-MS/MS.

# Chapter1

## Introduction

Proteomics, as a large scale comprehensive analysis tool for proteins, allows us to zoom in on biological processes at molecular level. Proteomics studies help researchers to explore the connections between genes, proteins and diseases and therefore plays a crucial role in disease recognition, drug development and molecular medicine. The application of nanomaterials in proteomics is expected to have significant impact on the future direction of research in this field.

Magnetic nanoparticles (MNPs), and particularly magnetite ( $\text{Fe}_3\text{O}_4$ ), as well established nanomaterials, have recently attracted a great deal of interest due to the important possibilities they can offer in biomedical studies. Synthetic magnetic nanoparticles have controllable sizes ranging from a few to several hundreds of nanometers – smaller than the size of a cell (10-100  $\mu\text{m}$ ) but comparable to the dimension of cell components such as proteins (5-50 nm). The similar size of nanoparticles and proteins makes them relatively easy to get close to each other and integrate. Magnetic nanoparticles can be easily surface-functionalized with a variety of ligands which can selectively bind to or interact with specific sites of proteins. Due to their ability to respond to magnetic fields, magnetic nanoparticles coated with various peptide reactive groups can be effectively used for protein isolation, purification and enrichment.

In this study we have utilized silica coated magnetic iron oxide nanoparticles ( $\text{Fe}_3\text{O}_4@ \text{SiO}_2$  MNPs) with well tailored surface functionalities for protein sample preparation and analysis. This thesis is divided into five parts. The introductory Chapter provides information about the key concepts that are related to the studies presented in this dissertation. The second Chapter describes the quantification of active functional groups on the surface of

Fe<sub>3</sub>O<sub>4</sub>@SiO<sub>2</sub>MNPs using different methods. The third Chapter evaluates the use of Fe<sub>3</sub>O<sub>4</sub>@SiO<sub>2</sub> MNPs in separation of lipid bound proteins such as ApoB-100 as well as application of these nanoparticles in labeling surface exposed lysine groups of ApoB-100 in native low density lipoprotein (LDL). The fourth Chapter is about the application of TCEP-immobilized Fe<sub>3</sub>O<sub>4</sub>@SiO<sub>2</sub> MNPs in reduction and alkylation of disulfide bonds in both cyclic peptides and proteins. The last Chapter summarizes the performed work and also provides suggestions for future studies.

## **1.1 Magnetic iron oxide nanoparticles-applications, synthesis, functionalization and quantification of surface ligands**

Nanoparticles are submicron entities (with the diameter ranging from 1-100 nm) composed of organic or inorganic materials.<sup>1</sup> Magnetic nanoparticles (MNPs), as one of the most well-established nanomaterials, possess unique magnetic properties such as superparamagnetism, high coercivity, low Curie temperature and high magnetic susceptibility.<sup>1</sup> MNPs have attracted a lot of attention due to their broad range of applications including magnetic fluids, data storage and catalysis.<sup>1-6</sup> In recent years MNPs have also been extensively used for various biological, diagnostic and therapeutic applications such as separation and detection of cells and cell compartments (protein, nucleic acids, enzymes), magnetic resonance imaging, magnetic fluid hyperthermia and targeted drug delivery.<sup>1, 7-10</sup>

Magnetite (Fe<sub>3</sub>O<sub>4</sub>) and maghemite (γ-Fe<sub>2</sub>O<sub>3</sub>) are two major forms of magnetic nanoparticles used in biomedical applications. The applications of iron oxide MNPs are highly influenced by their shape, size and size distribution, surface and magnetism.<sup>11</sup> Therefore, having good control over the properties of MNPs during the synthesis and functionalization is crucial for

their successful application. The most common methods to synthesize MNPs are: thermal decomposition, hydrothermal synthesis, co-precipitation, microemulsion and sonochemical synthesis.<sup>12</sup> Thermal decomposition and hydrothermal methods were employed to synthesize magnetic Fe<sub>3</sub>O<sub>4</sub> nanoparticles which have been used in our studies.

Thermal decomposition methods have been employed for fabrication of monodisperse size controlled magnetic iron oxide nanoparticles. Thermal decomposition of organoiron precursors such as iron penta carbonyl (Fe(CO)<sub>5</sub>) and iron (III) acetylacetonate (Fe(acac)<sub>3</sub>) in presence of surfactant generates nanoparticles with controlled size (ranging from 4 to 20nm).<sup>13-15</sup> More environmental friendly alternatives to the aforementioned precursors are iron chloride and other iron oxides which have been widely used in recent years.<sup>16-19</sup> The magnetic iron oxide nanoparticles generated by thermal decomposition methods are well dispersed in organic solvents.

The hydrothermal method is a simple and environmental friendly procedure for the synthesis of magnetic iron oxide nanoparticles that does not require organic solvents. The reactions are performed in aqueous solutions at high pressure (>2000 psi) and temperature<sup>20</sup> (200-300 °C). The nucleation and growth processes of the nanoparticles are influenced by several factors including reaction time, temperature and solvent composition<sup>21</sup>. To generate nanoparticles with well defined shape and narrow size distribution, polyols (such as ethylene glycol, diethylene glycol, polyethylene glycol) have been used as solvents.<sup>22,23</sup> Polyols also act as reducing and stabilizing agents that prevent the aggregation of nanoparticles.<sup>24</sup> The nanoparticles made by this method are coated with hydrophilic ligands, which make them well dispersible in polar solvents.

Surface coating of magnetic nanoparticles with inert materials such as silica increases the chemical stability and biocompatibility of magnetic nanoparticles.<sup>25</sup> Silica coating also enhances the colloidal stability of the magnetic nanoparticles due to the electrostatic repulsion induced by silica shell. Moreover, the silica layer serves as a platform for surface functionalization of magnetic nanoparticles.<sup>26</sup> In our studies, we followed the two most common approaches for silica coating of magnetic nanoparticles: the Stöber method and inverse microemulsions.

Stober method relies on hydrolysis-condensation reaction of tetraethyl orthosilicate (TEOS) as the silicon dioxide precursor.<sup>27</sup> The hydrolysis and polycondensation of TEOS in basic solution leads to formation of an amorphous silica shell. The thickness of the silica layer can be controlled by changing the concentration of TEOS, the type of solvent, the amount of water and the concentration of base.<sup>28-31</sup>

Water in oil microemulsions (W/O, also called inverse microemulsions) are well known methods for synthesis of silica coated magnetic nanoparticles with narrow size distribution.<sup>32</sup> In these methods, water nanodroplets are dispersed in the organic (oil) phase and stabilized by a nonionic surfactant. The water nanodroplets in the internal core of the micelles serve as nanoreactors in which the silica shell forms around the iron oxide cores via hydrolysis-condensation reaction of TEOS. The size of these water nanodroplets and consequently the size of the silica coated nanoparticles can be changed by varying the ratio between the organic and aqueous phase, the concentration of reactants, the reaction temperature and the type of surfactant.<sup>33</sup>

Functionalization of nanoparticles is a critical step in various bio-applications. Different functional groups such as carboxylic acid,<sup>34,35</sup> thiol<sup>36,37</sup> and amine<sup>38</sup> are immobilized on the surface of the nanoparticles before further conjugation to the biomolecules. The application of

the nanoparticles is usually defined by the ligands present on their surface. Accurate measurement of the active functional groups is very important to evaluate the efficiency of further chemical conjugation reactions.

Despite dramatic improvements in the synthesis of biocompatible nanoparticles, less attention has been paid to quantification of intermediate functional groups and exposed ligands on the surface of NPs. Common spectroscopic techniques such as IR and XPS showed low sensitivity towards the quantification of surface functional groups.<sup>39,40</sup> Fluorometric<sup>41,42</sup> and colorimetric techniques,<sup>43</sup> high resolution mass spectrometry,<sup>44</sup> combustion analysis<sup>45</sup> and ATR-FTIR<sup>39,40</sup> have also been used to quantify the surface functional groups. Each of these aforementioned methods has its own disadvantages that prevent accurate quantitative measurement of surface functional groups.

Chemical labeling approaches, which rely on covalent attachment of a chromophore/fluorophore to the surface functional groups, have also been employed for surface characterization of nanomaterials. These methods are simple, sensitive and nondestructive. However, the direct quantification of chromophore/fluorophore attached to the surface of nanoparticles could be problematic due to the possible fluorescence quenching effect of some type of nanoparticles. This problem can be solved by inducing a specific cleavage of conjugated fluorophore from NPs prior to measurements.<sup>46</sup> Dansyl derivatives have been widely used as fluorophores in covalent labeling and quantification of aldehyde, ketone and carboxylic acid functional groups on the surface of nanomaterials.<sup>47,48, 49</sup>

## 1.2 Cardiovascular diseases (CVD)

Cardiovascular disease (CVD) is a collective term to describe disorders that affect the function of the heart and the blood vessel system (arteries, veins and capillaries) including coronary heart diseases, cerebrovascular diseases (stroke), peripheral arterial diseases, rheumatic heart disease, congenital heart disease, deep vein thrombosis and pulmonary embolism. The two most important forms of CVD are coronary heart disease and stroke. Coronary heart disease refers to a blockage of the arteries that supply oxygen to the heart muscle, which results in a heart attack. Stroke occurs when the blood flow to the brain is blocked or interrupted as a result of either blockage (ischaemic stroke) or the rupture of a blood vessel<sup>50</sup> (hemorrhagic stroke).

Cardiovascular disease is the world's leading cause of death accounting for one third of all deaths globally. Figure 1.1 shows the trends in CVD mortality as well as the expected shift from infectious to chronic disease over the next few decades.<sup>51</sup> According to World Health Organization (WHO) estimates, 17 million people die each year from CVD. Of these, an estimated 7.2 million were attributed to coronary heart disease and 5.7 million were due to stroke.<sup>52</sup> The annual CVD deaths are expected to rise to 24 million by 2030.<sup>52</sup> The epidemic of CVD is also shifting from developed to developing nations and nearly 80 percent of the CVD deaths occur in low and middle income countries. The largest percentage increase in CVD deaths is expected to occur in the Eastern Mediterranean Region.<sup>52</sup>

Several risk factors are associated with CVD, which can be classified as modifiable and non-modifiable risk factors. Non-modifiable risk factors include gender, ethnicity, age and family history. Modifiable risk factors, which can be prevented, treated and controlled include tobacco smoking, insufficient physical activity, high blood pressure, high blood cholesterol, obesity and unhealthy diets.<sup>52,53</sup> It is an undeniable fact that diet has a crucial role in

development and prevention of CVD. A high level of blood cholesterol has been known as a major risk factor for cardiovascular disease.<sup>52,53</sup> Although studies show a declining trend in total average blood cholesterol level for adult Americans (Figure 1.2), elevated cholesterol should still be considered as a serious health threat.

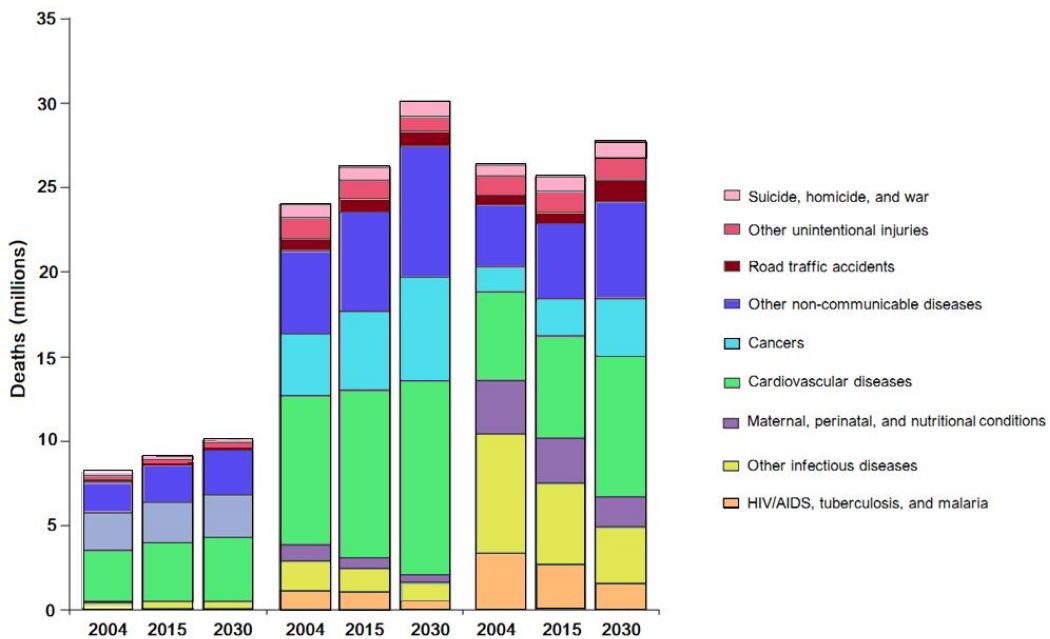


Figure 1.1: Global mortality projection by cause.<sup>51</sup>

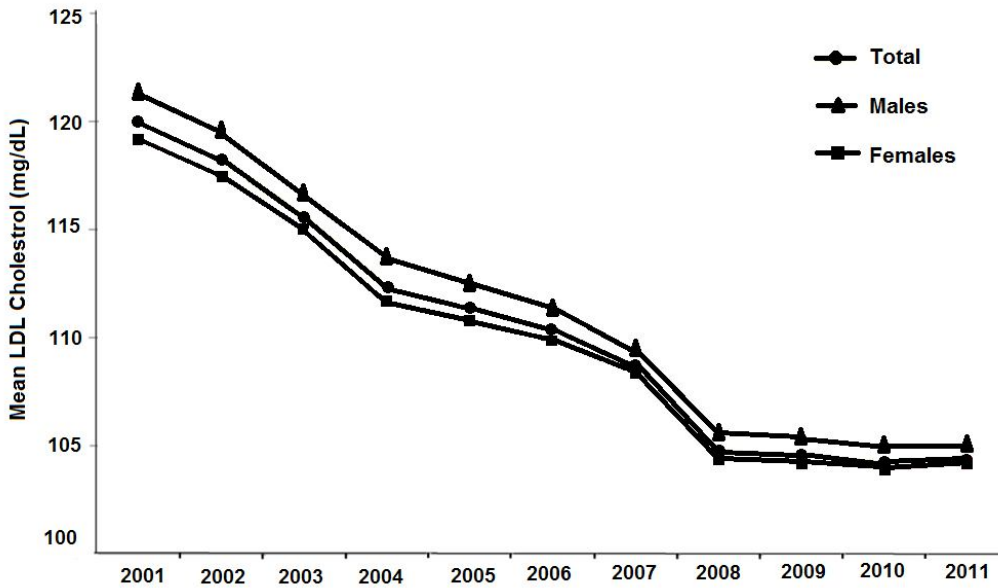


Figure 1.2: Age adjusted trends in mean plasma LDL-cholesterol for total population and by gender.<sup>54</sup>

### 1.3 Low density lipoproteins (LDL)

Lipoproteins are micelle-like particles consisting of lipids and proteins held together by non-covalent interactions that enable lipid transport in the aqueous environment of body fluids.<sup>55,56</sup> The main groups of lipoproteins are classified as chylomicrons, very low density lipoprotein, low density lipoproteins (LDL), intermediate density lipoproteins (IDL) and high density lipoproteins (HDL). LDL, as the main cholesterol carrier in the physiological system, is synthesized in the liver. LDL is often called "bad" cholesterol since an elevated level of LDL is associated with cardiovascular diseases.<sup>57,58</sup> Higher levels of HDL or "good" cholesterol reduce the risk of CVD.<sup>59,60</sup>

LDL particles (Figure 1.3), with an average molecular weight of 3 million Daltons, consist of a non-polar core including cholesteryl ester and triglycerides. The hydrophobic core of LDL is surrounded by an outer monolayer consists of phospholipids and free cholesterol. The

only protein component of LDL is apolipoprotein B-100<sup>61</sup> (apoB-100). Cholesterol, which is vital for proper function of cells, has several roles including stabilization of cell membranes. When needed, cholesterol is acquired by cells via receptor mediated endocytosis of LDL particles.<sup>62</sup> After binding to the LDL receptor on the cell surface, the LDL-bound protein is then internalized by endocytosis forming a clatherin-coated pit which will pinch off to form a clatherin vesicle. The acidic pH of the endosome leads to protonation of the LDL receptor and finally freeing of the bound LDL particles. The enzymatic digestion of LDL particles in lysosomes breaks down the ApoB-100 to amino acids and release cholesterol. The LDL receptors are recycled back to the cell membrane via transport vesicles.<sup>62</sup>

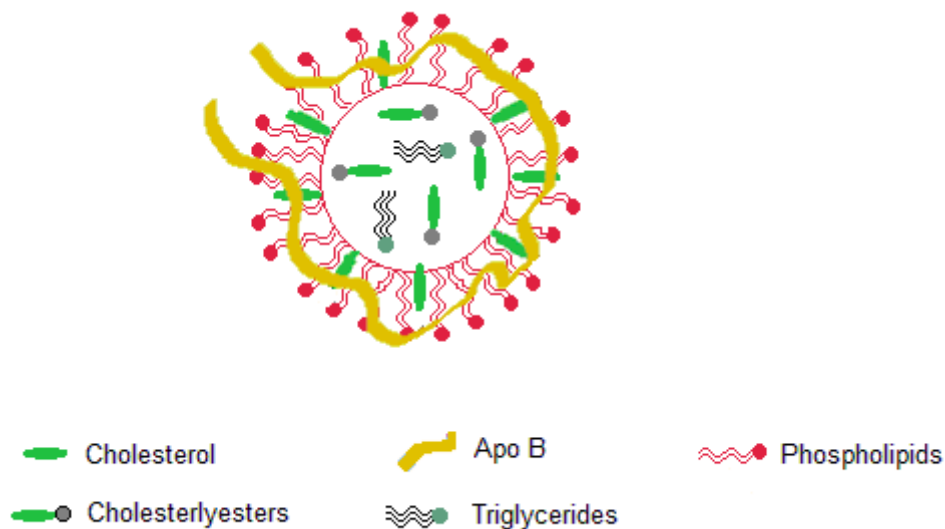


Figure 1.3: Schematic representation of an LDL particles.

## 1.4 Apolipoprotein B-100 (ApoB-100)

ApoB-100, the exclusive protein constituent of LDL, is one of the largest monomeric protein known with the molecular weight of 550 kDa.<sup>63-65</sup> Apo B-100, as a ligand for receptor-mediated endocytosis of LDL,<sup>66</sup> is produced in the liver and contains 4563 amino acids. It has been difficult to determine the structure of ApoB-100 due to the very large size of the molecule, which hinders the production of good quality X-ray diffraction crystals. ApoB-100 is insoluble in the aqueous environment once it is delipidated, which makes the structural analysis even more difficult.<sup>67</sup>

Despite extensive studies on APOB-100 structure over the last two decades,<sup>64, 68</sup> the structure of ApoB-100 is still not well characterized. The results from calorimetric and x-ray diffraction studies as well as cryo-electron microscopy indicated that ApoB-100 wraps around the outer surface of LDL particles.<sup>69-71</sup> Circular dichroism (CD) and helical wheel analysis showed the presence of 25%  $\alpha$  helical content.<sup>72</sup> These methods also provided some information about the role of disulfide linkage in the conformation of ApoB-100<sup>73</sup> as well as the lipid associating motifs of ApoB-100.<sup>74</sup> The presence of  $\beta$  sheet structure in ApoB-100 was also confirmed by infrared spectroscopy and CD studies. 1D NMR<sup>75</sup> and 2D NMR<sup>76</sup> were used to detect different populations of solvent exposed lysine groups of ApoB-100.

Molecular modeling techniques has shed some light on the ApoB structure using the ApoB sequence homology to lipovitellin, which is a protein found in egg yolk.<sup>77</sup> It was found that the N-terminal residues of ApoB and lipovitellin are very similar showing, up to 20.5% sequence match<sup>78</sup>. Further analysis using the homology search program (BLAST) showed that the sequence similarity between ApoB and lipovitellin extends beyond the N-terminal amino acids to include the first 1000 amino acid residues in ApoB-100.<sup>79</sup>

The oxidative modification of ApoB-100 in the presence of radicals has been studied in our lab.<sup>80, 81</sup> The oxidation was carried out prior to the delipidation process, and the modified peptides were analyzed by liquid chromatography tandem-mass spectrometry (LC-MS/MS). Covalent labeling of the solvent exposed amino acid residues is a challenging task due to the ability of small labeling reagents to cross the lipid layer and modify the internal amino acid residues embedded inside the structure of ApoB-100.

ApoB-100 contains both hydrophobic regions that bind to lipids and hydrophilic regions that interact with the aqueous phase. ApoB-100 has a pentapartite structure, NH<sub>2</sub> - β<sub>1</sub> - α<sub>1</sub> - β<sub>2</sub> - α<sub>2</sub> - β<sub>3</sub> - COOH, consisting of three α-helices and two β-strands in between the α-helices.<sup>62</sup> β-domains of ApoB-100 are rigid and irreversibly associated with the neutral lipid core of LDL particles, providing stability to the LDL particles, while α-helices give more elasticity to the ApoB molecule.<sup>62</sup> The amphiphilic characteristic of ApoB is crucial in preserving the integrity of LDL particles during lipid transport in the blood.

### **1.5 Mapping protein structure using Amino acid-specific covalent labeling**

Combining mass spectrometric analysis with covalent modification of specific amino acids residues in proteins is a very useful approach to obtain important information about the sequence, structure and surface topology of proteins,<sup>77</sup> specially in those systems which are difficult to study by other methods. Electrospray ionization (ESI) and matrix-assisted laser desorption ionization (MALDI) followed by tandem mass spectrometric analysis have been employed to identify the sites of covalent modifications, providing important site-specific structural information about proteins.<sup>78</sup> The covalent labeling methods rely on differential reactivity of amino acid side chain towards labeling reagents. The reactivity of amino acids in

proteins depends on several factors including accessibility of the side chain to the reagent, the inherent reactivity of the label and the reactivity of the amino acid side chain.<sup>78</sup>

Covalent labeling is usually performed using either non-specific or specific labels. Oxidative footprinting methods using radicals are an example of nonspecific covalent labeling.<sup>79-</sup><sup>81</sup> On the other hand, side chains of many amino acids have been selectively modified using covalent labels that target specific functionalities such as sulfhydryls (cysteine), amines (lysine) and carboxylic acids<sup>82-85</sup> (aspartic acid and glutamic acid).

Iodoacetic acid and iodoacetamide have been extensively used for probing cysteine groups in proteins. Maithal et.al used these reagents to determine the differential reactivity of cysteine residues in Plasmodium falciparum triose-phosphate isomerase.<sup>85</sup> Whitehurst et al. studied the accessibility of cysteine residues for covalent modification with iodoacetamide in the Sindbis virus E1 and E2 glycoproteins by incubation of the native virus particles with the labeling reagent.<sup>86</sup> Covalent modification of lysine groups with amine reactive reagents such as *N*-hydroxysuccinimidyl (NHS) esters,<sup>82,87</sup> sulfo-NHS esters,<sup>88</sup> isothiocyanates,<sup>89</sup> and isocyanates<sup>90</sup> has been of particular interest in protein structural studies due to the fact that lysine residues are more abundant compared to cysteine residues.<sup>82,91</sup> Solvent exposed lysine residues of ApoB-100 were modified by <sup>13</sup>C methyl groups followed by NMR characterization.<sup>92</sup> Patil et al. fabricated NHS ester modified Fe<sub>3</sub>O<sub>4</sub>@SiO<sub>2</sub> magnetic nanoparticles with a cleavable disulfide bond linker to label primary amine groups on the solvent accessible surface of bovine serum albumin<sup>82</sup> (BSA).

## 1.6 LC-MS/MS based proteomics

Proteomics is the large scale structural and functional analysis of protein molecules, which are vital components of living organisms. Proteomics is not only used for protein

sequencing but also provides detailed information about the protein abundances, protein-protein interactions and post translational modifications.<sup>79, 93-95</sup> Mass spectrometry, as one of the most sensitive analytical techniques, has made an enormous contribution in development of proteomics to its current capabilities. Initially, mass spectrometry was used in combination with 2-dimensional gel electrophoresis (2DE) for individual protein sequencing and identification of gel bands.<sup>96</sup> Analysis of complex protein and peptide mixtures became possible after combining the liquid chromatography separation techniques with mass spectrometry.<sup>97</sup>

In mass spectrometric analysis of proteins, two soft ionization techniques are commonly used. In MALDI technique,<sup>98</sup> the analyte is mixed with an organic matrix. The energy of the laser beam is then transferred to the sample through the matrix, which causes the simultaneous desorption and ionization of the analyte. In ESI method, a high voltage is applied to the analyte solution which results in formation of charged droplets that in turn rapidly evaporate and become smaller as they are dragged along the ion passage by potential and pressure gradients. As the droplets become smaller, they repel each other because of the increased surface charge density and burst into smaller droplets. Once the solvent is completely removed, the analyte ions enter the mass spectrometer and can be easily analyzed.

In our instrumental design, peptide ions entered a hybrid quadrupole time of flight mass spectrometer (Agilent 6520 Q-TOF mass spectrometer coupled with HPLC) after desolvation.<sup>99,100</sup> The quadrupole guides ions through the analyzer region in MS mode and also serves as a mass selection tool in MS/MS mode. A time-of-flight (TOF) analyzer, which is placed orthogonally to the ion beam exiting the quadrupole, resolves different mass ions in both MS and MS/MS

modes. In MS/MS analysis, the fragmentation takes place in the collision cell, which is located between the quadrupole and the TOF analyzer. Nitrogen was used as collision gas. The sample separation using liquid chromatography prior to mass detection, increases the sensitivity of the mass spectrometric analysis of complex protein and peptides samples.

## 1.7 Database Search

The data acquired in a common LC-MS/MS analysis includes a complex collection of precursor ions intensities and the associated MS/MS spectra from which we can obtain valuable information by performing a database search. Different search algorithms are available to identify the peptides in complex biological mixtures. In our studies, the full length cDNA sequences for ApoB-100 (Swiss-Prot accession # P04114) and bovine insulin (GenBank accession #550058A) were processed by the PEAKS database search program. After adding the sequence to a database, the software performs in-silico (performed via computer simulation) cleavage of the polypeptide sequence to create theoretical precursor ions. The fragmentation of these precursor ions generates corresponding product ions.

The PEAKS software matches the theoretical b (charge is retained on the N-terminus) and y (charge is retained on the C terminus) ions with the experimental tandem mass spectra and generates a score called the linear discriminative function (LDF) to evaluate the quality of match. The LDF score not only finds the most likely correct peptides in each spectrum of the tandem mass dataset, but also efficiently separates true and false identifications.<sup>101, 102</sup> The LDF score is then converted to a P-value to facilitate the data interpretation. For a given LDF score, its equivalent P-value is the probability that a false identification has a score > LDF. The smaller the

P-value the less likely the peptide-spectrum match is a random match<sup>101</sup>. The p value is then converted to  $-10 \cdot \log_{10}(\text{P-value})$ , which is a more human friendly representation. In this case, a better match has a higher  $-10 \log P$  value. AP-value of 1% is equal to  $-\log P$  of 20.<sup>102</sup>

## 1.8 Disulfide bonds in proteins

Disulfide bonds are covalent linkages between cysteine pairs, which are formed due to the oxidation of cysteines.<sup>103</sup> Disulfide bonds exist in proteins of both prokaryotic and eukaryotic cells. Disulfide bond containing proteins are usually found in the endoplasmic reticulum of prokaryotic cells or the preplasmic space of bacteria.<sup>103</sup> Both intermolecular (between different polypeptide chains) and intramolecular (within the polypeptide chain) disulfide bonds play crucial role in folding of proteins into their native, three dimensional and active structures.<sup>103</sup> Insulin, an example of disulfide bond containing proteins, is an essential hormone produced by the pancreas beta cells and plays a crucial role in metabolism of carbohydrates and fats. Mature insulin, with the molecular weight of 5733 Da, contains 51 amino acids in two polypeptide chains. The A chain has 21 amino acids (A1-A21), and the B chain has 30 amino acids (B1-B30). These chains are connected via two interchain disulfide bonds (A7-B7 and A19-B20). There is also an intrachain disulfide bond (A6-A11) within the A chain of insulin.<sup>102</sup> The first precursor of insulin (preproinsulin) contains an amino terminal signal sequence which is cleaved during the process of transferring to the endoplasmic reticulum. Cleavage of the signaling sequence generates the second insulin precursor called proinsulin, which is finally converted to the mature insulin by removing the internal connecting polypeptide<sup>105</sup> (C chain).

## 1.9 Reduction and alkylation of proteins

Generating protein fragments via proteolytic digestion is a crucial step in structural analysis of proteins by mass spectrometry. The efficiency of proteolytic digestion depends on the accessibility of the enzymes, such as trypsin, to their potential cleavage sites, which could be hindered if the protein is folded.<sup>106</sup> Disulfide bond reduction unfolds protein and improves the efficiency of the digestion process by making the cleavage sites accessible to the enzyme. This ultimately increases the protein sequence coverage and improves the protein identification by mass spectrometry.<sup>107, 108</sup>

Various reducing agents such as dithiothreitol (DTT),  $\beta$ -mercaptoethanol (BME), and tris-(2-carboxyethyl) phosphine hydrochloride (TCEP) have been used for the reduction of disulfide bonds in peptides and proteins.<sup>108</sup> The application of BME and DTT is limited by several factors including low stability, pH sensitivity and incompatibility with sulfhydryl modifying reagents. TCEP has been extensively employed for reduction of disulfide bonds in peptides and proteins due to its advantages of being odorless, active over a wide range of pH, more resistant to air oxidation and more water soluble.<sup>109-114</sup> Additionally, TCEP does not interfere with most of the thiol labeling reactions, which eliminates the need of its removal before the modification of free thiol groups.<sup>109, 115, 116</sup> The reduction of disulfide bonds using TCEP is typically done by simply mixing the reducing reagent with proteins over a specific time (ranging from 30 min - 24 hr) at a specific temperature<sup>109</sup> (ranging from room temperature to 60°C).

The free thiol groups generated by disulfide bond cleavage are highly reactive and could be oxidized easily to reform disulfide bonds. Reformation of disulfide bonds can often be avoided by blocking the free thiol groups via alkylation reactions. Vinylpyridine, iodoacetamide,

iodoacetic acid and iodoethanol are common alkylating reagents among which iodoacetamide has been extensively used since it is odorless and more stable.<sup>116,117</sup> The alkylation reaction using iodoacetamide is usually carried out in the dark at 37°C for a specific time ranging from 30min to 1hr.<sup>118</sup>

TCEP does not contain a thiol, which makes it unreactive towards most of the thiol labeling reagents. However, TCEP shows some degree of reactivity towards certain chemicals that are commonly used for labeling proteins and peptides.<sup>118,119</sup> In this case, TCEP should be removed before further modification of the reduced proteins. Immobilization of TCEP on solid supports such as hydrophilic PEG resins<sup>120</sup> and monolithic silica<sup>109</sup> chips eliminates the need to perform time consuming and laborious methods such as dialysis and gel filtration, which are commonly used for separation of reducing agents from protein solution.

## References

1. Wu W., He Q., Jiang C., *Nanoscale Research Letters*, 3(11):397-415, 2008.
2. Patel D., Moon J.Y., Chang Y., Kim T.J., Lee G.H., *Colloid Surf., A* 313–314, 91, 2008.
3. Zhao M., Josephson L., Tang Y., Weissleder R., *Angew. Chem. Int. Ed.*, 42, 1375, 2003.
4. Mornet S., Vasseur S., Grasset F., Veverka P., Goglio G., Demourgues A., et al., *Prog. Solid State Chem.*, 34, 237, 2006.
5. Stevens P.D., Fan J., Gardimalla H.M.R., Yen M., Gao Y., *Org. Lett.*, 7, 2085, 2005.
6. Jun Y., Choi J., Cheon J., *Chem. Commun. (Camb)*, 1203, 2007.
7. Horák D., *Polymer*, Volume 46, Issue 4, 7, Pages 1245-1255, February 2005.
8. Gupta A.K., Gupta M., *Biomaterials*, Volume 26, Issue 18, Pages 3995- 4021, Jun 2005.
9. Jordan A., et al., *Journal of Magnetism and Magnetic Materials*, Volume 225, Issues 1-2, Pages 118- 126, 2001.
10. Neuberger T., et al., *Journal of Magnetism and Magnetic Materials*, Volume 293, Issue 1, Pages 483-496, May 2005.
11. Laurent S., Forge D., Port M., Roch A., Robic C., Vander E. L., *Magnetic iron oxide nanoparticles: synthesis, stabilization, vectorization, physicochemical characterizations and biological applications*, *Chemical reviews*, 108:2064-110, 2008.
12. Wu W., He Q., Hu R., Huang J., Chen H., *Rare Metal Mater*, p. 238, 2007.
13. Rockenberger J., Scher E.C., Alivisatos A.P., *Journal of American Chemical Society*, 121, 11595-6, 1999.
14. Hyeon T., Lee S.S., Park J., Chung Y., Bin Na H., *Journal of American Chemical Society*, 123, 12798-801, 2001.

15. Sun S., Zeng H., Robinson D.B., Raoux S., Rice P.M., Wang S.X., et al., *Journal of American Chemical Society*, 126, 273-9, 2004.
16. Park J., An K., Hwang Y., Park J.G., Noh H.J., Kim J.Y., et al., *Nature Materials*, 3, 891-5, 2004.
17. Jana N.R., Chen Y., Peng X., *Chemistry of Materials*, 16, 3931-5, 2004.
18. Yu W.W., Falkner J.C., Yavuz C.T., Colvin V.L., *Chemical Communications*, 2306-7, 2004.
19. Lin C.R., Chiang R.K., Wang J.S., Sung T.W., *Journal of Applied Physics*, 99, 08N710, 2006.
20. Fievet F., Lagier J.P., Blin B., Beaudoin B., Figlarz M., *Solid State Ionics.*, 32-33, 198-205, 1989.
21. Sue K., Kimura K., Arai K., *Materials Letters*, 58, 3229- 31, 2004.
22. Chen D., Xu R., *Materials Research Bulletin*, 33, 1015-21, 1998.
23. Liu W. B., Bing J. Y., Wan L. Y., Wen L., Jiao Y., and Mei Z. G., In *Advanced Materials Research*, Volume 631, Pages 490-493, 2013.
24. Jezequel D., Guenot J., Jouini N., Fievet F., *Journal of Materials Research*, 10, 77-83, 1995.
25. Chen, W. Y., and Chen, Y. C., *Anal. Bioanal. Chem.*, Volume 386, Issue 3, Pages 699–704, 2006.
26. Li Y. S., Church J. S., Woodhead A. L., and Moussa F., *Spectrochim. Acta, Part A* 76 (5), 484–489, 2010.
27. Stoeber W., Fink A., Bohn E., *Journal of Colloid and Interface Science*, 26, 62-9, 1968.
28. Im S.H., Herricks T., Lee Y.T., Xia Y., *Chemical Physics Letters*, 401, 19-23, 2005.
29. Lu Y., Yin Y., Mayers B.T., Xia Y., *Nano Letters*, 2, 183-6, 2002.

30. Deng Y.H., Wang C.C., Hu J.H., Yang W.L., Fu S.K., *Physicochemical and Engineering Aspects*, 262, 87-93, 2005.
31. Barnakov Y.A., Yu M.H., Rosenzweig Z., *Langmuir*, 21, 7524-7, 2005.
32. Liu H.M., Wu S.H., Lu C.W., Yao M., Hsiao J.K., Hung Y., et al., *Small*, 4, 619-26, 2008.
33. Santra S., Tapeç, R., Theodoropoulou N., Dobson J., Hebard A., Tan W., *Langmuir*, 17, 2900, 2001.
34. Tadmor R., Rosensweig R. E., Frey J., and Klein J., *Langmuir*, Volume 16, no. 24, pp. 9117–9120, 2000.
35. Rosensweig R. E., Kaiser R., and Miskolczy G., *Journal of Colloid and Interface Science*, vol. 29, no. 4, pp. 680–686, 1969.
36. Lu J., Fan J., Xu R., Roy S., Ali N., and Gao Y., *Journal of Colloid and Interface Science*, vol. 258, no. 2, pp. 427–431, 2003.
37. Kataby G., Ulman A., Prozorov R., and Gedanken A., *Langmuir*, vol. 14, no. 7, pp. 1512–1515, 1998.
38. Rockenberger J., Scher E. C., and Alivisatos A. P., *Journal of the American Chemical Society*, vol. 121, no. 49, pp. 11595–11596, 1999.
39. Noel S., Liberelle B., Robitaille L. and De Crescenzo G., *Bioconjugate Chem.*, 22, 1690-1699, 2011.
40. Dauginet L., Duwez A. S., Legras R., and Demoustier C. S., *Langmuir*, 17, 3952-3957, 2001.
41. Chen Y., Chi Y., Wen H. and Lu Z., *Anal. Chem.*, 79, 960-965, 2006.
42. Corsi K., Chellat F., Yahia L. H. and Fernandes J. C., *Biomaterials*, 24, 1255-1264, 2003.
43. Bravo-Osuna I., Teutonico D., Arpicco S., Vauthier C. and Ponchel G., *Int.J. Pharma.*, 340, 173-181, 2007.

44. Kim J., Shon H. K., Jung D., Moon D. W., Han S. Y. and Lee T. G., *Anal. Chem.*, 77, 4137-4141, 2005.
45. Waterbeemd M., Sen T., Biagini S. and Bruce I. J., *Micro & Nano Lett.*, IET, 5, 282-285, 2010.
46. Liu Y. and Yan B., *Comb. chem. high throughput screening*, 14, 191-197, 2011.
47. Feng X., Dementev N., Feng W., Vidic R., and Borguet E., *Carbon*, 44, 1203-1209, 2006.
48. Dementev N., Feng X. and Borguet E., *Langmuir*, 25, 7573-7577, 2009.
49. Pellenbarg T., Dementev N., Jean-Gilles R., Bessel C., Borguet E., Dollahon N. and Giuliano R., *Carbon*, 48, 4256-4267, 2010.
50. Mackay J., Mensah G.A., Geneve: World Health Organization, 2004.
51. Fuster V., Kelly B., *Promoting cardiovascular health in the developing world: a critical challenge to achieve global health*. Washington, DC: The National Academies Press, 2010.  
Available from: [http://www.nap.edu/nap-cgi/report.cgi?record\\_id=12815&type=pdfxsum](http://www.nap.edu/nap-cgi/report.cgi?record_id=12815&type=pdfxsum) [cited 8 November 2011][[PubMed](#)]
52. <http://www.who.int/mediacentre/factsheets/fs317/en/index.html>.
53. Lloyd-Jones D., Adams R. J., Brown T. M., Carnethon M., Dai S., De Simone G., Ferguson T. B., Ford E., Furie K., Gillespie C., Go A., Greenlund K., Haase N., Hailpern S., Ho P. M., Howard V., Kissela B., Kittner S., Lackland D., Lisabeth L., Marelli A., McDermott M. M., Meigs J., Mozaffarian D., Mussolino M., Nichol G., Roger V., Rosamond W., Sacco R., Sorlie P., Stafford R., Thom T., Wasserthiel-Smoller S., Wong N. D., Wylie-Rosett J., *A Report From the American Heart Association*. *Circulation* 2009, CIRCULATIONAHA.109.192667-CIRCULATIONAHA.192109.192667.

54. Kaufman H.W., Blatt A.J., Huang X., Odeh M.A., Superko H.R., Blood Cholesterol Trends 2001–2011 in the United States: Analysis of 105 Million Patient Records, PLoS ONE 8(5): e63416, 2013.
55. Chapman M., J. Lipid Res., Volume 21, Issue 7, Pages 789-853, 1980.
56. Mahley R., Innerarity T., Rall S. Jr, Weisgraber K., J. Lipid Res., Volume 25, Issue 12, 1277-1294, 1984.
57. Assmann, G., Nofer J.R., Annu. Rev. Med., 54, 321-341, 2003.
58. Stein O., Stein Y., Atherosclerosis, Volume 144, Issue 2, 285-301, 1999.
59. Berg J. M., Tymoczko J. L., Stryer L., Biochemistry, 5<sup>th</sup> ed., W.H. Freeman: New York, p 1 v. (various pagings), 2002.
60. Lehninger A. L., Nelson D. L., Cox M. M., Principles of biochemistry, 2<sup>nd</sup> ed., Worth Publishers: New York, NY, p xli, 1013, [1077] p, 1993.
61. Segrest J. P., Jones M. K., De Loof H., Dashti N., J. Lipid Res., Volume 42, Issue 9, 1346-1367, 2001.
62. Goldstein J. L., Brown M. S., Anderson R. G. W., Russell D. W., Schneider W. J., Annu. Rev. Cell Biol, Volume1, Issue 1, 1-39, 1985.
63. Knott T. J., Pease R. J., Powell L. M., Wallis S. C., Rall S. C., Innerarity T. L., Blackhart B., Taylor W. H., Marcel Y., et al., Nature (London, United Kingdom), 323 (6090), 734-738, 1986.
64. Yang C. Y., Chen S. H., Gianturco S. H., Bradley W. A., Sparrow J. T., Tanimura M., Li W. H., Sparrow D. A., DeLoof H., et al., Nature (London, United Kingdom), 323 (6090), 738-742, 1986.

65. Yang C. Y., Lee F. S., Chan L., Sparrow D. A., Sparrow J. T., Gotto A. M., *Biochem. J.*, 239 (3), 777-780, 1986.
66. Whitfield A.J., Barrett P.H., Van Bockxmeer F.M., Burnett J.R., *Clin Chem.*, 50(10):1725-32, 2004.
67. Law S.W., Lackner K.J., Hospattankar A.V., et al., *Proceedings of the National Academy of Sciences of the United States of America*. Volume 82, Issue 24, Pages 8340-8344, 1985.
68. Yang C. Y., Gu Z. W., Weng S. A., Kim T. W., Chen S. H., Pownall H. J., Sharp P. M., Liu S. W., Li W. H., et al., *Arterioscler. Thromb. Vasc. Biol.*, Volume 9, Issue 1, Pages 96-108, 1989.
69. Richardson P.E., Manchekar M., Dashti N., Jones M.K., Beigneux A., Young S.G., Harvey S.C., Segrest J.P., *Biophys J.*, Volume 88, Issue 4, Pages 2789-800, Apr. 2005.
70. Atkinson D., Deckelbaum R. J., Small D. M., and Shipley G. G., *Natl. Acad. Sci., USA*, 74, Pages 1042–1046, 1977.
71. Muller K., Laggner P., Glatter O., and Kostner G., *Eur. J. Biochem.*, 82, Pages 73–90, 1978.
72. Scanu A., Hirz R., *Nature.*, Volume 218, Issue 5137, Pages 200-1, Apr. 1968.
73. Singh S., Lee D.M., *BiochimBiophysActa.*, Volume 876, Issue 3, Pages 460-8, May 1986.
74. Wei C.F., Chen S.H., Yang C.Y., Marcel Y.L., Milne R.W., Li W.H., Sparrow J.T., Gotto A.M. J.r., Chan L., *ProcNatlAcadSci U S A*, Volume 82, Issue 21, Pages 7265-9, Nov. 1985.
75. Aviram M., Lund-Katz S., Phillips M.C., Chait A., *J. Biol Chem.*, Volume 263, Issue 32, Pages 16842-8, Nov. 1988.
76. Blanco F.J., Villegas S., Benítez S., Bancells C., Diercks T., Ordóñez-Llanos J., Sánchez-Quesada J.L., *J. Lipid Res.*, Volume 51, Issue 6, Pages 1560-5, Jun. 2010.

77. Fung Y.M.E., Liu H.C., Chan T.W.D., *J. Am. Soc. Mass Spectrom.*, Volume 17, Pages 757-771, 2006.
78. Mendoza V.L., Vachet R.W., *Mass Spectrom Rev.*, Volume 28, Issue 5, Pages 785-815, Sep-Oct 2009.
79. Aebersold R., Mann M., *Nature*, Volume 422, Issue 6928, Pages 198-207, 2003.
80. Chakraborty S., Cai Y., Tarr M.A., *Anal Biochem.*, Volume 404, Issue 2, Pages 109-17, Sep 2010.
81. Chakraborty S., Cai Y., Tarr M.A., *Proteomics*, Volume 14, Issues 21-22, Pages :2614-22, Nov. 2014.
82. Patil U.S., Qu H., Caruntu D., et al., *Bioconjugate chemistry.*, Volume 24, Issue 9, Pages 10.1021, 2013.
83. Hermanson G. T., *Bioconjugate Techniques*, pp 3–26, Chapter 1, Academic Press, San Diego, 1996.
84. Weber C., Reiss S., and Langer K., *Int. J. Pharm.*, Volume 211, Issues 1–2, Pages 67–78, 2000.
85. Maithal K., Ravindra G., Balaram H., Balaram P., *J. Biol Chem.*, Volume 277, Pages 25106–25114, 2002.
86. Whitehurst C.B., Soderblom E.J., West M.L., Hernandez R., Goshe M.B., Brown D.T., *J. Virol.* Volume 81, Pages 6231–6240, 2007.
87. Cheng K., El-Boubbou, Kheireddine L., and Christopher C., *ACS Appl. Mater. Interfaces*, Volume 4, Issue 1, Pages 235–243, 2011.
88. Qian J., Cole R. B., and Cai Y., *J. Mass. Spectrom.*, Volume 46, Issue 1, Pages 1–11, 2011.

89. Zhao L. Y., Zhang Y. J., Wei J. Y., Cao D., Liu K. H., and Qian X. H., *Proteomics*, Volume 9, Issue 18, Pages 4416–4420, 2009.
90. Rifai A., and Wong S. S., *J. Immunol. Methods*, Volume 94, Issues 1–2, Pages 25–30, 1986.
91. Voet D., Voet J. G., and Pratt C. W., *Fundamentals of Biochemistry: Life at the Molecular Level*, 3<sup>rd</sup>ed., Wiley & Sons, Inc. Press, New York, 2008.
92. Lund-Katz S., Ibdah J.A., Letizia J.Y., Thomas M.T., Phillips M.C., *J.Biol Chem.*, Volume 263, Issue 27, Pages 13831-8, Sep. 1988.
93. Sevier C. S. and Kaiser C. A., *Nature Reviews Molecular Cell Biology*, Volume 3, Pages 836-847, 2002.
94. Steen H., Mann M., *Nat. Rev. Mol. Cell Biol.*, Volume 5, Issue 9, Pages 699-711, 2004.
95. Balestrieri M. L., Giovane A., Mancini F. P., Napoli C., *Curr. Med. Chem.*, Volume 15, Issue 6, Pages 555-572, 2008.
96. Corthals G. L., Wasinger V. C., Hochstrasser D. F., Sanchez J. C., *Electrophoresis*, Volume 21, Issue 6, Pages 1104- 1, 2000.
97. Makarov A., Scigelova M., *Coupling. J. Chromatogr.*, Volume 1217, Issue 25, Pages 3938-45, 2010.
98. Skoog D. A., Holler F. J., Nieman T. A., *Principles of Instrumental Analysis*, 5<sup>th</sup> ed., Thomson, Singapore, 2003.
99. [http://www.chem.agilent.com/Library/technicaloverviews/Public/5989-7408EN\\_HI.pdf](http://www.chem.agilent.com/Library/technicaloverviews/Public/5989-7408EN_HI.pdf)
100. [http://www.chem.agilent.com/Library/usermanuals/Public/G3335-90142\\_TOF\\_Q-TOF\\_Concepts.pdf](http://www.chem.agilent.com/Library/usermanuals/Public/G3335-90142_TOF_Q-TOF_Concepts.pdf).
101. <http://www.bioinfor.com/peaks/tutorials/peaksdbscore.html>

102. Zhang J., Xin L., Shan B., Chen W., Xie M., Yuen D., Zhang W., Zhang Z., Lajoie G. A., and Ma B., *Mol. Cell. Proteomics*, Volume 11, M111.010587, 2012.
103. Braakman I. and Hebert D. N., *Current Protocols in Protein Science*, John Wiley & Sons, New York, 2001.
104. Kohn W. D., Micanovic R., Myers S. L., Vick A. M., Kahl S. D., Zhang L., Striffler B. A., S. Li, Shang J., Beals J. M., Mayer J. P. and DiMarchi R. D., *Peptides*, 28, 935-948, 2007.
105. Chang S.G., Choi K.D., Jang S.H., Shin H.C. *Mol Cells*. Dec 31, Volume 16, Issue 3, Pages 323-30, 2003.
106. Scigelova M., Green P., Giannakopoulos A., Rodger A., Crout D. and Derrick P., *European Journal of Mass Spectrometry*, Volume 7, Pages 29-34, 2001.
107. Hauser N. J. and Basile F., *Journal of Proteome Research*, Volume 7, Pages 1012-1026, 2008.
108. Tzanavaras P. D., Mitani C., Anthemidis A. and Themelis D. G., *Talanta*, Volume 96, Pages 21-25, 2012.
109. Alzahrani E. and Welham K., *Analytical Methods*, Volume 6, Issue 2, Pages 558-568, 2014.
110. Getz E. B., Xiao M., Chakrabarty T., Cooke R. and Selvin P. R., *Analytical Biochemistry*, Volume 273, Pages 73-80, 1999.
111. Begg G. E. and Speicher D. W., *Journal of Biomolecular Techniques*, Volume 10, Pages 17-20, 1999.
112. Rhee S. S. and Burke D. H., *Analytical Biochemistry*, Volume 325, Pages 137-143, 2004.
113. Han J. C. and Han G. Y., *Analytical Biochemistry*, Volume 220, Pages 5-10, 1994.

114. Wang S., Liu K. and Lu Y., *Biochemical and Biophysical Research Communications*, Volume 381, Pages 639-642, 2009.
115. Fischer W. H., Behan D. P., Park M., Potter E., Lowry P. J. and Vale W., *Journal of Biological Chemistry*, Volume 269, Pages 4313-4316, 1994.
116. Bai F., Liu S. and Witzmann F. A., *Proteomics*, Volume 5, Pages 2043-2047, 2005.
117. Gehanne S., Cecconi D., Carboni L., Righetti P. G., Domenici E. and Hamdan M., *Rapid Communications in Mass Spectrometry*, Volume 16, Pages 1692-1698, 2002.
118. Hale J. and Knierman M., *Indiana Proteomics Consortium LLC*, USA, 2006.
119. Shriver-Lake L.C., North S.H., Rowe Taitt C., *Biotechniques*, Volume 55, Issue 6, Pages 292-4, 2013.
120. Miralles G., Verdíe P., Subra G., *ACS Comb. Sci.*, Volume 15, Pages 169–173, 2013.

## Chapter 2

### Protein surface labeling reactivity of *N*-hydroxysuccinimide ester group conjugated to Fe<sub>3</sub>O<sub>4</sub>@SiO<sub>2</sub> magnetic nanoparticles

This Chapter presents a collaborative work between Parisa Pirani, Ujwal S. Patil, Tushar Dattu Apsunde, Mark L. Trudell, Yang Cai, and Matthew A. Tarr. However, the experiments are predominantly performed by Parisa Pirani.

#### 2.1 Introduction

Among different types of nanomaterials, iron oxide magnetic nanoparticles have attracted great deal of interest mainly due to their superparamagnetization properties<sup>1,2</sup> as well as simple preparation. Separation of ligands that are covalently or non-covalently attached to the iron oxide nanoparticles can be easily done using an external magnet, and the nanoparticle-ligand conjugates are easily re-dispersible in solution by removing the magnetic field. The synthesis of magnetic iron oxide nanoparticles is quite simple, and the stability and aqueous compatibility<sup>3</sup> of these nanoparticles could be significantly improved by coating them with silica, polyethylene glycol, dextran and other coating agents. The surface of MNPs could be easily modified with different functional groups, such as amine, thiol and carboxylic acid before further conjugation of other ligands.<sup>4</sup> The application of nanomaterials such as MNPs is usually defined by the ligands present on their surface.

Accurate quantification of reactive functional groups (amine, thiol, carboxyl, etc.) on the surface of nanomaterials is essential for further conjugation of biomolecules to the surface. Although

numerous efforts have been made on preparation and surface functionalization of biocompatible nanoparticles, less research has been carried out on quantification of intermediate functional groups and exposed ligands on the nanomaterials' surface. A common approach to quantify ligands on solid surfaces involves covalent or non-covalent conjugation of a chromophore/fluorophore to the surface functional groups. Quantification of the conjugated chromophore/fluorophore determines the equivalent amount of ligands on the solid surfaces.<sup>5</sup> Amine groups on solid surfaces have been quantified via covalent interaction with a chromophore/fluorophore. Few examples include fluorescamine assay<sup>6,7,8</sup> fluorescent Fmoc-CL assay,<sup>9,10</sup> NHS-fluorescein assay,<sup>11</sup> 4-nitrobenzaldehyde detection using UV-Vis spectroscopy<sup>12,13,14</sup> and bromophenol blue assay.<sup>14</sup> Amine groups on a glass slide were quantified via covalent conjugation to a carboxyl modified fluorescent dye (4,4-difluoro-5,7-dimethyl-4-bora-3a,4a-diaza-s-indacene-3-propionic acid) followed by fluorometric quantification of the fluorophore conjugated amine groups.<sup>15</sup> To quantify thiol groups on solid surfaces, Ellman's reagent was covalently conjugated to the free thiol groups followed by measuring the yellow colored fluorophore conjugated product.<sup>16</sup> Aldehyde groups on a glass slide were quantified by covalent conjugation of this functional group to a hydrazine modified fluorescent dye (4,4-difluoro-5,7-dimethyl-4-bora-3a,4a-diaza-s-indacene-3-propionic acid, hydrazide), followed by fluorometric measurement.<sup>15</sup> Cleave-analyze quantification approach has been employed to avoid any interference from solid surfaces. In this method, fluorophores/chromophores covalently conjugated to the surface are detached prior to the fluorometric measurement.<sup>17</sup> Quantification of amine groups on solid surfaces has also been performed via non-covalent attachment of chromophores/fluorophores such as orange II dye<sup>18</sup> or coomassie brilliant blue (Bradford assay)<sup>19</sup> to amine groups.

Time of flight-secondary ion mass spectrometry (ToF-SIMS),<sup>20</sup> carbon-hydrogen-nitrogen combustion analysis,<sup>21</sup> and X-ray photoelectron spectroscopy (XPS) were used to quantify primary amine groups.<sup>18,22</sup> Thiol groups on the surface of gold nanoparticles were quantified by using inductively coupled plasma-mass spectrometry (ICP-MS).<sup>23,24</sup> Yan et al recently quantified dopamine anchoring group on the surface of MNPs by using laser desorption ionization mass spectrometry (LDI-MS).<sup>25</sup> These elemental analysis approaches (ToF-SIMS, XPS, ICP-MS, and LDI-MS) are more suitable for smaller nanoparticles such as gold nanoparticles with less atoms.<sup>18</sup> Indirect quantification of ligands on solid surfaces has been also performed by measurement of the side-products in the reactions that further modify the ligands. For example, the heterobifunctional crosslinkers *N*-(succinimidyl 3-(2-pyridyldithio) propionate (SPDP) and succinimidyl 6-[3'-(2-pyridyldithio)-propionamido] hexanoate (LC-SPDP) react with primary amine groups and quantitatively yield pyridine-2-thione. The amount of amine groups immobilized on solid surfaces has been determined by Spectrophotometric measurement of pyridine-2-thione.<sup>26,18,27</sup> Thiol groups on chitosan MNPs were quantified via an indirect iodine titration in which thiol groups were oxidized by iodine, and the remaining iodine in solution was determined by the brilliant blue colour resulting from the starch-iodine complex.<sup>16</sup> To calculate the amount of thiol groups, the unconsumed iodine was subtracted from the initial amount of iodine added. These indirect measurement methods are ligand specific and highly dependent on the ligand modification reaction. Hydroxyl, carboxylic acid and aldehyde/ketone groups on solid surfaces were quantified via depletion approach that measures the difference between initial and final amount of fluorophore after covalent conjugation to the surface.<sup>28,29,30</sup> Moreover, Fourier transform-infrared (FTIR) absorbance spectroscopy was used for quantitative monitoring of ester carbonyl and aldehyde carbonyl groups in benzimidazole synthesis reaction

on solid phase,<sup>31</sup> and relative quantification of carbonyl containing ligands on the surface of gold nanoparticles.<sup>32</sup>

NHS ester modified Fe<sub>3</sub>O<sub>4</sub>@SiO<sub>2</sub> MNPs with cleavable disulfide bond linker have been recently employed in our lab to label primary amine groups on the solvent accessible surface of proteins.<sup>33</sup> The reaction between NHS ester moiety and primary amine group was performed under conditions that the native structure of protein was preserved. To confirm the presence of NHS ester moiety on the surface of Fe<sub>3</sub>O<sub>4</sub>@SiO<sub>2</sub> MNPs, we developed a sensitive fluorescence microscopic approach based on covalent attachment of fluorophore dansylcadaverine to MNPs. The amount of dansylcadaverine<sup>34</sup> conjugated to Fe<sub>3</sub>O<sub>4</sub>@SiO<sub>2</sub> MNPs was determined through a cleave-analyze approach. Quantification of released/modified fluorophore via fluorometric HPLC analyses, determined the equivalent amount of NHS ester/thiol groups on MNPs surface. Accurate quantification of NHS ester groups on Fe<sub>3</sub>O<sub>4</sub>@SiO<sub>2</sub> MNPs surface provided the basis for investigations on the reactivity of the magnetic nanoparticle reagent in labelling native proteins.

## **2.2 Experimental procedures**

### **2.2.1 Materials**

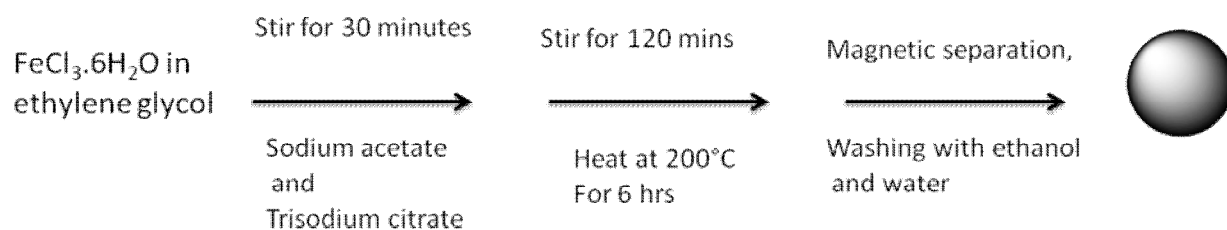
All chemicals were of reagent grade, obtained from commercial sources and used as received without further purification unless specified otherwise. Ferric (III) chloride hexahydrate, (99%), iron (III)oxide hydrated FeO(OH), oleic acid, dimethyl sulfoxide (DMSO, anhydrous), (3-mercaptopropyl)trimethoxysilane (MPTMS, 99%), tetraethylorthosilicate (TEOS, 99%), Igepal CO-520, cyclohexane, dansylcadaverine, (≥97%) and bovine serum albumin (BSA)

were purchased from Sigma-Aldrich (St. Louis, MO). Anhydrous trisodiumcitrate (99%), 1-octadecene, and anhydrous sodium acetate (99%) were purchased from Alfa Aesar (Ward Hill, MA). Sodium citrate dihydrate was purchased from J. T. Baker Chemicals (Center Valley, PA). Ammonium hydroxide, hydrochloric acid and Phosphate buffered saline (PBS) were purchased from EMD Millipore (Billerica, MA). Ethylene glycol was purchased from VWR (Radnor, PA). (3,3'-Dithiobis[sulfosuccinimidylpropionate]) (DTSSP) and a micro bicinchoninic acid (BCA) protein assay kit were purchased from Pierce (Rockford, IL). (*N*-succinimidyl 3-[2-pyridyldithio]propionate (SPDP, 99+%) was purchased from Molecular Biosciences (Boulder, CO). Tris(2-carboxyethyl)phosphine hydrochloride (TCEP-HCl) was purchased from Amresco (Solon, OH). Ethanol was purchased from Pharmco-AAPER (Brookfield, CT). Nanopure water (18.2 MΩ, Millipore Co. Billerica, MA) was used for all experiments.

### **2.2. 2 Synthesis of silica coated iron oxide nanoparticles ( $\text{Fe}_3\text{O}_4@ \text{SiO}_2$ NPs, diameter 100 nm)**

The  $\text{Fe}_3\text{O}_4@ \text{SiO}_2$  NPs (100 nm diameter) were prepared according to a previously reported method<sup>1</sup>. Initially,  $\text{FeCl}_3 \cdot 6\text{H}_2\text{O}$  (0.67 g) was dissolved in ethylene glycol (12.5 mL) under constant magnetic stirring for 30 min in a Teflon<sup>®</sup> coated 30 mL autoclave container (Parr Instrument Company, St. Moline, IL). To the  $\text{FeCl}_3$  solution, anhydrous sodium acetate (1.35 g) and anhydrous trisodium citrate (0.5 g) were added, and the mixture was stirred vigorously for 120 min. The autoclave container was sealed tightly and heated at 200°C for 6 hr. The black suspension of  $\text{Fe}_3\text{O}_4$  NPs was washed several times with ethanol and water using magnetic separation and air dried at room temperature (Scheme 2.1). The  $\text{Fe}_3\text{O}_4$  NPs (0.1g) were put into

1M HCl (15 mL) and stirred on a vortex mixer for 10 min. The magnetic NPs were isolated by a magnet, washed with water and re-suspended in aqueous sodium citrate (10wt%) followed by stirring for 30 min. The citrate complexed Fe<sub>3</sub>O<sub>4</sub> NPs were magnetically separated and resuspended in a mixture of ethanol (80 mL), water (20 mL) and ammonia solution (2 mL, 28 wt%) under ultrasonication for 15 min. TEOS (99%, 1 mL) was added dropwise to the above mixture followed by mechanical stirring (400 rpm) for 12 hr at room temperature. The prepared silica coated magnetite (Fe<sub>3</sub>O<sub>4</sub>@SiO<sub>2</sub>) nanoparticles were magnetically separated and washed repeatedly with ethanol. Empty silica shells were carefully removed during the process. The Fe<sub>3</sub>O<sub>4</sub>@SiO<sub>2</sub> NPs (100 nm diameter) were immersed in freshly prepared HCl (4N) for 10 min to remove bare iron oxide NPs. The separated particles were then washed with nanopure water and air dried at room temperature.



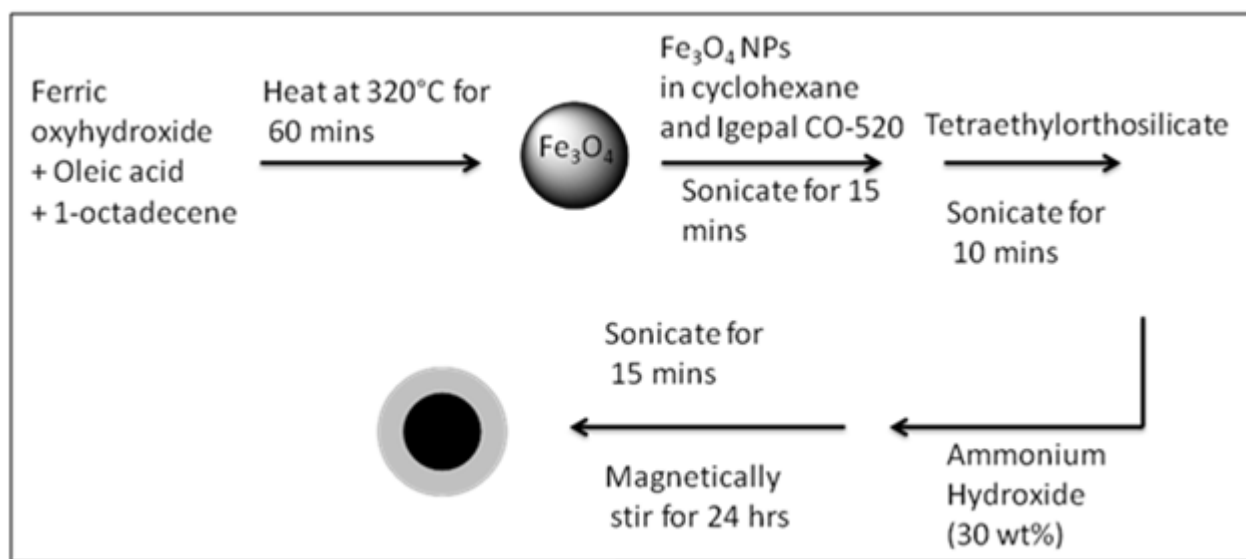
Schematic 2.1: Synthesis of Fe<sub>3</sub>O<sub>4</sub> MNPs (80 nm in diameter) by hydrothermal method.

### 2.2.3 Synthesis of silica coated iron oxide nanoparticles (Fe<sub>3</sub>O<sub>4</sub>@SiO<sub>2</sub> NPs, 20 nm diameter)

The iron oxide core was prepared by previously reported method.<sup>2</sup> To prepare iron oxide core, FeO(OH) (0.178 g), oleic acid (2.26 g) and 1-octadecene (5.00 g) were mixed in a three neck flask and heated at 320°C for 60 minutes. The resulting brown colored solution was washed

with ethanol using magnetic separation and re-suspended in 25 mL toluene to prepare 10 mg/mL solution (Scheme 2.2).

The iron oxide core (400  $\mu\text{L}$  of 10 mg/mL) was re-suspended in cyclohexane (4 mL) and Igepal-CO-520 (0.247 g) and sonicated for 15 minutes. TEOS (25  $\mu\text{L}$ ) was added and sonicated further for 10 minutes followed by addition of aqueous ammonium hydroxide (50  $\mu\text{L}$ , 30 wt%) with additional sonication for 15 minutes. This solution was stirred at room temperature for 24 hours. The  $\text{Fe}_3\text{O}_4@ \text{SiO}_2$  NPs (20 nm diameter) were washed with water and ethanol three times followed by treatment with 4N hydrochloric acid. The resulting silica coated magnetic nanoparticles were washed several times with nanopure water and air dried at room temperature prior to TEM observation.



Schematic 2.2: Preparation of  $\text{Fe}_3\text{O}_4@ \text{SiO}_2$  MNPs (~20 nm in diameter, with a iron oxide core of (~10 nm in diameter) by thermal decomposition plus reverse microemulsion method.

#### **2.2. 4 Surface functionalization of Fe<sub>3</sub>O<sub>4</sub>@SiO<sub>2</sub> NPs (100 nm and 20 nm in diameter) with NHS ester groups**

Similar protocols<sup>3</sup> were used to coat both the larger Fe<sub>3</sub>O<sub>4</sub>@SiO<sub>2</sub> NPs(100 nm diameter) and smaller Fe<sub>3</sub>O<sub>4</sub>@SiO<sub>2</sub> NPs (20 nm diameter) with NHS ester groups. Briefly, Fe<sub>3</sub>O<sub>4</sub>@SiO<sub>2</sub> NPs (100 nm diameter, 0.1 g) were resuspended in a solution containing ethanol (90 mL) and nanopure water (10 mL) followed by sonication for 15 min. MPTMS (95 %, 1 mL) was added drop wise and the mixture was mechanically stirred at room temperature for 15 hrs. The thiol coated nanoparticles were separated from the solution using an external magnet, washed several times with ethanol and air dried at room temperature.

The thiol coated Fe<sub>3</sub>O<sub>4</sub>@SiO<sub>2</sub> NPs were treated with TCEP-HCl solution in water (10mM) prior to NHS ester conjugation to cleave any disulfide bonds formed between surface thiol groups. The NPs were washed multiple times with water, ethanol and acetonitrile to remove excess TCEP. *N*-Succinimidyl 3-(2-pyridyldithio)-propionate (SPDP) was first dissolved in anhydrous DMSO (10 mg/mL SPDP in DMSO) and then added to thiol coated NPs and stirred at room temperature for 1 hr. The NHS ester coated NPs were magnetically separated, washed several times with ethanol and dried under vacuum before use.

#### **2.2. 5 Conjugation of dansylcadaverine to NHS ester modified Fe<sub>3</sub>O<sub>4</sub>@SiO<sub>2</sub> MNPs**

NHS ester coated Fe<sub>3</sub>O<sub>4</sub>@SiO<sub>2</sub> MNPs (100 nm diameter, 7 mg) or smaller NHS ester coated Fe<sub>3</sub>O<sub>4</sub>@SiO<sub>2</sub> MNPs (20 nm diameter, 6 mg) were incubated with dansylcadaverine (2mM, 1 mL in ethanol) in the dark at room temperature for 1 hr. The dansylcadaverine conjugated MNPs were collected by an external magnet and washed repeatedly with dimethyl

sulfoxide (DMSO), ethanol, and water. Dansylcadaverine modified MNPs were treated with TCEP (50 mM) solution in water (300  $\mu$ L) at room temperature for 1 hr. The cleaved product (3-mercaptopropanamido dansylcadaverine, 3-MPA-Dansyl) was recovered by repeatedly washing the MNPs and by magnetic separation. The supernatant and wash solutions were combined and dried under vacuum. The cleaved 3-MPA-Dansyl samples were dissolved in 20:80 acetonitrile:water (1 mL) prior to HPLC analysis.

### **2.2. 6 Synthesis of 3-Mercaptopropanamido dansylcadaverine (3-MPA-Dansyl)**

Dansylcadaverine (10 mg, 0.032 mmol, 2 equiv.) was added to a well stirred solution of DTSSP (10mg, 0.016 mmol, 1 equiv.) in dichloromethane/methanol (10:1) and triethylamine (4.5  $\mu$ L, 0.032 mmol, 2 equiv.). The reaction mixture was stirred for 12 hours at room temperature. After 12 hours, the solvent was evaporated under reduced pressure and the crude product was dispersed in water (5 mL) and extracted with ethyl acetate (3 $\times$ 5 mL). The combined organic extract was dehydrated by mixing with sodium sulphate and evaporated under reduced pressure. The product was purified by flash chromatography technique using 50% ethyl acetate/hexane to get white solid (5.22 mg, 0.0072 mmol, 45% yield). TCEP $\cdot$ HCl (20.55 mg, 0.0822 mmol, 4 equiv) was added to a well stirred solution of the obtained product (15 mg, 0.02 mmol, 1 equiv) in methanol with 4-5 drops of water. The reaction mixture was stirred for 2 hours at room temperature. After 2 hours, the solvent was evaporated under reduced pressure. Water (5 mL) was added to the crude product and extraction of crude product was carried out with ethyl acetate (3 $\times$ 5 mL). The combined organic extract was dehydrated by mixing with sodium sulphate and evaporated under reduced pressure to furnish solid product. (1.7 mg, 20% yield).

### 2.2.7 Characterization of 3-MPA- Dansyl

Excitation and emission spectra of 3-MPA-Dansyl were obtained using a PerkinelmerLS55 fluorescence spectrometer with a pulsed Xe lamp as the light source. The sample was dissolved in 20% acetonitrile-80% water and transferred to a 1-cm quartz cuvette. The excitation and emission were scanned over ranges of 200-500 nm and 400-700 nm respectively. 3-MPA-Dansyl was also analyzed by a Finnigan LTQ ion trap mass spectrometer (Thermo Electron, San Jose, CA). The flow rate for direct infusion was set to 1  $\mu$ L/min. Electrospray capillary voltage was set to 2.65 kV with temperature at 200 °C. Mass spectrometric analysis of 3-MPA-Dansyl showed the peak at  $m/z$  424.1 Da which corresponded to  $[M+H]^+$  of 3-MPA-Dansyl.

NMR Chemical Shifts of 3-MPA- Dansyl:

$^1\text{H}$  NMR (400MHz,  $\text{CDCl}_3$ ) =  $\delta$  1.23-1.44 (m, 6H), 2.60 (t,  $J = 7.2\text{Hz}$ , 2H), 2.86 (q,  $J = 6.4\text{Hz}$ , 2H), 2.88 (s, 6H), 3.03 (t,  $J = 6.4\text{Hz}$ , 2H), 3.13 (q,  $J = 6.0\text{Hz}$ , 2H) 5.35 (t,  $J = 6.0\text{Hz}$ , 1H), 6.27 (t,  $J = 5.6\text{Hz}$ , 1H), 7.17 (d,  $J = 8.0\text{Hz}$ , 2H), 7.49-7.56 (m, 2H), 8.21 (d,  $J = 7.2\text{Hz}$ , 2H), 8.32 (d,  $J = 8.8\text{Hz}$ , 2H), 8.53 (d,  $J = 8.4\text{Hz}$ , 2H).

### 2.2.8 HPLC instrumentation and chromatography conditions

An Agilent 1100 HPLC systems (Agilent, Santa Clara, CA) with 1100 series quaternary gradient pump, vacuum degasser and HP 1046A fluorescence detector was used for all measurements. Isocratic elution with a mobile phase of 80% acetonitrile and 20% water was used for all measurements. The detector was set at 335 nm for excitation and 530 nm for emission. A GRACE VisionHT™ C18 Classic 5 $\mu$ m 150 x 4.6 mm column (Grace, Columbia,

MD) was used for all analyses at ambient temperature with a flow rate of 0.8 mL/min.

### **2.2. 9 Fluorescence microscopy imaging of dansylcadaverine modified Fe<sub>3</sub>O<sub>4</sub>@SiO<sub>2</sub> MNPs**

NHS ester modified Fe<sub>3</sub>O<sub>4</sub>@SiO<sub>2</sub> MNPs (100 nm diameter, 1 mg) were incubated at room temperature with 1 mL of 2 mM dansylcadaverine in ethanol for 1 hr. The nanoparticles were separated by a magnetic field and washed multiple times with DMSO, water and ethanol. The fluorophore-conjugated magnetic nanoparticles were re-dispersed in ethanol (1 mL), and small aliquots were transferred to a glass slide and air-dried in the dark prior to fluorescence microscopy imaging. An Olympus IX 71 inverted fluorescence microscope with a high performance 16 bit resolution, back illuminated CCD camera (Roper Scientific) and a 100 W Hg lamp as the light source was used for the measurements. The fluorescence images were taken through a 40X microscope objective with numerical aperture (NA) = 0.75. The filter cube of the microscope contained a 450 ±10 nm band-pass excitation filter, a 505 nm dichroic mirror, and a 515-nm long pass emission filter.

A program run under MATLAB<sup>®37</sup> was written for fluorescence intensity integration.

The fluorescence intensities of dansylcadaverine conjugated MNPs in a fluorescence microscope image were calculated in two steps. First, the color image (red, green, blue) was converted to a grayscale image. Second, the intensities of bright spots on this grayscale image were calculated by adding the intensities of pixels together. In the grayscale image, the background pixels were converted to black pixels. Therefore, the background was removed from the intensity integration. The brightness of a pixel was normalized to the scale from 0 to 1.

### **2.2. 10 Fluorescence intensity calculations using MATLAB**

The fluorescence images were processed in two steps. First, the color image (Figure 2.1A) was converted to a grayscale image (Figure 2.1B). In the second step, the intensity of the

grayscale image was calculated by integration of all pixels intensities. Since the background pixels are black (Figure 2.1B) with the intensity value of zero, the total intensity of the image is not affected by the background. The total intensity value,  $I_T$ , for a 8-Bit grayscale image was obtained as equation (1).

$$I_T = \sum_{i=0}^{256^2} I_i \quad (1)$$

Where  $I_i$  is intensity of pixel  $i^{\text{th}}$  and  $255^2$  is the number of all pixels.

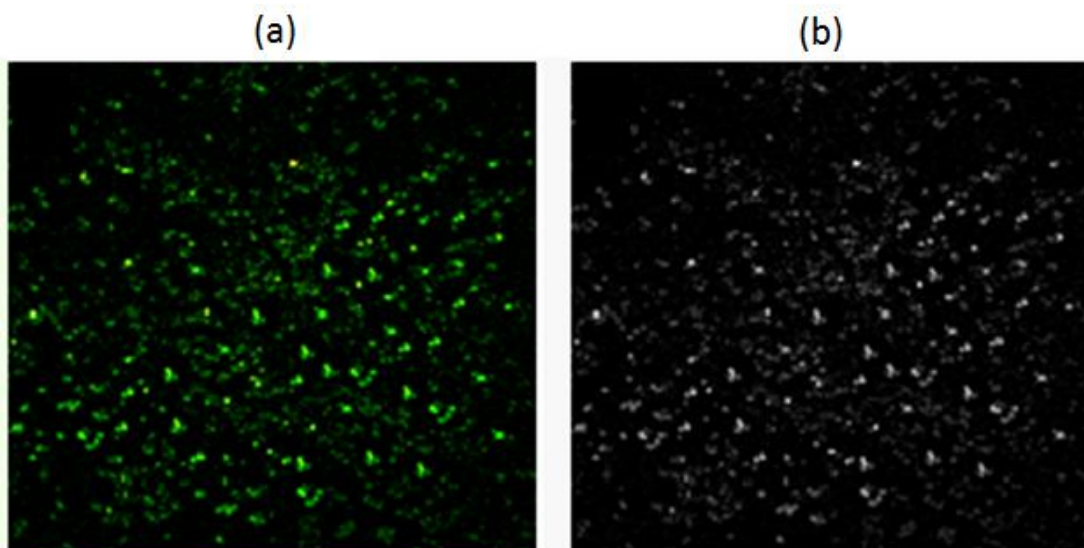
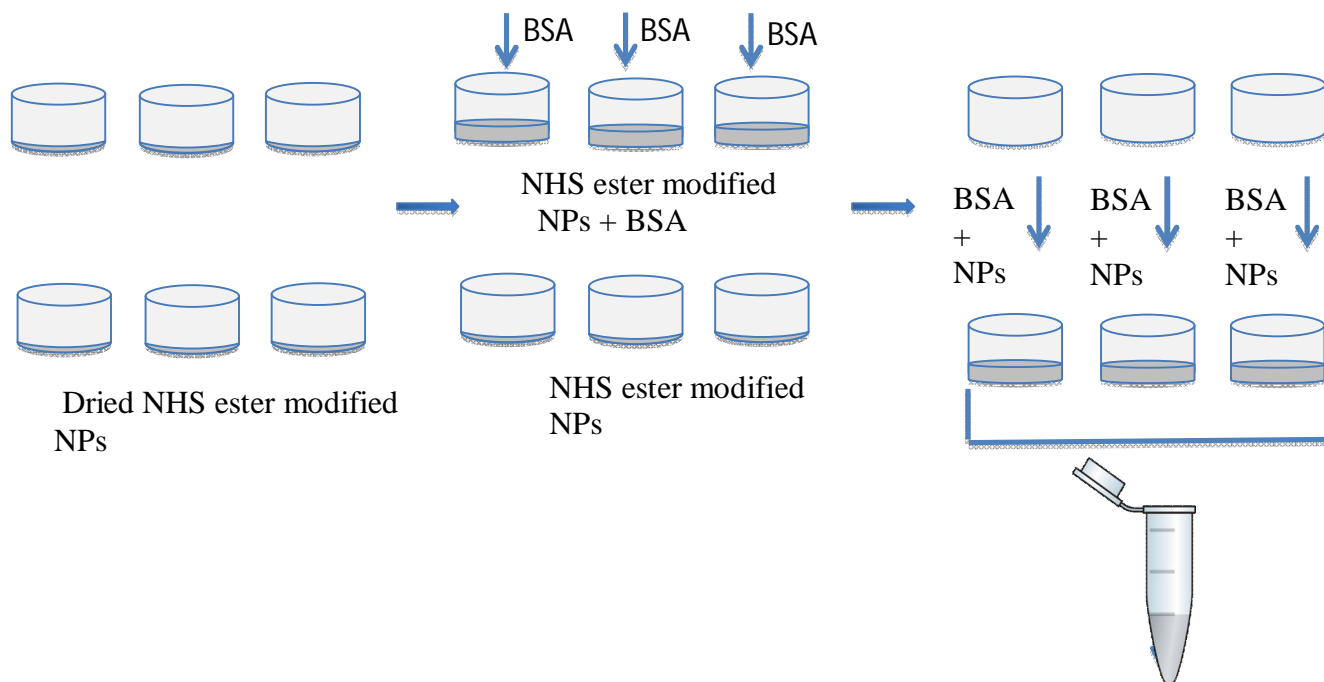


Figure 2.1: Conversion of RGB image (a) to grayscale image (b) in order to calculate the image intensity.

## 2.2. 11 Measurement of BSA conjugated to $\text{Fe}_3\text{O}_4@ \text{SiO}_2$ nanoparticles

Bovine serum albumin (BSA) solution (1 mL of 1 mg/mL) in phosphate buffered saline (PBS, 10 mM, pH 7.4) was incubated with iodoacetamide (20 mM) in the dark at 37°C for 1 hr, then the mixture was diluted with PBS to 0.5 mg/mL of BSA. Mixing of the NHS ester modified

Fe<sub>3</sub>O<sub>4</sub>@SiO<sub>2</sub> (100 nm diameter) MNPs with the BSA solution (0.5 mg/mL in PBS pH 7.4) was performed according to Scheme 2.3. The MNPs were washed several times with water and acetonitrile (70%). All the washes were combined, centrifuged, dried under vacuum, and re-dissolved in 10 μL of nanopure water. The un-conjugated BSA in the combined washes was quantified by using a BCA according to the protocol provided by the manufacturer. The amount of BSA conjugated to the MNPs labelling reagent was calculated by subtraction of un-conjugated BSA from the initial amount of fresh BSA used for labelling reaction.



Schematic 2.3: Mixing method for labeling BSA by NHS ester modified Fe<sub>3</sub>O<sub>4</sub>@SiO<sub>2</sub> MNPs.

## 2.3 Results and discussion

The size and shape of Fe<sub>3</sub>O<sub>4</sub>@SiO<sub>2</sub> MNPs employed in this study was significantly improved compared to that of the Fe<sub>3</sub>O<sub>4</sub>@SiO<sub>2</sub> MNPs in previous proof of concept study performed in our lab.<sup>33</sup> Although Fe<sub>3</sub>O<sub>4</sub>@SiO<sub>2</sub> MNPs with irregular shapes were

superparamagnetic, it was difficult to estimate the surface area of these particles as well as the number of intermediate functional groups (e.g. primary amine, thiol) per MNP. Additionally, MNPs with irregular shapes might have less binding sites that are sterically accessible for the approaching protein molecules. This affects the number of protein molecules that could bind to the MNPs. TEM analysis confirmed the uniformity in size and shape for both larger  $\text{Fe}_3\text{O}_4@\text{SiO}_2$  MNPs (100 nm diameter) and smaller  $\text{Fe}_3\text{O}_4@\text{SiO}_2$  MNPs (20 nm diameter). Such size and shape uniformity, facilitated improved characterization of the surface modified MNPs.

### **2.3.1 NHS ester conjugated $\text{Fe}_3\text{O}_4@\text{SiO}_2$ MNPs**

The spherical and uniform nature of the magnetite core of silica coated MNP with diameters of  $80 \pm 5$  nm (Figures 2.2a) and  $\text{Fe}_3\text{O}_4@\text{SiO}_2$  MNPs with  $100 \pm 10$  nm diameters was confirmed by TEM image analysis (Figures 2.2 a). Smaller  $\text{Fe}_3\text{O}_4@\text{SiO}_2$  MNPs (20 nm diameter, Figure 2.2b) with improved uniformity in size and shape were prepared and employed in this study, however the majority of the experiments were performed on larger MNPs. The silica coating improved aqueous stability, protected the MNPs from oxidation and reduced nonspecific interactions with ligands.

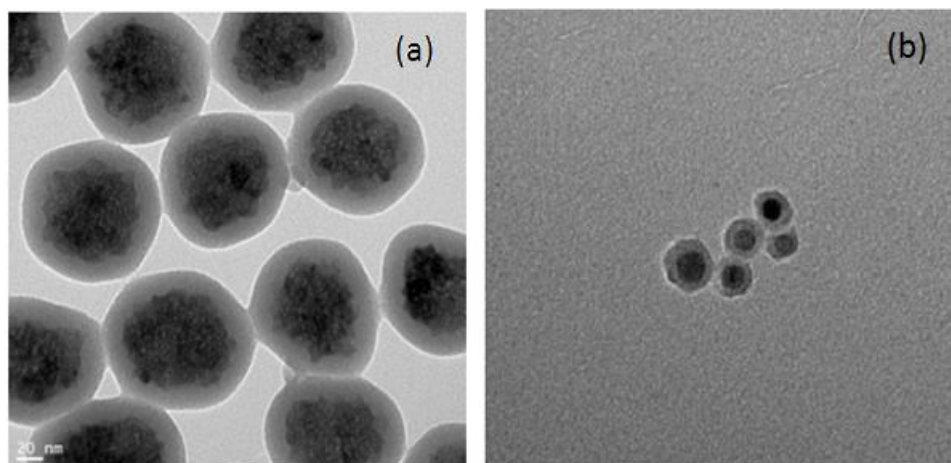
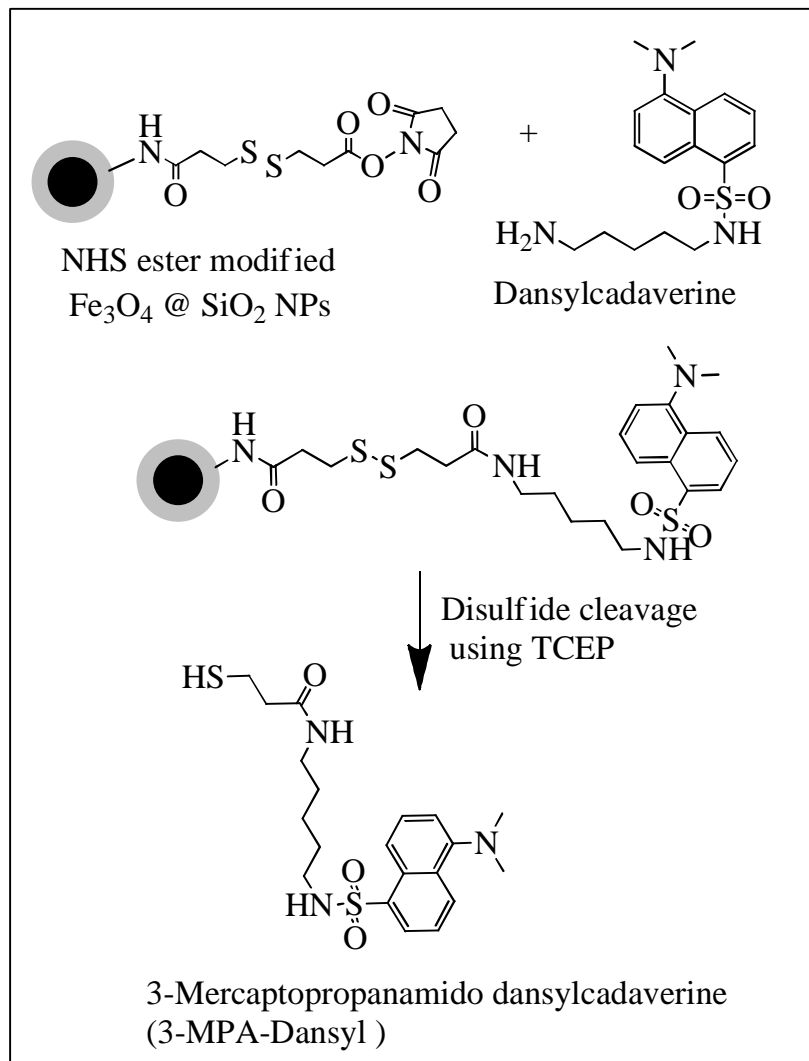


Figure 2.2: TEM image of a)  $\text{Fe}_3\text{O}_4@SiO_2$  nanoparticles (100 nm diameter) and b)  $\text{Fe}_3\text{O}_4@SiO_2$  nanoparticles (20 nm diameter). MNPs were uniform in size and shape, and well dispersible in aqueous solvents.

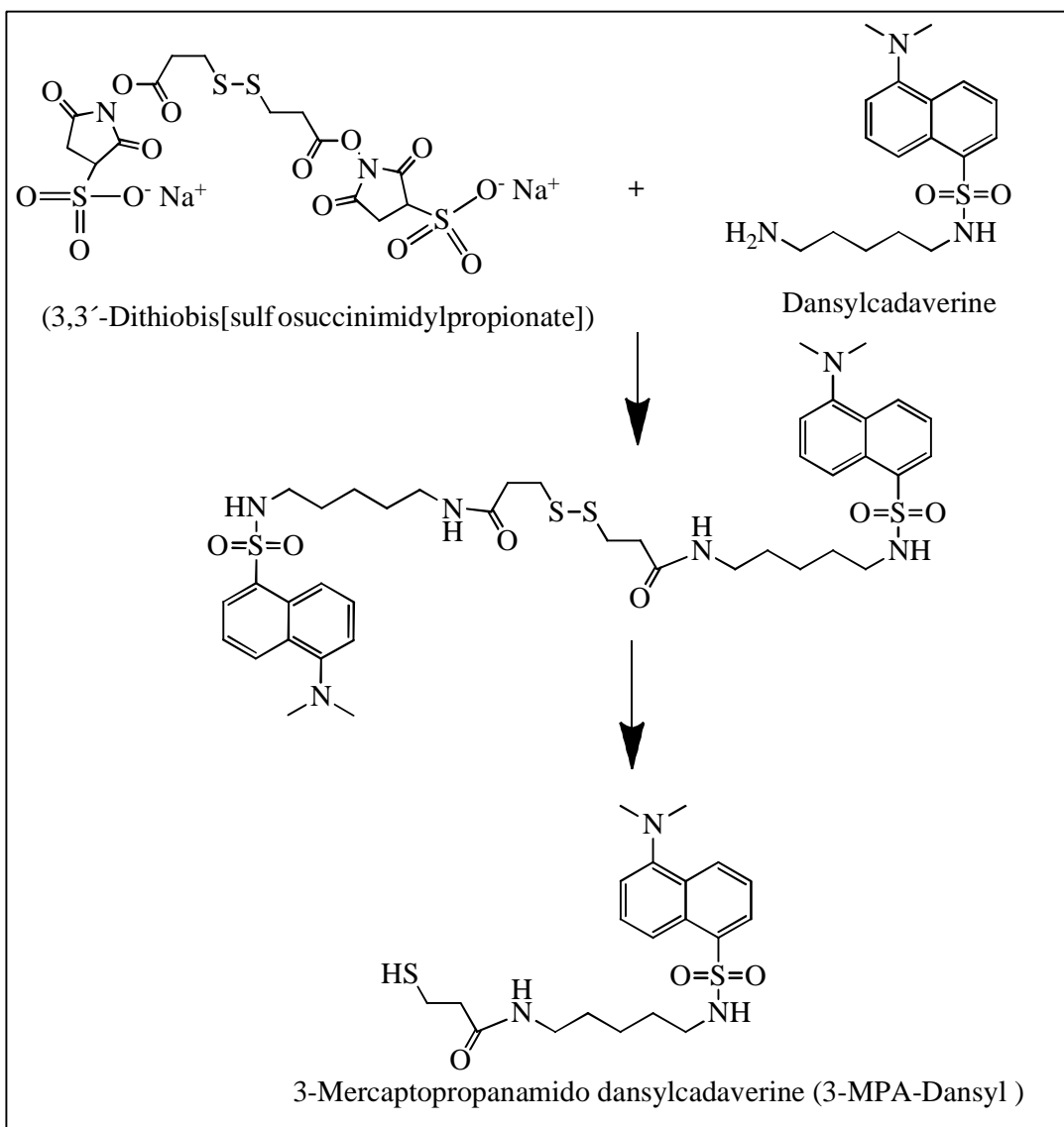
MPTMS was used to further functionalize the 100 and 20 nm  $\text{Fe}_3\text{O}_4@SiO_2$  MNPs with thiol groups. The theoretical number of thiol groups that could be conjugated to the surface of each 100 nm  $\text{Fe}_3\text{O}_4@SiO_2$  MNP was calculated to be about  $10^5$ . The estimation was based on the following parameters: density of MNPs ( $4.5 \text{ g/cm}^3$ ), total mass of MNPs (1 mg), bond length of Si-O (171 picometer), and bond angle of O-Si-O ( $109.5^\circ$ ). To determine the theoretical number of surface groups after modification, the total surface area of the particles and the estimated surface area required per MPTMS were calculated. Based on the theoretical number of thiol groups on MNPs surface, the amount of SPDP for free thiol group conjugation could be estimated. Based on these calculations, 1 mg of 100 nm  $\text{Fe}_3\text{O}_4@SiO_2$  MNPs should be able to react with 22  $\mu\text{g}$  of SPDP.

### **2.3.2 Fluorescence-based quantification of active NHS ester groups on the surface of $\text{Fe}_3\text{O}_4@\text{SiO}_2$ MNPs**

Since dansylcadaverine contains a primary amine group similar to that in the side chain of the amino acid lysine, it can be covalently attached to NHS ester conjugated  $\text{Fe}_3\text{O}_4@\text{SiO}_2$  MNPs via a nucleophilic substitution reaction between the NHS ester and the primary amine. A disulfide bond is incorporated in the spacer/linker between the fluorophore moiety and the  $\text{Fe}_3\text{O}_4@\text{SiO}_2$  MNPs moiety (Scheme 2.4). The fluorophore moiety can be cleaved from the modified  $\text{Fe}_3\text{O}_4@\text{SiO}_2$  MNPs by reductive cleavage of the disulfide bond in the spacer/linker. The fluorescent dansylcadaverine serves as an indicator for quantification of NHS ester groups on the surface of  $\text{Fe}_3\text{O}_4@\text{SiO}_2$  MNPs.



Schematic 2.4: A cleave-analyze approach for quantification of 3-MPA-Dansyl released upon cleaving disulfide bond between nanoparticles and dansylcadaverine.



Schematic 2.50: Synthesis of 3-Mercaptopropanamido dansylcadaverine (3MPA-Dansyl, a calibration standard for fluorometric measurements)

### 2.3.3 Quantification of NHS ester groups by cleave-analyze approach

3-MPA-Dansyl was released by reductive cleavage of the disulfide bond in the linker between the dansylcadaverine moiety and the Fe<sub>3</sub>O<sub>4</sub>@SiO<sub>2</sub> MNPs (structure in Scheme 2.4) and analyzed by HPLC with fluorescence detection. HPLC analysis also facilitated the separation of TCEP, which is reported to affect the fluorescence of various fluorophores.<sup>40</sup> In order to accurately quantify dansylcadaverine released from the fluorophore modified Fe<sub>3</sub>O<sub>4</sub>@SiO<sub>2</sub> MNPs, the calibration standard 3-MPA-Dansyl(Scheme2.5), was synthesized and characterized by fluorescence spectroscopy (Figure 2.3), mass spectrometry and NMR. The synthesized calibration standard (3-MPA-Dansyl) showed the same retention time as that of 3-MPA-Dansyl released from MNPs but eluted from the HPLC column faster than unmodified dansylcadaverine (Figure 2.4).

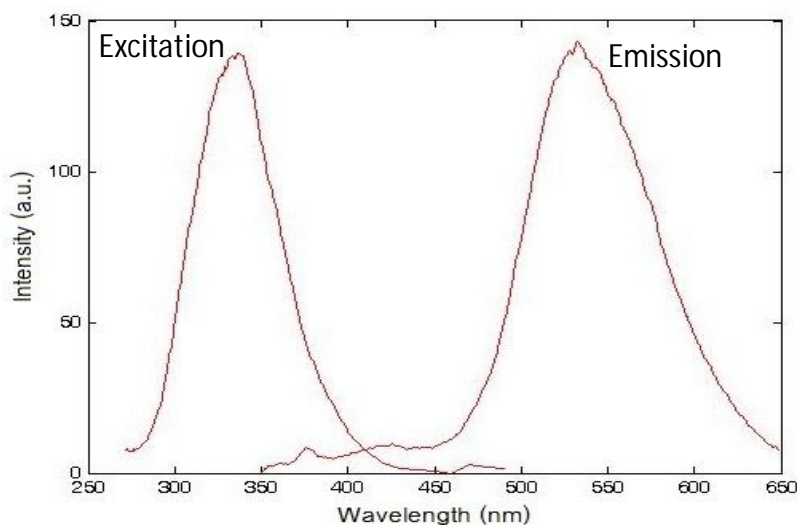


Figure 2.3: Fluorescence spectrum of 3-MPA Dansylcadaverine Excitation: 335 nm and Emission: 530 nm.

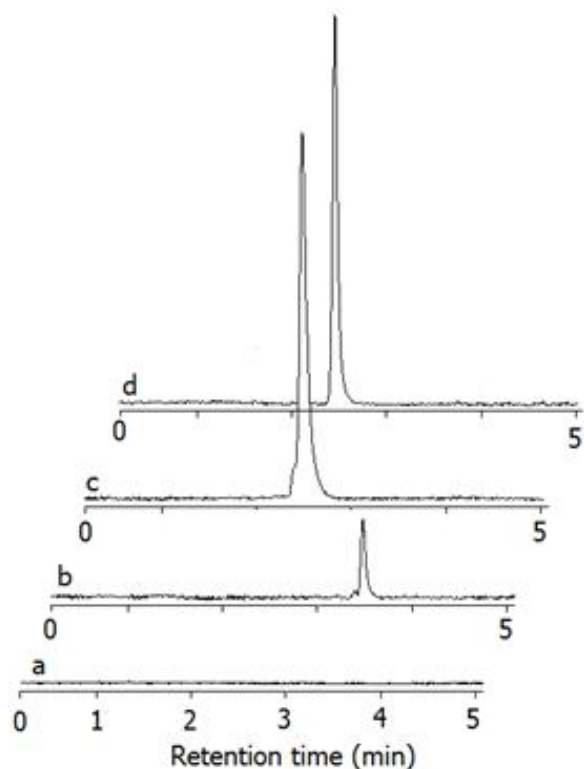


Figure 2.4: Chromatogram obtained by HPLC-fluorescence analysis of (a) Control, (b) dansylcadaverine (5 $\mu$ M) (c) 3-MPA-Dansyl (20 $\mu$ M) and (d) 3-MPA- Dansyl released from 7 mg of Fe<sub>3</sub>O<sub>4</sub>@SiO<sub>2</sub> MNPs (100nm in diameter) upon cleaving the disulfide bond. For all samples the injection volume was 100 $\mu$ L. The isocratic elution with mobile phase of 80% ACN and 20% H<sub>2</sub>O was performed for all samples. The control sample was prepared by reacting thiol coated MNPs (7 mg) with dansylcadaverine.

Based on the following parameters ,the number of dansylcadaverine molecules per Fe<sub>3</sub>O<sub>4</sub>@SiO<sub>2</sub> MNP was estimated: size of the nanoparticle (determined by TEM), density of MNPs (estimated based on the structure of Fe<sub>3</sub>O<sub>4</sub>@SiO<sub>2</sub>, i.e., the size of magnetite core and the thickness of the silica coating layer), and the amount of 3-MPA-Dansyl released from dansylcadaverine conjugated Fe<sub>3</sub>O<sub>4</sub>@SiO<sub>2</sub> MNPs. For the smaller Fe<sub>3</sub>O<sub>4</sub>@SiO<sub>2</sub> MNPs (20 nm diameter, 6 mg), the amount of conjugated dansylcadaverine was determined by HPLC to be

$2.4 \times 10^{-7}$  mol. The number of dansylcadaverine molecules per MNP was calculated based on the following assumptions. The density of 20 nm diameter  $\text{Fe}_3\text{O}_4@\text{SiO}_2$  MNPs was estimated to be  $2.5 \text{ g/cm}^3$  according to the density values of  $\text{Fe}_3\text{O}_4$  ( $5.17 \text{ g/cm}^3$ ) and  $\text{SiO}_2$  ( $2.2 \text{ g/cm}^3$ ).<sup>41</sup> Consequently, 6 mg of these MNP contained approximately  $5.62 \times 10^{14}$  particles, the average number of dansylcadaverine conjugated to one nanoparticle was about  $2.6 \times 10^2$ , and the number of conjugated dansylcadaverine per milligram of 20 nm MNPs was  $2.4 \times 10^{16}$ . Similarly, it can be estimated for 100 nm  $\text{Fe}_3\text{O}_4@\text{SiO}_2$  MNPs, the average number of dansylcadaverine conjugated to one nanoparticle surface was about  $3.4 \times 10^3$ , and the number of conjugated dansylcadaverine per milligram of 100 nm MNPs that approximately contained  $4.27 \times 10^{11}$  particles, was  $1.4 \times 10^{15}$ . Assuming a 1:1 stoichiometry and optimum efficiency, the number of NHS ester groups on the MNP surface should be equal to the number of released 3-MPA-Dansyl molecules. The actual number of NHS ester groups on each 100 nm  $\text{Fe}_3\text{O}_4@\text{SiO}_2$  MNP was less than the theoretical maximum number of thiol groups that could attach to the MNP surface ( $\sim 10^5$ ). Steric hindrance and hydrolysis of NHS ester groups in contact with moisture in the solvent or air between preparation of the particles and binding to the fluorophore are two important factors that may contribute to the observed difference in conjugation efficiency.

#### **2.3.4 Semiquantitative fluorescence microscopic characterization of dansylcadaverine modified $\text{Fe}_3\text{O}_4@\text{SiO}_2$ MNPs**

As a rapid and sensitive technique, fluorescence microscopy was used for qualitative and semi-quantitative characterization of active NHS ester groups covalently attached to dansylcadaverine. The presence of NHS esters on the surface of  $\text{Fe}_3\text{O}_4@\text{SiO}_2$  MNPs was

confirmed by detecting the green fluorescence of dansylcadaverine conjugated  $\text{Fe}_3\text{O}_4@\text{SiO}_2$  MNPs using a fluorescence microscope (Figure 2.5a). No fluorescence signal was detected for thiol coated  $\text{Fe}_3\text{O}_4@\text{SiO}_2$  MNPs that were used as a negative control (i.e. no dansylcadaverine) under the same conditions (data not shown). By measuring the fluorescence intensity of microscope images, the quantity of dansylcadaverine conjugated to NHS ester coated  $\text{Fe}_3\text{O}_4@\text{SiO}_2$  MNPs can be calculated. Even though similar fluorescence image processing software were reported in the literature,<sup>42,43</sup> the fluorescence image processing program employed in this study was developed independently and run in MATLAB environment (Figure 2.1). As we see in Figures 2.5a and 2.5b, the fluorescence intensities increased with the increasing amount of dansylcadaverine coated  $\text{Fe}_3\text{O}_4@\text{SiO}_2$  MNPs. To prove that the fluorophore molecules were immobilized onto the MNPs surface only through covalent attachment, a control experiment (Figure 2.5 a7) was performed in which the NHS groups on the surface of  $\text{Fe}_3\text{O}_4@\text{SiO}_2$  MNPs were hydrolyzed by incubation. The carboxylic acid coated  $\text{Fe}_3\text{O}_4@\text{SiO}_2$  MNPs (product of NHS ester hydrolysis) were then treated with dansylcadaverine, followed by fluorescence microscopy observation of the extensively washed MNP. No fluorescence was detected for such hydrolyzed MNPs incubated with dansylcadaverine (Figure 2.5 a7). This observation confirmed that nonspecific adsorption of fluorophore to the surface of  $\text{Fe}_3\text{O}_4@\text{SiO}_2$  MNPs was minimal.

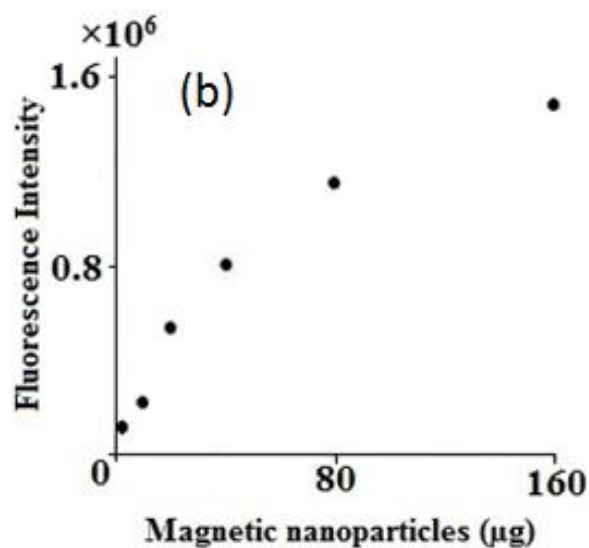
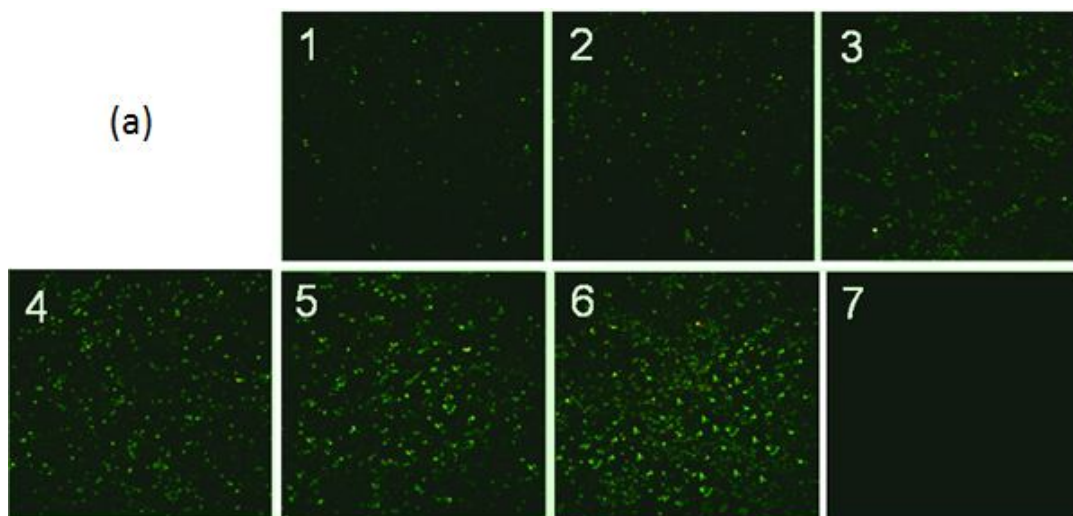


Figure 2.5: Fluorescence micrographs of  $\text{Fe}_3\text{O}_4@\text{SiO}_2$  MNPs labeled with dansylcadaverine. a) Micrographs (a1-a6) represent fluorescence images obtained from 5, 10, 20, 40, 80 and 160  $\mu\text{g}$  of dansylcadaverine labeled  $\text{Fe}_3\text{O}_4 @\text{SiO}_2$  MNPs. The control sample (a7, 20 $\mu\text{g}$ ) was prepared by reacting the hydrolyzed NHS ester coated  $\text{Fe}_3\text{O}_4 @\text{SiO}_2$  MNPs with dansylcadaverine. The fluorescence intensity on a7 is below detection limit. b) Integrated fluorescence intensities of the images in (a) were plotted against quantity of MNPs.

The fluorescence microscopic method employed for detection of dansylcadaverine coated  $\text{Fe}_3\text{O}_4@\text{SiO}_2$  MNPs, could be considered as semi-quantitative method since it revealed

the trend of elevated fluorescence intensities with the increasing amount of fluorophore coated MNPs. We were also able to detect the fluorescence signal from 5  $\mu\text{g}$  of dansylcadaverine coated  $\text{Fe}_3\text{O}_4@\text{SiO}_2$  MNPs using the abovementioned highly sensitive fluorescence microscopy approach. Compared to the HPLC method that was employed for accurate quantification of NHS ester groups on  $\text{Fe}_3\text{O}_4@\text{SiO}_2$  MNPs surface, the fluorescence microscopy approach is more convenient for monitoring the incorporation of NHS ester group on nanoparticle surface. For the application of NHS ester coated magnetic nanoparticle reagent in labelling the exposed lysine residues of native proteins, the presence of NHS ester on  $\text{Fe}_3\text{O}_4@\text{SiO}_2$  MNPs surface is essential.<sup>33</sup>

### **2.3.5 Labeling efficiencies of exposed lysine residues in native protein by NHS ester conjugated $\text{Fe}_3\text{O}_4@\text{SiO}_2$ MNPs**

The reaction of primary amine groups in proteins with NHS/sulfo-NHS ester has been extensively used for protein conjugation.<sup>4</sup> The conjugation reaction can be done at room temperature in aqueous solution, which allow us to detect exposed lysine residues in the native structures of proteins. A large volume of solvent is required to re-disperse the bulky MNPs labelling reagent compared to equivalent amount of small molecule labelling reagents such as sulfo-NHS-SS-biotin. This requirement on solvent would results in dilution of protein in the reaction system and reduced the primary amine labelling efficiency. For the same initial amount of BSA (100  $\mu\text{g}$ ), a larger quantity of NHS ester coated MNPs (7 mg) dissolved in larger volume of the solvent (400  $\mu\text{L}$  PBS), captured a smaller amount of protein (27  $\mu\text{g}$ ), compared to a smaller quantity of MNPs in a smaller volume of solvent (3 mg MNPs in 200  $\mu\text{L}$  PBS) that

captured 52  $\mu\text{g}$  of BSA. If the protein concentration in aqueous solvent was below 0.5 mg/mL, the efficiency of the reaction between the primary amine and the NHS ester groups (conjugated to the MNPs) was dramatically decreased due to the hydrolysis of NHS/sulfo-NHS ester.

To solve the above mentioned issues, a special sample mixing method was employed in labelling the exposed lysine residues of native BSA with NHS ester coated  $\text{Fe}_3\text{O}_4@\text{SiO}_2$  MNPs (Scheme 2.3). Instead of mixing the NHS ester coated  $\text{Fe}_3\text{O}_4@\text{SiO}_2$  MNPs with BSA in one step, the MNPs were divided to smaller portions and added to the BSA solution separately. After the first addition of the MNPs, the labelling reaction was allowed to proceed for 30 minutes followed by addition of the remaining fresh NHS ester coated MNPs with an additional 30 minutes of shaking. The reaction volume was kept minimal in order to maintain the initial high concentration of BSA. The addition of fresh NHS ester coated  $\text{Fe}_3\text{O}_4@\text{SiO}_2$  MNPs allows us to label those lysine residues that were not modified in the first step due to hydrolysis of NHS ester groups.

Two types of experiments were designed and performed to investigate the effect of quantity of MNPs and proteins on labelling efficiency. In the first set of experiments, the same amount of MNPs was reacted with different amounts of BSA. The second set of experiments were performed by mixing the same amount of BSA with different amounts of MNPs. The above mentioned sample mixing methods was used in both experiments to mix MNPs with BSA, and BCA assay was performed to measure the unbound BSA. In order to understand the effects on labelling efficiency either by increasing the ratio of BSA/MNP (Figure 2.6a) or by increasing the ratio of MNP/BSA (Figure 2.6b), the amounts of BSA conjugated to MNPs were compared in

both experiments. With increasing amount of BSA, the quantity of BSA conjugated to the NHS ester coated  $\text{Fe}_3\text{O}_4@\text{SiO}_2$  MNPs (0.5 mg) increased until reaching a maximum at 16  $\mu\text{g}$  of BSA added. After this maximum point, the quantity of captured BSA did not change by adding more BSA to the reaction, indicating that 0.5 mg of labelled MNP can bind a maximum of 16  $\mu\text{g}$  of BSA. A similar pattern was observed in the second set of experiments, where an increase in the amount of BSA conjugated to  $\text{Fe}_3\text{O}_4@\text{SiO}_2$  MNPs reached to plateau once all the available BSA were labelled. The results from these experiments were in agreement with the constant MNP experiment, with 0.5 mg of labelled MNPs binding about 18  $\mu\text{g}$  of protein. The molar ratio of BSA to available NHS ester groups determined by fluorescence quantification was 1:12.

In case of increasing MNP/BSA ratio ( the first type of experiment), few MNPs can be conjugated to one BSA molecule when the number of BSA molecules was small. As we increase the amount of BSA, one magnetic nanoparticle can be conjugated to several BSA molecules. In the second type of experiment that involved increasing BSA/MNP ratio, when amount of MNPs were low, some of the BSA molecules could have multiple sites labelled, and some might have one site labelled, and some might not be labelled at all. In this case, it is also possible that one MNP could label several BSA molecules. By increasing the amount of MNPs, more sites in one BSA molecule could be labelled , but due to large number of bulky MNPs present in the system ,the average number of BSA molecules attached per magnetic nanoparticle could be reduced. The sample mixing method described previously, might not be required when the BSA/MNPs ratio was large due to the fact that BSA concentration was high enough for most of the MNPs to be conjugated by at least one BSA molecule. The first set of experiments (increasing MNP/BSA

ratio) could be used as an effective approach to label multiple sites in one protein molecule. On the other hand, the second set of experiments (increasing BSA/MNP ratio) can be employed when preserving the native structure of the protein during the labelling process is highly desired.

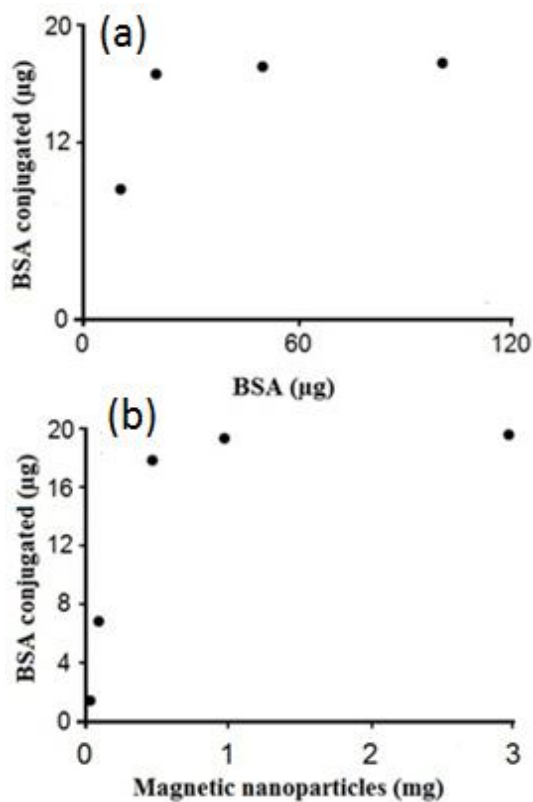


Figure 2.6: Quantitative study of labeling BSA by NHS ester modified  $\text{Fe}_3\text{O}_4@SiO_2$  MNPs. The amount of BSA conjugated to the NHS ester coated  $\text{Fe}_3\text{O}_4@SiO_2$  MNPs was calculated by subtracting the amount of remaining BSA from the initial amount of BSA. In the series of experiments presented in Fig. 2.6a, the amount of NHS ester coated  $\text{Fe}_3\text{O}_4@SiO_2$  MNPs (0.5 mg) was kept constant and amount of BSA was varied (20,40,60,80 and 100  $\mu\text{g}$ ). In Fig. 2.6 B, the quantity of BSA (20  $\mu\text{g}$ ) conjugated was kept constant, and the quantity of NHS ester modified MNPs was varied (0.05, 0.1, 0.5, 1 and 3 mg).

## 2.4 Conclusions

The reactivity of NHS ester groups conjugated on  $\text{Fe}_3\text{O}_4@\text{SiO}_2$  MNPs surface towards primary amine containing molecules such as the fluorophore dansylcadaverine provides the possibility of qualitative and quantitative characterization of the amount of NHS ester groups immobilized on  $\text{Fe}_3\text{O}_4@\text{SiO}_2$  MNPs surfaces. Accurate quantification of NHS ester groups was performed by HPLC analysis of modified fluorophore that was detached from  $\text{Fe}_3\text{O}_4@\text{SiO}_2$  MNPs via reductive cleavage of disulfide bond in the linker between the fluorophore and MNPs. On the other hand, fluorescence microscopy was employed as a fast and sensitive approach for direct measurement of fluorophore conjugated  $\text{Fe}_3\text{O}_4@\text{SiO}_2$  MNPs, and to determine if NHS ester groups were immobilized on the magnetic nanoparticle surface. In case of using bulky labelling reagents such as NHS ester coated  $\text{Fe}_3\text{O}_4@\text{SiO}_2$  MNPs, maintaining the concentration of fresh NHS ester groups in the reaction system is very important to increase the labelling efficiency. This can be achieved by adding multiple doses of NHS ester coated MNPs to each aliquot of protein during the labelling reaction. In case of labelling minimum sites in a protein of high concentration, maintaining the concentration of fresh NHS ester groups may not be necessary. However, it is critical to maintain the concentration of fresh NHS ester groups if labelling as many sites as possible in a protein with multiple sites or protein mixtures such as a cell surface proteome is desired.

## References

1. A. K. Gupta and M. Gupta, *Biomaterials*, 2005, 26, 3995-4021.
2. J. He, M. Huang, D. Wang, Z. Zhang and G. Li, *J. Pharm. Biomed. Anal.*, 2014, 101, 84-101.
3. K. Turcheniuk, A. V. Tarasevych, V. P. Kukhar, R. Boukherroub and S. Szunerits, *Nanoscale*, 2013, 5, 10729-10752.
4. K. E. Sapsford, W. R. Algar, L. Berti, K. B. Gemmill, B. J. Casey, E. Oh, M. H. Stewart and I. L. Medintz, *Chem. Rev.*, 2013, 113, 1904-2074.
5. Y. Xing, N. Dementev and E. Borguet, *Curr. Opin. Solid State Mater. Sci.*, 2007, 11, 86-91.
6. Y. Chen, Y. Chi, H. Wen and Z. Lu, *Anal. Chem.*, 2006, 79, 960-965.
7. K. Corsi, F. Chellat, L. H. Yahia and J. C. Fernandes, *Biomaterials*, 2003, 24, 1255-1264.
8. A. J. Kell and B. Simard, *Chem. Comm.*, 2007, 1227-1229.
9. Y. Chen and Y. Zhang, *Anal. Bioanal. Chem.*, 2011, 399, 2503-2509.
10. Y. Zhang and Y. Chen, *IET Nanobiotechnol.*, 2012, 6, 76-80.
11. L. Maus, J. P. Spatz and R. Fiammengo, *Langmuir*, 2009, 25, 7910-7917.
12. I. J. Bruce and T. Sen, *Langmuir*, 2005, 21, 7029-7035.
13. J. Kim, D. Jung, Y. Park, Y. Kim, D. W. Moon and T. G. Lee, *Appl. Surf. Sci.*, 2007, 253, 4112-4118.
14. M. Ghasemi, M. Minier, M. Tatoulian and F. Arefi-Khonsari, *Langmuir*, 2007, 23, 11554-11561.
15. Y. Xing and E. Borguet, *Langmuir*, 2006, 23, 684-688.

16. I. Bravo-Osuna, D. Teutonico, S. Arpicco, C. Vauthier and G. Ponchel, *Int.J. Pharma.*, 2007, 340, 173-181.
17. Y. Liu and B. Yan, *Comb. chem. high throughput screening*, 2011, 14, 191-197.
18. S. Noel, B. Liberelle, and G. De Cresc, *Bioconjugate Chem.*, 2011, 22, 1690-99.
19. G. Coussot, E. Nicol, A. Commeyras, I. Desvignes, R. Pascal and O. Vandenabeele-Trambouze, *Polym. Int.*, 2009, 58, 511-518.
20. J. Kim, H. K. Shon, D. Jung, S. Y. Han and T. G. Lee, *Anal. Chem.*, 2005, 77, 4137-41.
21. M. van de Waterbeemd, T. Sen, S. Biagini and I. J. Bruce, *Micro & Nano Lett., IET*, 2010, 5, 282-285.
22. L. Dauginet, A. S. Duwez, R. Legras and S. Demoustier-Champagne, *Langmuir*, 2001, 17, 3952-3957.
23. H. Hinterwirth, S. Kappel, T. Waitz, T. Prohaska, W. Lindner and M. Lammerhofer, *ACS nano*, 2013, 7, 1129-1136.
24. S. Elzey, D. H. Tsai, S. A. Rabb, L. L. Yu, M. R. Winchester and V. A. Hackley, *Anal. Bioanal. Chem.*, 2012, 403, 145-149.
25. B. Yan, Y. Jeong, L. A. Mercante, G. Y. Tonga, C. Kim, Z.-J. Zhu, R. W. Vachet and V. M. Rotello, *Nanoscale*, 2013, 5, 5063-5066.
26. E. A. Schellenberger, D. Sosnovik, R. Weissleder and L. Josephson, *Bioconjugate Chem.*, 2004, 15, 1062-1067.
27. C. Fang, N. Bhattarai, C. Sun and M. Zhang, *Small*, 2009, 5, 1637-1641.
28. X. Feng, N. Dementev, W. Feng, R. Vidic and E. Borguet, *Carbon*, 2006, 44, 1203-1209.

29. N. Dementev, X. Feng and E. Borguet, *Langmuir*, 2009, 25, 7573-7577.
30. T. Pellenbarg, N. Dementev, R. Jean-Gilles, C. Bessel, E. Borguet, N. Dollahon and R. Giuliano, *Carbon*, 2010, 48, 4256-4267.
31. Q. Sun and B. Yan, *Bioorg. Med. Chem. Lett.*, 1998, 8, 361-364.
32. H. Zhou, X. Li, A. Lemoff, B. Zhang and B. Yan, *Analyst*, 2010, 135, 1210-1213.
33. U. S. Patil, H. Qu, D. Caruntu, C. J. O'Connor, A. Sharma, Y. Cai and M. A. Tarr, *Bioconjugate Chem.*, 2013, 24, 1562-1569.
34. A. Ikari, A. Takiguchi, K. Atomi and J. Sugatani, *J. Cell. Physiol.*, 2011, 226, 2448-2456.
35. W. W. Yu, J. C. Falkner, C. T. Yavuz and V. L. Colvin, *Chem. Comm.*, 2004, 2306-07.
36. B. J. Yang, W. Liu, W. Yang, W. Li, and M. Gao, *Adv. Mat. Res.*, 2013, 631-32, 490-93.
37. MATLAB and Statistics Toolbox Release R2013a, Inc., Natick, MA, USA, 2013.
38. Y. Lu, Y. Yin, B. T. Mayers and Y. Xia, *Nano Lett.*, 2002, 2, 183-186.
39. C. Cannas, A. Musinu, A. Ardu, F. Orrù, D. Peddis, M. Casu, R. Sanna, F. Angius, G. Diaz and G. Piccaluga, *Chem. Mater.*, 2010, 22, 3353-3361.
40. J. C. Vaughan, G. T. Dempsey, and X. Zhuan, *J. Am. Chem. Soc.*, 2013, 135, 1197-1200.
41. K. K. N. Simon, and M. Sze, *Physics of Semiconductor Devices*, John Wiley and Sons, Inc, New York, 1981.
42. H. Fekkar, N. Benbernou, S. Esnault, H. C. Shin and M. Guenounou, *Proceedings of Society of Photographic Instrumentation Engineers-3260*, San Jose, CA, 1998.
43. Rasband, W.S., *IMAGEJ*, U. S. National Institutes of Health, Bethesda, Maryland, USA, 1997-2014.

## Chapter 3

### Solvent Exposed Lysine Residues of Native Apolipoprotein B-100

#### 3.1 Introduction

Low density lipoproteins (LDL) which is also referred to as 'bad cholesterol' transports cholesterol in blood and interstitial fluids. Elevated levels of LDL and other lipoproteins containing apolipoprotein B-100 (apoB-100) is a major cause of pathogenesis of atherosclerosis. LDL particles usually range from 18-30 nm in diameter,<sup>1,2</sup> and contain variable number of lipids with one molecule of apoB-100.<sup>3,4</sup> The hydrophilic core of LDL is surrounded by hydrophobic phospholipids and fatty acids. The protein molecule provides stability to structure of lipids and are responsible for recognition of cell surface receptors present on lipid molecules. In addition to a single apoB-100 molecule, LDL contains linoleic acid, esterified and non-esterified cholesterol, triglycerides, phospholipids containing phosphatidylcholine and sphingomyelin.<sup>5</sup> The variability of lipids adds a great amount of heterogeneity to the structure of LDL, which makes it a challenging task to elucidate the structure of ApoB.

ApoB-100 is a large hydrophobic glycoprotein containing 4536 amino acids (mature form). ApoB exists in two isoforms; apoB-100 and apoB-48 of which apoB-48 lack the receptor binding domain and cannot bind to lipid receptor domain. However, since apoB-48 is produced after RNA editing of apoB-100, both of these isoforms share similar *N*-terminal sequence. Cryo-electron microscopic results determined the length of detergent solubilized apo B-100 to be around 650 Å.<sup>17</sup> The large size and insolubility in aqueous solvents makes it difficult to obtain structural information about apoB-100. Great amount of efforts were poured into studying the

receptor binding domains of apoB-100 interacting with lipids. Circular dichroism (CD) and helical wheel analysis shed light on the presence of 25%  $\alpha$  helical content,<sup>7</sup> role of intramolecular disulfide linkage in conformation of ApoB-100<sup>8</sup> and the lipid associating motifs of ApoB-100.<sup>6</sup> Infrared spectroscopy and CD analysis of ApoB-100 also confirmed the presence of  $\beta$  sheet structure in ApoB-100. Using a computer program called LOCATE, Segrest et al. proposed a pentapartite structure of ApoB-100 containing two  $\beta$  strands alternating with two  $\alpha$  helices and an *N*-terminal  $\alpha$  helical domain.<sup>10</sup> Further, Chen et al suggested the parallel orientation of  $\beta$  sheets with phospholipid monolayer of LDL using FTIR, which might contribute to the high affinity of ApoB-100 to lipid receptors.<sup>9</sup> The interaction of ApoB-100 with lipid receptors is highly influenced by the presence of solvent exposed lysine and arginine residues.<sup>11</sup> Use of trypsin to release the surface exposed portion of apoB-100 may provide information about the composition of amino acids present on the surface of apo B-100. Fractionation of trypsin accessible peptides of apoB-100 coupled with two dimensional fingerprinting and amino acid analysis divided trypsin releasable peptides into four categories according to size, amino acid composition and C-terminal residues. All the four categories showed abundance of arginine and lysine residues along with relative positioning of arginine and lysine residues on the surface of apoB-100.<sup>18</sup> Yang et al. used trypsin to release lipid associating peptides of apoB-100 and Edman degradation to identify sequence of 13 tryptic peptides in 5 domains based on their trypsin releasability.<sup>20</sup>

Solvent exposed lysine residues were chemically modified by <sup>13</sup>C methyl groups followed by NMR characterization. NMR technique revealed presence of 53 active and 172 normal lysine residues on the solvent exposed surface of ApoB-100<sup>13</sup> The 1D NMR,<sup>15, 16</sup> and 2D NMR<sup>14</sup> was also used to detect different populations of solvent exposed lysine groups of apoB.

The NMR studies were focused on determination of number of active solvent exposed lysine residues irrespective to the position on the lysine residues located on the exposed surface of apo B-100. Chemical modification/labeling of active sites of proteins coupled with mass spectrometry has been preferred to study tricky proteins which are not suitable for NMR and X-ray crystallography due to size, purification, hydrophobic nature and inability to crystallize. Posttranslational modification of LDL which include oxidative modifications of tryptophan,<sup>19</sup> phenylalanine and proline were reported earlier. In our lab, oxidation of lysine, phenylalanine, proline, tryptophan and histidine amino acids upon exposure to hydroxyl radicals, peroxyntite and sodium hypochlorite was studied along with the position of modified amino acids in peptides. The modification was carried out prior to delipidation process and dialysis was used to remove lipids before LC-MS/MS analysis.<sup>21,22</sup> However, it has been a challenging task to ensure the modification of solvent exposed amino acid residues due to ability of small chemical modification reagents to cross the lipid bilayer and modify the internal amino acid residues embedded inside the structure of apoB-100.

In order to ensure the specific modification of solvent exposed peptides, we have utilized the large size of silica coated iron oxide magnetic nanoparticles ( $\text{Fe}_3\text{O}_4@\text{SiO}_2$  MNPs) which carries NHS ester group to modify solvent exposed free amine groups of apoB-100.<sup>23</sup> NHS ester modified  $\text{Fe}_3\text{O}_4@\text{SiO}_2$  MNPs contain a cleavable disulfide bond to isolate MNPs upon labeling and introduces a distinct mass shift on lysine residues which helps the identification of labeled peptides using mass spectrometry. In this work, we extend the application of NHS ester modified  $\text{Fe}_3\text{O}_4@\text{SiO}_2$  MNPs to label the solvent exposed amine groups of native apoB-100. The modification was performed at room temperature and in physiological conditions to maintain the native structure of apo B-100. Upon labeling, samples were delipidated using SDS treatment and

magnetic separation allowed the efficient and quick removal of SDS from the labeled apoB-100. After tryptic digestion, disulfide bond was cleaved in aqueous conditions to elute labeled peptides. LC-MS/MS analysis identified 28 solvent exposed peptides of native apoB-100.

### **3.2 Materials and Methods**

Ferric (III) chloride hexahydrate, ( $\text{FeCl}_3 \cdot 6\text{H}_2\text{O}$ , 99%), dimethyl sulfoxide (DMSO, anhydrous), (3-mercaptopropyl)trimethoxysilane (MPTMS, 99%), tetraethylorthosilicate (TEOS, 99%), sodium dodecyl sulfate (SDS) and ammonium bicarbonate were purchased from Sigma-aldrich (St. Louis, MO). Trisodium citrate, anhydrous, 99%, and sodium acetate, anhydrous, 99% were purchased from Alfa Aesar (Ward Hill, MA). Sodium citrate dihydrate was purchased from J. T. Baker Chemicals (Center Valley, PA). Ammonium hydroxide, was purchased from EMD Millipore (Billerica, MA). Ethylene glycol was purchased from VWR international (Radnor, PA). Succinimidyl 6-(3-[2-pyridyldithio]-propionamido)hexanoate (LC-SPDP) was purchased from Proteochem (Loves Park, IL, USA). Human low density lipoprotein (LDL) was purchased from Calbiochem (Billerica, MA) and Biovendor (Asheville, NC). Trypsin was purchased from Promega (Madison, WI). Tris(2-carboxyethyl)phosphine hydrochloride (TCEP-HCl) was purchased from Amresco (Solon, OH). Phosphate buffered saline (PBS) was purchased from Calbiochem (Billerica, MA). Ethanol was purchased from Pharmco-AAPER (Brookfield, CT). Nanopure water (18.2 M $\Omega$ ) was used for all experiments.

### **3.3 Synthesis of silica coated iron oxide magnetic nanoparticles ( $\text{Fe}_3\text{O}_4@ \text{SiO}_2$ MNPs)**

Superparamagnetic nanoparticles ( $\text{Fe}_3\text{O}_4$ ) were prepared by the hydrothermal method and then coated with silica ( $\text{Fe}_3\text{O}_4@ \text{SiO}_2$ ) using the modified Stober method as described in details in Chapter 2.

### **3.4 Surface functionalization of $\text{Fe}_3\text{O}_4 @ \text{SiO}_2$ MNPs with NHS ester groups**

The synthesized  $\text{Fe}_3\text{O}_4@ \text{SiO}_2$  MNPs were coated with thiol groups using MPTMS and then treated with TCEP prior to NHS ester coating as described previously (Chapter 2). The thiol coated MNPs (5 mg, 100 nm diameter) were dispersed in 200  $\mu\text{L}$  of ethanol and sonicated for 1 min. A solution of Succinimidyl 6-(3-[2-pyridyldithio]-propionamido)hexanoate (LC-SPDP, 8 mg) in anhydrous dimethyl sulfoxide (DMSO, 50  $\mu\text{L}$ ) was added to the nanoparticles suspension. The mixture was stirred at room temperature for 90 min and the NHS ester coated MNPs were collected by magnetic separation and then washed several times with ethanol to remove unreacted LC-SPDP.

To evaluate the success of NHS ester coating, 1 mg of the prepared NHS ester modified nanoparticles were dispersed in 100  $\mu\text{L}$  of 0.5 mM solution of dansylcadaverine in ethanol and the mixture was stirred at room temperature for 90 min. The fluorophore coated MNPs were washed several times with DMSO, ethanol and water to remove unreacted fluorophore. Fluorophore-nanoparticle conjugates were re-dispersed in 50  $\mu\text{L}$  of ethanol. 10  $\mu\text{L}$  of this solution was transferred to a microscope slide and observed under Olympus IX 71 inverted fluorescence microscope with a high performance 16 bit resolution, back illuminated CCD camera (Roper Scientific) and a 100 W Hg lamp as a light source.

### **3.5 Labeling solvent exposed lysine groups of ApoB-100 in native human low density lipoprotein (LDL) using NHS ester functionalized Fe<sub>3</sub>O<sub>4</sub>@SiO<sub>2</sub> MNPs**

The NHS ester modified Fe<sub>3</sub>O<sub>4</sub>@SiO<sub>2</sub>MNPs were re-dispersed in 200  $\mu$ L of ethanol and equally distributed among four micro centrifuge tubes (1.5 mL). The solvent (ethanol) was then removed under vacuum.

Low density lipoprotein solution (protein concentration of 5  $\mu$ g/ $\mu$ L, 20  $\mu$ L) was diluted to 80  $\mu$ L using phosphate buffered saline (PBS, 100 mM) with iodoacetamide (final concentration of 30 mM). The protein solution was mixed on a mechanical stirrer in dark at 37°C for one hour. The LDL solution was then distributed between four centrifuge tubes each containing 1mg of NHS ester coated nanoparticle. The nanoparticle - LDL suspensions were mixed for 30 min, combined and then mixed for another 60 min. The unreacted NHS ester groups were quenched using tris-HCl (100  $\mu$ L, 1M). LDL- MNPs conjugates were separated using a magnet and washed multiple times with 2% SDS, 20, 50 and 70 % acetonitrile (ACN) in water and finally water containing IAA (30 mM).

The ApoB - MNPs conjugates were dispersed in methanol/ammonium bicarbonate mixture (3: 2, v/v, 1mL) containing IAA (30mM) followed by addition of trypsin (14  $\mu$ L of 0.5  $\mu$ g / $\mu$ L solution, 7  $\mu$ g). The tryptic digestion was carried out at pH 8 for 15 hrs at 37°C. The tryptic peptides conjugated to the MNPs were collected by magnetic separation and the supernatant was acidified and stored at -20°C for further analysis. The MNPs were washed with 20, 50 and 70% ACN in water and finally nanopure water multiple times.

To release the tryptic peptides from Fe<sub>3</sub>O<sub>4</sub>@SiO<sub>2</sub> nanoparticles, the peptide-MNPs conjugates were dispersed in TCEP solution in water (1mL, 30 mM) and the suspension was mixed for 1hr at room temperature. The supernatant containing cleaved modified peptides was

collected and the Fe<sub>3</sub>O<sub>4</sub>@SiO<sub>2</sub> nanoparticles were washed multiple times with 20, 50 and 70% ACN in water. The supernatant and washes were combined and then dried under vacuum. The peptides were then re-suspended in 500 μL of water and the sample was desalted using C18 spin columns (Pierce, Rockford, IL) and dried under vacuum. The peptides were re-suspended in 50 μL of water/ acetonitrile / formic acid (92: 5: 3, v/v) prior to LC-MS/MS analysis.

### **3.6 LC-MS/MS and data analysis of ApoB-100 peptides labeled with NHS ester modified Fe<sub>3</sub>O<sub>4</sub>@SiO<sub>2</sub> MNPs**

All Mass spectrometric analyses were performed using an Agilent 1200 HPLC system and an Agilent 6520 Q- TOF tandem mass spectrometer (Agilent Technologies, Santa Clara, CA) coupled with a chip cube interface. Peptide sample (2 μL) was loaded to the HPLC-Chip system (160 nL enrichment column , 150 mm analytical column packed with C18, 5 μm beads with 300 Å pores) using a capillary pump at 4 μL/min flow rate. The peptides were then separated in the analytical column using a nano pump at a flow rate of 600 nL/min. The MS ion source was operated at 300°C with nitrogen as drying gas at flow rate of 5 L/min and a fragmentor voltage of 175 V. Nitrogen was used as the collision gas and the collision energy varied as a function of mass and charge using a slope of 3.7V/100 Da and an offset of 2.5V. The reference compounds with the mass of 322.048121 and 1,221.990637 Da were constantly infused into the ion source during the analysis. All analyses were performed in positive ion mode. Table 3.1 shows solvent gradient used for LC-MS/MS analysis.

Time	Solvent A (%)	Solvent B (%)
0.00	97	3
2.00	90	10
15.00	70	30
20.00	0	100
22.00	0	100
25.00	97	3

Table 3.1: Solvent gradient used for analysis of tryptic digests of labeled apoB-100. Solvent A: water (100%), formic acid (0.1%). Solvent B: Acetonitrile: water (90:10), formic acid (0.1%).

The acquired MS/MS spectra were processed using PEAKS software (Bioinformatics Solutions Inc, Ontario, Canada). A full length cDNA sequence of Apo B-100 (accession # P04114) was used in database search. Trypsin was selected as proteolytic enzyme and the number of missed cleavage sites was set to three. The search parameters were set as follow: differential mass increase of 201.28 Da for lysine residues, 57.07 Da for carbamidomethylated cysteine residues and 15.99 Da for oxidation of methionine residues. The presence of b and y ions for the peptides with high matching scores was confirmed by manual examination of MS /MS spectra.

### 3.7 Results and Discussion

#### 3.7.1 Synthesis of NHS ester functionalized Fe<sub>3</sub>O<sub>4</sub>@SiO<sub>2</sub> MNPs

The Fe<sub>3</sub>O<sub>4</sub> MNPs (80 nm diameter) were prepared using hydrothermal method, coated with silica shell by modified Stober method and finally functionalized with thiol groups using MPTMS as described in details previously (Chapter2). The synthesized thiol coated Fe<sub>3</sub>O<sub>4</sub>@SiO<sub>2</sub> were approximately 100 nm in diameter, spherical in shape (confirmed by TEM)

and well- dispersible in both aqueous and organic solvents. LC-SPDP was used to further decorate the surface of thiol coated MNPs with NHS ester groups via disulfide exchange reaction. To confirm the successful NHS ester functionalization, Dansylcadaverine was conjugated to the surface of nanoparticles through the amide bond formation between the amine group of fluorophore and the NHS ester moiety on the nanoparticles. The nanoparticles-fluorophore conjugates were extensively washed with different solvents (DMSO, water and ethanol) to ensure the removal of unreacted fluorophore and then observed under the fluorescence microscope. The green fluorescence of dansylcadaverin proved the presence of NHS ester groups on the surface of nanoparticles.

### **3.7.2 Labeling solvent exposed amine groups of ApoB-100 in native human LDL using NHS ester modified Fe<sub>3</sub>O<sub>4</sub>@SiO<sub>2</sub> MNPs**

The main steps for covalent modification of solvent exposed lysine groups of ApoB-100 using NHS ester modified Fe<sub>3</sub>O<sub>4</sub>@SiO<sub>2</sub> labeling reagent were summarized in Figure 3.1. The quantity of NHS ester coated Fe<sub>3</sub>O<sub>4</sub>@SiO<sub>2</sub> MNPs for labeling specific amount of ApoB was calculated based on the accurate quantification of NHS ester groups on the surface of MNPs presented in Chapter 2. To preserve the native structure of LDL, the labeling reaction was performed at room temperature and in aqueous-based buffer solution (PBS, pH 7.5). Cysteine residues of ApoB were alkylated using iodoacetamide prior to labeling reaction to ensure that the disulfide linkage between the NHS ester groups and MNPs stays intact. The concentration of protein solution was kept very high during the conjugation reaction to minimize the chance of NHS ester hydrolysis and improve the efficiency of the conjugation reaction. Tris HCl was used to quench unreacted NHS ester groups prior to delipidation and digestion of protein. This step is

necessary to prevent modification of those lysine groups which became accessible to the labeling reagent during the lipid removal or digestion process.

The LDL - MNPs conjugates can be washed several times with a variety of solvents to efficiently remove lipids associated with ApoB-100. Compare to conventional time consuming and tedious methods for delipidation of membrane or lipid bound proteins (such as gel based methods), magnetic separation provides fast and easy lipid removal. Different solvents (chloroform, isopropyl alcohol, methanol, acetone, etc) or solvent combinations (chloroform /diethyl ether/ water, chloroform/ methanol, etc) have been used for lipid removal which were not found to be effective. In this case, the efficiency of protein digestion decreases dramatically since lipid-bound protein is not accessible to the proteolytic enzyme and the generated peptides usually have poor solubility and a high tendency to aggregate. The efficient delipidation was achieved using 3% SDS followed by several washes with 20-70% ACN solution in water.

The magnetic separation also eliminated the need to perform commontime consuming procedures such as dialysis to remove surfactant from protein solution. Due to strong magnetization of nanoparticles, the protein-MNPs conjugates can be washed several times with different solvents to quickly, simply and efficiently remove SDS prior to proteolytic digestion. The efficient removal of detergent is crucial to maintain the activity of proteolytic enzymes such as trypsin. Additionally, the presence of SDS in peptide solution is highly detrimental to MS analysis since it can suppress the ionization of peptides.

After tryptic digestion of ApoB which was covalently bound to MNPs, the MNP-tryptic peptide conjugates were collected by magnetic separation and extensively washed to remove those peptides that are nonspecifically adsorbed on the surface of nanoparticles. Labeled peptides were finally released from the surface of MNPs by reductive cleavage of the disulfide bonds

between the peptides and MNPs. After magnetic separation of nanoparticles, the supernatant containing the labeled tryptic peptides was desalted and then analyzed by LC-MS/MS.

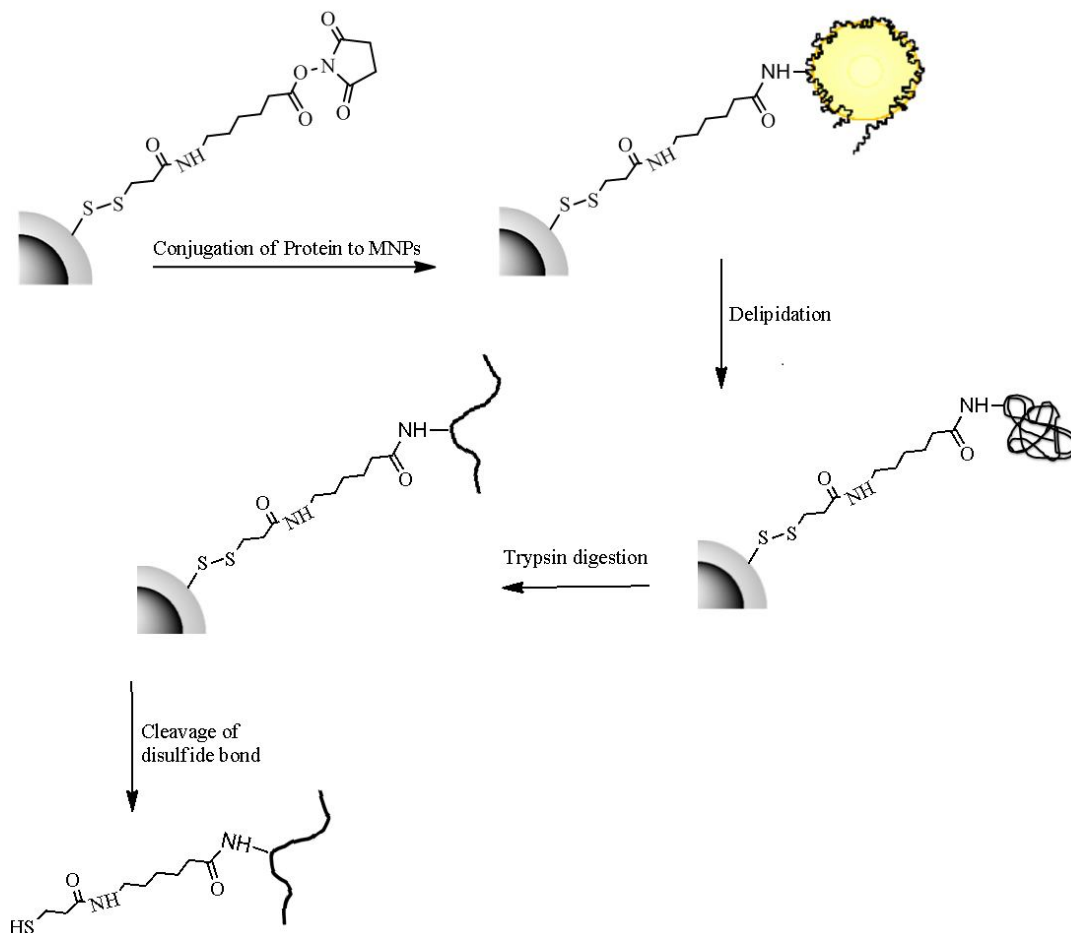


Figure 3.1: Labeling surface exposed lysine residues of apoB-100 in intact LDL using NHS ester modified Fe<sub>3</sub>O<sub>4</sub>@SiO<sub>2</sub> MNPs.

Labeling surface exposed primary amine groups in ApoB-100 with the NHS ester coated MNPs caused a 201.28 Da mass shift for lysine residues. LC-MS/MS analysis of tryptic digests of ApoB-100 generated 28 MS/MS spectra corresponding to 28 labeled peptides which we believe are located on the surface of intact LDL particles. Table 3.2 presents the amino acid sequence of the labeled peptides as well as the exact position of amino acids in the full length sequence of human apoB-100.

Labeled peptides	Peptide sequence	- log p
1078-1089	(R)VNDESTEGK(+201.28)TSYR(L)	90.02
28-45	E(+201.28)EEM(+15.99)LENVSLVCPK(D)	78.44
3235-3244	(K)AEK(+201.28)SHDELPR(T)	73.4
3521-3537	(R)SSVK(+201.28)LQGTSK(I)	71.7
2695-2705	(R)DLK(+201.28)VEDIPLAR(I)	68.44
3508-3527	(R)EYSGTIASEANTYLNSK(+201.28)STR(S)	68.19
208-219	(R)DLGQCDRFK(+201.28)PIR(T)	64.85
3936-3946	(K)IEDGTLASK(+201.28)TK(G)	62.75
3498-3507	(K)GDVK(+201.28)GSVLSR(E)	59.26
288-297	(K)LEDTPK(+201.28)INSR(F)	58.58
116-128	(K)TK(+201.28)NSEEFAAAMSR(Y)	57.33
1296-1308	(K)IEIPLPFGGK(+201.28)SSR(D)	56.4
1120-1128	(K)IK(+201.28)GVISIPR(L)	55.49
743-760	(K)DDK(+201.28)HEQDM(+15.99)VNGIM(+15.99)LSVEK(L)	52.54
1309-1317	(R)DLK(+201.28)MLETVR(T)	47.5
1692-1702	(R)EHNAK(+201.28)FSLDGK(A)	47.07
1853-1867	(K)ADTVAK(+201.28)VQGVFESHRL(L)	45.85
3207-3212	(R)HFEK(+201.28)NR(N)	44.12
1287-1295	(K)YTLNK(+201.28)NSLK(I)	43.9
764-774	(K)DLK(+201.28)SK(+201.28)EVPEAR(A)	40.5
3156-3163	(K)TGLK(+201.28)EFLK(T)	40.08
2140-2147	(K)EK(+201.28)LTALTK(K)	38.34
1636-1646	(K)INSGAHK(+201.28)ATLR(I)	37.84
4036-4044	(K)LTIFK(+201.28)TELR(V)	36.13
4479-4486	(K)SQAIATK(+201.28)K(I)	33.74
2003-2012	(K)DK(+201.28)IGVELTGR(T)	32.55
2098-2109	(R)NLK(+201.28)HINIDQFVR(K)	31.93
1044-1055	(K)QTEATM(+15.99)TFK(+201.28)YNR(Q)	30.51

Table 3.2: List of apoB-100 peptides with lysine (represented K) residues being labeled with NHS ester coated Fe<sub>3</sub>O<sub>4</sub>@SiO<sub>2</sub> MNPs and detected by LC-MS/MS analysis.

Labeled lysine residues are no longer a cleavage site for trypsin, therefore modified lysine groups are usually located in the middle of peptide sequence and not at the C-terminus. Although NHS ester has some reactivity toward hydroxyl group, we did not observe modification of amino acids such as serine and tyrosine which have hydroxyl group in their side chain. We were also able to detect labeled N terminal amino acid (glutamic acid) of mature apoB-100. The MS/MS spectra of labeled peptides were manually examined and the presence of b and y ions in the tandem mass spectra confirmed the quality of peptide identification (Figure 3.2).

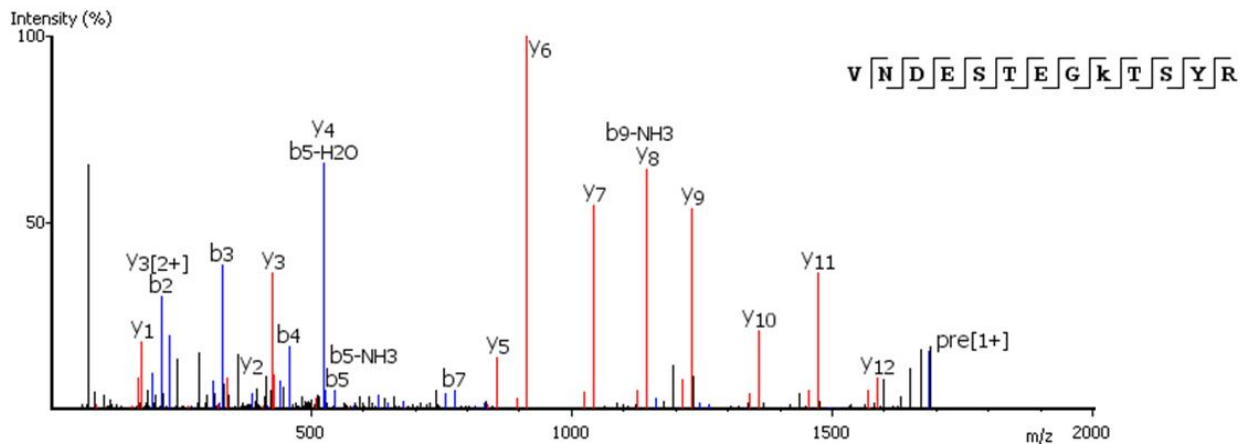


Figure 3.2:MS/MS spectrum of the labeled peptide "VNDESTEGKTSYR" of m/z 843.89 (molecular mass of 1685.76 Da).

Our labeling protocol revealed the presence of considerably lower number of lysine residues on the surface of intact LDL particles compare to the other approaches that utilize small covalent modification reagents such as formaldehyde to probe surface exposed lysine groups.<sup>13</sup> There are 357 lysine residues present in Human ApoB-100 molecule<sup>13</sup>. NMR studies on <sup>13</sup>C-labeled human LDL have revealed the presence of approximately 225 exposed lysine residues. The rest of the apoB lysine groups (132 lysine residues) are buried in the lipid layer and therefore they are not accessible to the labeling reagents.

Although the  $^{13}\text{C}$ -labeling reaction was performed on intact LDL and in aqueous medium, the modification of the surface lysine groups using the small labeling reagent ( $^{13}\text{C}$ -formaldehyde) remains challenging. The long reaction time (18 hr) and very small size of the modification reagent (compare to the size of LDL particles, 20-28 nm in diameter), increases the chance for the labeling reagent to cross the lipid layer and modify those lysine residues which are embedded in the hydrophobic core of LDL. Therefore, the labeling protocols that utilize small modification reagents may overestimate the number of lysine groups exposed on surface of intact LDL particles.

Due to the large size of our labeling reagent (NHS ester coated MNPs, 100 nm), the covalent modification is restricted to those amine groups that are located on the surface of LDL particles while the rest of lysine groups buried inside the LDL particles stay intact. The longer spacer arm utilized in LC-SPDP crosslinkers improves the accessibility of further ligands to the potential binding sites on the surface of each MNP which could result in higher conjugation efficiency. Smaller labeling reagent (20 nm NHS ester coated  $\text{Fe}_3\text{O}_4@ \text{SiO}_2$  MNPs) has been also employed in our lab for the modification of surface lysine groups in proteins. In this case, lower magnetization of small MNPs and consequently poor magnetic separation results in significant protein loss.

### 3.8 Conclusion

Thiol coated  $\text{Fe}_3\text{O}_4@\text{SiO}_2$  MNPs were functionalized with NHS ester groups (using LCSPDP) to label surface lysine groups of ApoB-100 in native LDL particles. Conjugation of LC-SPDP to thiol coated MNPs was characterized by attaching a fluorophore which is reactive towards NHS ester group. Labeling native apoB-100 by NHS ester modified  $\text{Fe}_3\text{O}_4@\text{SiO}_2$  MNPs was efficient at pH 7.4 and at room temp. Prior to MNP labeling, free thiol groups in apoB-100 were alkylated with iodoacetamide to prevent undesired disulfide bond exchange. Conjugation of apoB-100 to MNPs facilitated SDS treatment to remove lipids and washes by various solvents to clean the sample. Quick and efficient removal of lipids and detergent by magnetic separation can be advantageous over conventional techniques such as dialysis, ion exchange chromatography or precipitation. In the last step, the labeled peptides were released from MNPs by reductive cleavage of disulfide bond in aqueous medium. MS/MS analysis of labeled peptides found 28 tryptic peptides containing labeled lysine residues. These labeled lysine residues should be on the solvent exposed surface of LDL since the large size of MNPs prevents contact of the reagent to those lysine residues embedded inside the structure of apoB-100. Moreover, identification of the labeled lysine residues includes the exact positions of this amino acid residue in the full-length sequence; and such detailed positioning of lysine residue provides additional structural information complementary to that obtained from different methods such as NMR analysis. Due to its ability to specifically target solvent accessible amine groups and magnetically separate labeled peptides from detergents, NHS ester modified  $\text{Fe}_3\text{O}_4@\text{SiO}_2$  MNPs can be a potential tool for sample preparation and identification of surface peptides of large and hydrophobic proteins.

## References

1. Fisher W. R., *Ann Clin Lab Sci*, Volume 2, Issue 3, 198-208, 1972.
2. Williams P. T., Vranizan K. M., Krauss R. M., *J Lipid Res*, Volume 33, Issue 5, 765-74, 1992.
3. Kane J. P., *Annu Rev Physiol*, Volume 45, 637-50, 1983.
4. Luc G., Turpin G., De Gennes J. L., *Ann Med Interne (Paris)*, Volume 134, Issue 8, 695-701, 1983.
5. Hevonoja T., Pentikainen M. O., Hyvonen M. T., Kovanen P. T., Ala-Korpela M., *Biochim Biophys Acta*, Volume 1488, Issue 3, 189-210, 2000.
6. Wei C. F., Chen S. H., Yang C. Y., Marcel Y. L., Milne R. W., Li W. H., Sparrow J. T., Gotto A. M., Chan L., *Proc Natl Acad Sci U S A*, Volume 82, Issue 21, 7265-9, 1985.
7. Scanu A., Hirz R., *Nature*, Volume 218, Issue 5137, 200-1, 1968.
8. Singh S., Lee D. M., *Biochim Biophys Acta*, Volume 876, Issue 3, 460-8, 1986.
9. Chen G. C., Hardman D. A., Hamilton R. L., Mendel C. M., Schilling J. W., Zhu S., Lau K., Wong J. S., Kane J. P., *Biochemistry*, Volume 28, Issue 6, 2477-84, 1989.
10. Segrest J. P., Jones M. K., Mishra V. K., Anantharamaiah G. M., Garber D. W., *Arterioscler Thromb*, Volume 14, Issue 10, 674-85, 1994.
11. Weisgraber K. H., Innerarity T. L., Mahley R. W., *J Biol Chem*, Volume 253, Issue 24, 9053-62, 1978.
12. Weisgraber K. H., Innerarity T. L., Mahley R. W., *J Biol Chem*, Volume 253, Issue 24, 9053-62, 1978.

13. Lund-Katz S., Ibdah J. A., etizia J. Y., Thomas M. T., Phillips M. C., J Biol Chem, Volume 263, Issue 27, 13831-8, 1988.
14. Blanco F. J., Villegas S., Benitez S., Bancells C., Diercks T., Ordonez-Llanos J., Sanchez-Quesada J. L., J Lipid Res., Volume 51, Issue 6, 1560-5, 2010.
15. Aviram M., Lund-Katz S., Phillips M. C., Chait A., J Biol Chem, Volume 263, Issue 32, 16842-8, 1988.
16. Lund-Katz S., Laplaud P. M., Phillips M. C., Chapman M. J., Biochemistry, Volume 37, Issue 37, 2867-74, 1998.
17. Gantz D. L., Walsh M. T., Small D. M., J Lipid Res, Volume 41, Issue 9, 1464-72, 2000.
18. Chakraborty Sourav, Cai Yang, Tarr Matthew A., Analytical Biochemistry, Volume 404, Issue 2, 109-117, 2010.
19. Chakraborty S., Cai Y., Tarr M. A., Proteomics, Volume 14, Issue 21-22, 2614-22, 2014.
20. Patil Ujwal S., Qu, Haiou Caruntu, Daniela O'Connor, Charles J., Sharma Arjun, Cai Yang, Tarr Matthew A., Bioconjugate Chemistry, Volume 24, Issue 9, 1562-69, 2013.
21. Hoofnagle A. N., Heinecke J. W., J Lipid Res., Volume 50, Issue 10, 1967-75, 2009.
22. Karlsson H., Leanderson P., Tagesson C., Lindahl M., Proteomics, Volume 5, Issue 5, 1431-45, 2005.
23. Karlsson H., Leanderson P., Tagesson C., Lindahl M., Proteomics, Volume 5, Issue 2, 551-65, 2005.
24. Banks R. E., Dunn M. J., Hochstrasser D. F., Sanchez J. C., Blackstock W., Pappin D. J., Selby P. J., Lancet, Volume 356, Issue 9243, 1749-56, 2000.

25. Yang C. Y., Gu Z. W., Weng S. A., Kim T. W., et al., *Arteriosclerosis*, Volume 9, Issue 1, 96-108, 1989.

## Chapter 4

### Reduction of Disulfide Bonds In Peptides and Proteins Using TCEP

#### Immobilized Fe<sub>3</sub>O<sub>4</sub>@SiO<sub>2</sub> Magnetic Nanoparticles

##### 4.1 Introduction

Disulfide bonds in proteins are formed by covalent interaction between pairs of cysteine residues. Disulfide bonds, which mostly exist in extracellular and secreted proteins,<sup>1</sup> are formed through the oxidative folding process in the endoplasmic reticulum.<sup>2</sup> These covalent bonds are essential in protein structure in many aspects including folding, assembly and stabilization of proteins. In bacteria, the formation and reduction of disulfide bonds serves as an on-off switch, which protects the organism against oxidative conditions.<sup>3</sup> There are two types of disulfide bonds in protein structures, intra- and intermolecular bonds. The former exist between two cysteine residues within a polypeptide chain (single molecule), while the later forms between the cysteine groups of two separate molecules of the same polypeptide or distinct proteins. Intramolecular disulfide bonds are responsible for maintaining the tertiary structure of a protein, while the intermolecular disulfide bonds stabilize the quaternary structure.<sup>4</sup>

The success of mass spectrometric-based analysis for identification and structural elucidation of proteins is highly dependent on the efficiency of protein digestion steps. To ensure efficient proteolysis, the protein should be unfolded through disulfide bond reduction and other denaturing. The disruption of disulfide bonds enhances the accessibility of the proteolytic enzymes to their potential cleaving sites, which consequently improves the sequence coverage

and protein identification by mass spectrometry.<sup>5</sup> The cleavage of disulfide bonds, which generates free active sulfhydryl groups occurs via a reduction reaction. The reductive cleavage of disulfide bonds in proteins is commonly carried out by simply mixing the protein solution with a reducing agent over a specific time (ranging from 30 min to 24 hrs) at a specific temperature<sup>6</sup> (ranging from room temperature to 60° C). The most commonly used reducing agents are thiol-containing reductants, including dithiothreitol (DTT) and  $\beta$ -mercaptoethanol (BME), and trialkylphosphines such as tris(2-carboxyethyl) phosphine (TCEP). Since DTT and BME function via a thiol-disulfide exchange reaction, which requires the formation of a thiolate anion, the reaction is usually inhibited at low pH<sup>7</sup> (typically less than 8). In addition to the abovementioned limitations, the excess amount of ME and DTT should be removed from the reaction mixture, especially in those applications that involve the determination or modification of free thiol groups<sup>8,9</sup> (for example histidine tagged protein purification and maleimide conjugations). On the other hand, trialkyl phosphines have poor water solubility and an irritant odor, which has hindered their widespread applications as reducing agents.<sup>10</sup>

TCEP was first synthesized and used as a disulfide reducing agent by Levinson et al.<sup>11</sup> in 1969 and Rüegg et al.<sup>12</sup> in 1977, respectively. However, the widespread adoption of TCEP as a disulfide bond reducing agent did not start until Burns et al.<sup>13</sup> established a protocol to synthesize large quantities of TCEP. Apart from being non-volatile, non-toxic and odorless, TCEP offers several advantages over other phosphines and thiol reducing agents, including higher resistance to air oxidation, higher specificity and efficiency in reducing disulfide bonds and a better ability to work over a wide range of pH (1.5-8.5). Unlike DTT and  $\beta$ -ME, TCEP does not have to be removed before the chemical modification of cysteine groups in reduced protein and peptides.<sup>7</sup>

However, in some cases the TCEP removal is required since it can react with iodoacetic acid and iodoacetamide compounds which are common reagents for modification of peptides and proteins.<sup>14,15</sup> To avoid time-consuming and laborious methods such as gel filtration or dialysis that are common for separation of reducing agents from protein and peptides, using a solid supported reducing agent could be an effective alternative. Immobilized TCEP disulfide reducing agarose gel has been commercially developed which provides fast separation of reducing agent from reduced proteins and peptides, however the application of the agarose gel-immobilized TCEP is limited to aqueous based solutions.<sup>16</sup> Subra et al. reported the synthesis and application of TCEP-immobilized hydrophilic crosslinked PEG resins in conjugation with microwave irradiation for reduction of disulfide bridges in peptides.<sup>16</sup> Welham et al. recently reported the fabrication and use of a TCEP-immobilized silica monolith in a glass microchip for the reduction of disulfide bonds in insulin at 60°C<sup>17</sup>.

The immobilization of biological, organic and inorganic molecules on the surface of magnetic nanomaterials has attracted a great deal of interest in recent decades.<sup>18</sup> Magnetic nanoparticles offer several advantages over other types and shapes of nanomaterials due to their unique characteristics, such as high surface area, large surface to volume ratio and superparamagnetism, which provides the possibility of fast and easy separation of the nanoparticle-bound ligands from the complex reaction mixture by simply using an external magnetic field.<sup>19</sup> In this study we have fabricated TCEP-immobilized Fe<sub>3</sub>O<sub>4</sub>@SiO<sub>2</sub> magnetic nanoparticles (MNPs) for reduction of disulfide bridges in peptides and proteins. The silica shell protects the iron oxide core from oxidation and also prevents the interaction of iron oxide with peptides and proteins. The silica shell also provides anchoring sites for additional

functionalization with a variety of organic groups, such as amino groups through co-condensation processes.<sup>20</sup> Due to the magnetic properties of the iron oxide core, the reducing agent-bound nanoparticles could be isolated under mild magnetic separation conditions, which minimizes the mechanical stress on biological samples such as proteins. The reduction reaction was done at room temperature followed by alkylation of the generated free thiol groups to prevent reformation of disulfide bonds. LC-ESI-MS/MS analysis was performed for qualitative detection of alkylated cysteine groups in peptide and protein samples. The reduction of disulfide bonds required a small amount of solid supported reducing agent and could be successfully done in aqueous as well as organic solvents. The TCEP-immobilized silica coated magnetic nanoparticles could be added to biological samples to maintain the reductive conditions that are required to preserve the free sulfhydryl groups against oxidation.

## **4.2 Experimental procedures**

### **4.2.1 Materials**

(3-Aminopropyl) triethoxysilane (APTES), iodoacetamide, ammonium bicarbonate, urea and bovine pancreas insulin were purchased from Sigma-Aldrich (St. Louis, MO). Tris (2-carboxyethyl) phosphine hydrochloride (TCEP-HCl) was purchased from Amresco (Solon, OH). Sulfo-NHS and 1-ethyl-3-(3-dimethylaminopropyl) carbodiimide hydrochloride (EDC-HCl) was purchased from ProteoChem (Loves Park, IL). Peptides containing a disulfide bridge (NGR and Oxytocin) were purchased from Ana Spec (Fremont, CA). 4-morpholineethanesulfonic acid (MES) buffer was purchased from Pierce (Rockford, IL). Nanopure water (18.2 M $\Omega$ , Millipore Co. Billerica, MA) was used for all experiments.

#### **4.2.2 Preparation of amino-functionalized $\text{Fe}_3\text{O}_4@\text{SiO}_2$ magnetic nanoparticles**

Superparamagnetic nanoparticles ( $\text{Fe}_3\text{O}_4$ ) were prepared by the hydrothermal method and then coated with silica ( $\text{Fe}_3\text{O}_4@\text{SiO}_2$ ) using the modified stober method as described in details in Chapter 2. To 100 mg of  $\text{Fe}_3\text{O}_4@\text{SiO}_2$ MNP was added 80 mL of ethanol and 20 mL of water followed by ultrasonication for 5 min. APTES (1mL) was added dropwise to the nanoparticle suspension followed by mechanical stirring (400 rpm) for 12 hr. The amine coated  $\text{Fe}_3\text{O}_4@\text{SiO}_2$ MNPs were isolated using an external magnet, washed several times with water and ethanol and finally air dried at room temperature.

#### **4.2.3 Synthesis of TCEP coated $\text{Fe}_3\text{O}_4@\text{SiO}_2$ magnetic nanoparticles**

A mixture of EDC-HCl (57 mg, 0.3 mmol) and sulfo-NHS (33 mg, 0.15 mmol) in 1mL of 4-morpholineethanesulfonic acid (MES) buffer (100 mM, pH 6) was added dropwise to 500  $\mu\text{L}$  MES buffer containing 100mg (0.3 mmol) TCEP under constant stirring over 15 min at room temperature. The above mixture was then added to a 500  $\mu\text{L}$  suspension of amine coated  $\text{Fe}_3\text{O}_4@\text{SiO}_2$ MNP in MES buffer followed by mechanical stirring at room temperature for 24 hr. The TCEP coated nanoparticles were washed with 3 $\times$ 1 mL MES buffer, 3 $\times$ 1 mL water and then dried under vacuum.

#### **4.2.4 Nanoparticle characterization with transmission electron microscopy (TEM) and dynamic light scattering (DLS)**

The shape and diameter of magnetic silica coated nanoparticles was identified using transmission electron microscopy (JEOL Model 2010 LaB6 at 200 kV voltage). The modification of nanoparticles with amine and TCEP groups was confirmed by measuring the zeta potential values using a Mobius dynamic light scattering (DLS) instrument (Wyatt Technology Corporation, Santa Barbara, CA). Samples were dissolved in phosphate buffered saline (PBS, 10mM, pH7) prior to analysis.

#### **4.2.5 Reduction of disulfide bond in cyclic peptides using TCEP-immobilized $\text{Fe}_3\text{O}_4@ \text{SiO}_2$ magnetic nanoparticles**

Cyclic peptides containing a disulfide bridge (100  $\mu\text{g}$ ) were dissolved in 500  $\mu\text{L}$  of 20% ethanol in water. The above solution was added to 5 mg of TCEP-functionalized MNPs followed by mechanical stirring at room temperature for 1hr. Aqueous iodoacetamide (IAA) solution (75  $\mu\text{L}$  of 200 mM IAA, pH 8, 50 mM ammonium bicarbonate buffer) was added to the mixture of peptides and nanoparticles under stirring in the dark at room temperature for 30 min. The solvent was then removed under reduced pressure and the peptides were re-suspended in 500  $\mu\text{L}$  of water. The sample was run through a C18 spin column (Pierce, Rockford, IL) to remove the salts and then dried under vacuum. The peptides were re-suspended in 50  $\mu\text{L}$  of water/ acetonitrile/formic acid (92: 5: 3, v/v) prior to LC-MS/MS analysis.

#### **4.2.6 Reduction of disulfide bonds in bovine pancreas insulin using TCEP-immobilized Fe<sub>3</sub>O<sub>4</sub>@SiO<sub>2</sub> magnetic nanoparticles**

Insulin solution (20  $\mu$ L of 5  $\mu$ g/ $\mu$ L) in 50 mM hydrochloric acid was diluted to 400  $\mu$ L using 50 mM ammonium bicarbonate buffer solution (pH 8). 100  $\mu$ L of 8M urea solution in water was added to the protein solution and the mixture was stirred at 37 °C for 1 hr. The insulin solution was treated with 5 mg of TCEP coated nanoparticles and then alkylated by IAA under the same condition used for cyclic peptides. The MNPs were separated by an external magnet and the reduced and alkylated protein solution was then diluted to 1mL using 50 mM ammonium bicarbonate buffer prior to tryptic digestion. After that, the alkylated insulin sample was digested by adding 8  $\mu$ L of trypsin solution (trypsin:insulin ratio 1:30) followed by an 18 hr incubation at 37 °C. The sample was frozen using liquid nitrogen and the solvent was removed under vacuum. The desalting step was performed as described previously followed by solvent removal under reduced pressure. The reduced/alkylated tryptic peptides were then re-suspended in the proper solvent before LC-MS/MS analysis.

#### **4.2.7 LC-MS/MS and data analysis of reduced/ alkylated peptides**

All Mass spectrometric analyses were performed using an Agilent 1200 HPLC system and an Agilent 6520 Q-TOF tandem mass spectrometer (Agilent Technologies, Santa Clara, CA) coupled with a chip cube interface. Peptide sample (2  $\mu$ L) was loaded to the HPLC-Chip system (160 nL enrichment column, 150 mm analytical column packed with C18, 5  $\mu$ m beads with 300  $\text{Å}$  pores) using a capillary pump at 4  $\mu$ L/min flow rate. The peptides were then separated in the analytical column using a nano pump at a flow rate of 600 nL/min. The MS ion source was

operated at 300°C with nitrogen as drying gas at flow rate of 5 L/min and a fragment or voltage of 175 V. Nitrogen was used as the collision gas and the collision energy varied as a function of mass and charge using a slope of 3.7V/100 Da and an offset of 2.5V. The reference compounds with the mass of 322.048121 and 1,221.990637 Da were constantly infused into the ion source during the analysis. All analyses were performed in positive ion mode. LC chromatogram and mass spectra were analyzed using Mass-Hunter (Version B.0301; Agilent Technologies) and PEAKS (Bioinformatics Solutions Inc, Ontario1, Canada) software.

## **4.3 Result and discussion**

### **4.3.1 Surface modification of Fe<sub>3</sub>O<sub>4</sub>@SiO<sub>2</sub> nanoparticles with TCEP**

The magnetite core and the Fe<sub>3</sub>O<sub>4</sub>@SiO<sub>2</sub> nanoparticles were prepared following the same methods that have been described in Chapter 2. The Fe<sub>3</sub>O<sub>4</sub>@SiO<sub>2</sub> nanoparticles were spherical with the average diameter of 100 nm. The surface of silica coated nanoparticles was functionalized by amino groups via co-condensation reaction of silanol groups of the silica shell and APTES (Figure 4.1a). The APTES coating did not change the shape and size of the nanoparticles as confirmed by TEM (data not shown). The successful functionalization of silica coated nanoparticles with amino groups was investigated by measuring the zeta potential values of nanoparticle solutions in 10mM PBS buffer (pH 7) using DLS. The zeta potential for Fe<sub>3</sub>O<sub>4</sub>@SiO<sub>2</sub> and amine coated Fe<sub>3</sub>O<sub>4</sub>@SiO<sub>2</sub> were found to be -23±5 mV and +28±2 mV, respectively. The negative zeta potential value for silica coated iron oxide nanoparticles is associated with deprotonation of silanol groups at pH 7<sup>21</sup>. On the other hand, the positive zeta potential value for the amine coated Fe<sub>3</sub>O<sub>4</sub>@SiO<sub>2</sub>MNPs was due to amine groups which were

protonated at neutral pH<sup>22</sup>. The large change in zeta potential confirms modification of the particles with APTES.

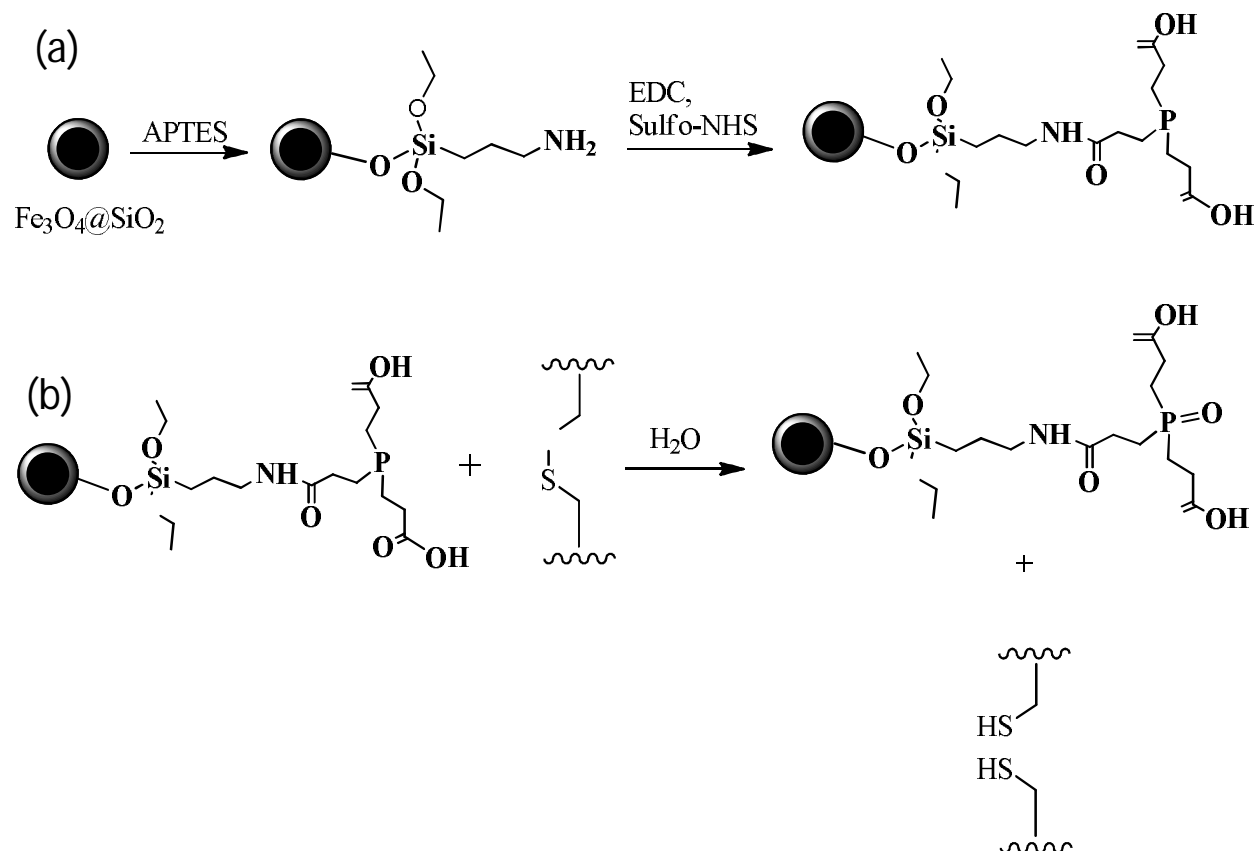


Figure 4.1: (a) Synthesis of TCEP-immobilized  $\text{Fe}_3\text{O}_4@\text{SiO}_2$  MNPs and (b) reduction of disulfide bonds in proteins and peptides using TCEP functionalized magnetic nanoparticles.

The amino groups on the surface of  $\text{Fe}_3\text{O}_4@\text{SiO}_2$  nanoparticles were then utilized for immobilization of TCEP groups on the nanoparticles surface via an amide bond formation between the surface amine groups and the carboxylic acid group of TCEP. The coupling reaction was accomplished by activation of one carboxylic acid group of TCEP with one equivalent of EDC coupling reagent in the presence of sulfo-NHS (Figure 4.1a). The Sulfo-NHS was used along with EDC to improve the efficiency of the coupling reaction by generating a more stable

amine reactive intermediate.<sup>23</sup> Due to higher reactivity of EDC in acidic condition,<sup>24</sup> the coupling reaction was performed in MES buffer solution (100 mM, pH 6). To minimize the chance of nanoparticle cross-linking, the EDC and sulfo NHS mixtures was added dropwise to the TCEP solution. The activated TCEP was then coupled to the amine groups on the surface of nanoparticles. The TCEP coated nanoparticles were then washed multiple times with MES buffer solution and water to remove byproducts and unreacted materials. The zeta potential of the TCEP coated nanoparticles in PBS buffer (10 mM, pH 7) was found to be  $-33\pm 5$  mV. The negative zeta potential, which was due to the deprotonation of TCEP carboxylic acid groups, indicated the replacement of amine groups with TCEP groups on the surface of the nanoparticles.

#### **4.3.2 Reduction and alkylation of cyclic peptides**

To evaluate the ability of TCEP-immobilized  $\text{Fe}_3\text{O}_4@\text{SiO}_2$  MNPs to cleave disulfide bonds, two cyclic peptides, NGR and oxytocin (Table 4.1), were selected as models for disulfide bond reduction. Each peptide had two cysteine groups linked by a disulfide bond. Table 4.1 shows the sequence as well as m/z values for singly protonated ions of cyclic NGR and oxytocin peptides employed in this study. No evidence of in-source disulfide bond cleavage was observed in the ESI-MS/MS spectrum of each cyclic peptide, which is expected under low energy CID conditions.<sup>25</sup>

Cyclic peptides	Peptide sequence	MW calculated	( M+ H <sup>+</sup> ) m/z found
NGR	H-Cys-Asn-Gly-Arg-Cys-Gly-Gly-Leu-Val-Thr-Thr-OH	1078.3	1079.9
Oxytocin	H-Gly-Leu-Pro-Cys-Asn-Gln-Ile-Tyr-Cys-OH	1008.2	1007.7

Table 4.1: Sequences of cyclic peptides used in this study. Each peptide contains two cysteine residues connected by an intramolecular disulfide bond.

Reduction of the cyclic peptides was performed in 20% ethanol/water mixture, with a final peptide concentration of 0.2 mg/mL. TCEP immobilized nanoparticles were added to the peptide solution and the reaction was carried out at room temperature. During the incubation of the peptide solution with TCEP coated nanoparticles, the disulfide bonds in the peptides reacted with the reducing agent, resulting in cleavage of the disulfide bond and the oxidation of TCEP to the phosphine oxide (Scheme 4.1b). After the reduction reaction, The MNPs were separated and the reduced peptides were immediately treated with iodoacetamide to protect the reactive sulfhydryl groups from oxidation and reformation of disulfide bond via carbamidomethylation reaction. The sample was then desalted using a C18 spin column (Pierce, Rockford, IL) and dried. The reduced and alkylated peptides were re-suspended in a mixture of water/acetonitrile/formic acid (92: 5: 3, v/v) and analyzed with LC/MS/MS using an Agilent 1200 LC system, an Agilent Chip Cube interface, and an Agilent 6520 Q-TOF tandem mass spectrometer (Agilent Technologies, Santa Clara, CA). The disulfide bond reduction followed by the addition of carbamidomethyl group to the thiol moieties resulted in a mass increase of 57.07 Da for each modified cysteine in NGR and oxytocin peptides. The LC/MS spectra of reduced

and alkylated oxytocin and NGR showed the presence of the peptides with two cysteine groups being alkylated with IAA. In the ESI/MS spectrum of the reduced/alkylated NGR (Figure 4.2a), the singly charged ion at  $m/z$  1193.94 and the doubly charged ion at  $m/z$  597.47 correspond to NGR with both cysteine residues being modified by carbamidomethyl groups. In the case of oxytocin (Figure 4.3a), the alkylation of two cysteine residues was confirmed by the appearance of singly and doubly charged ions at  $m/z$  1121.74 and 561.37, respectively. The collision induced dissociation (CID) of alkylated, doubly charged NGR and oxytocin precursor ions at  $m/z$  597.47 and 561.37 generated a series of fragment ions (Figures 4.2b and 4.3b) which were matched with the theoretically calculated b and y ions. The presence of b and y ions in the MS/MS spectrum, confirmed the successful reduction/alkylation of the disulfide bond in both peptides.

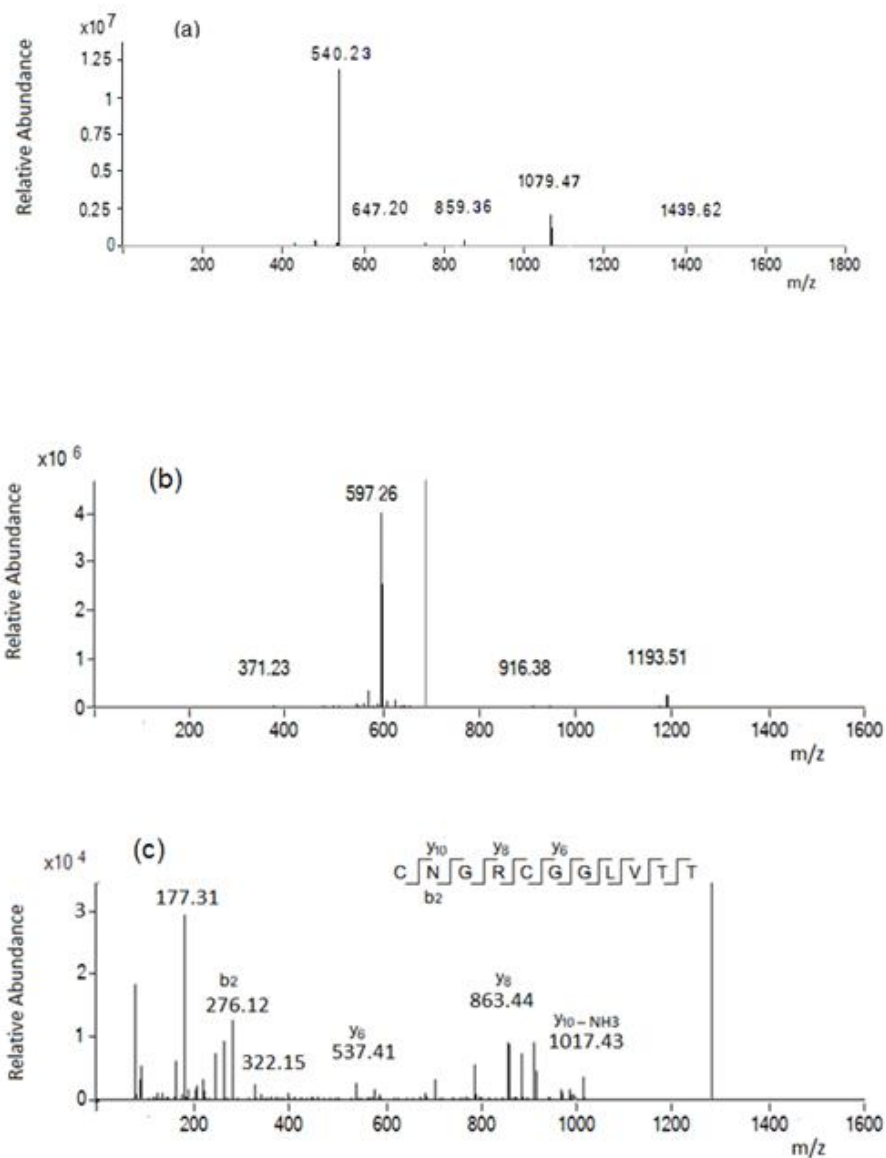


Figure 4.2: ESI analysis of NGR peptide before (a) and after (b) reduction reaction using TCEP-coated MNPs. a) In this mass spectrum, the peaks at m/z 1079.47 and 540.23 correspond to singly and doubly charged ions, respectively. c) The singly charged ion at m/z 1193.51 and doubly charged ion at m/z 597.26 correspond to reduced NGR with both cysteine residues modified with carbamidomethyl group. b) MS/MS spectra of the doubly charged reduced/alkylated NGR.

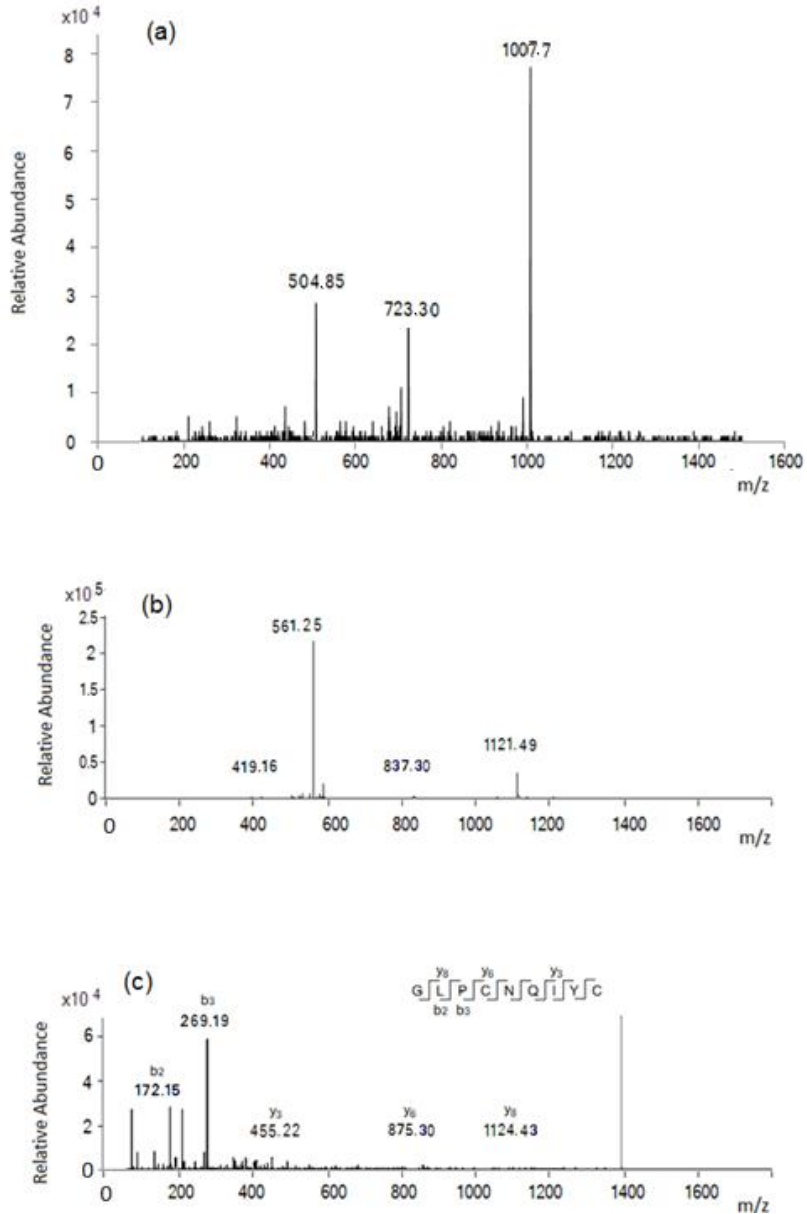


Figure 4.3: ESI analysis of oxytocin peptide before (a) and after (b) reduction reaction using TCEP-coated MNPs. a). In this mass spectrum, the peaks at m/z 1007.7 and 504.85 correspond to singly and doubly charged ions, respectively. c) The singly charged ion at m/z 1121.48 and the doubly charged ion at m/z 561.25 correspond to reduced NGR with both cysteine residues modified with carbamidomethyl group. b) MS/MS spectra of the doubly charged reduced/alkylated oxytocin.

### 4.3.3 Reduction and alkylation of bovine pancreas insulin

To assess the ability of TCEP-immobilized  $\text{Fe}_3\text{O}_4@\text{SiO}_2$ MNPs to reduce disulfide bonds in proteins, bovine pancreas insulin was selected as the target protein. To prepare the sample solution, insulin (100  $\mu\text{g}$  in 400  $\mu\text{L}$  ammonium bicarbonate buffer, pH 8) was first denatured by reacting with urea (100  $\mu\text{L}$  of 8 M urea solution) at 37°C for 1 hr. The reduction of insulin disulfide bonds using TCEP coated nanoparticles was performed in a similar way as with the cyclic peptides. The reduced protein was then alkylated using IAA as described in the previous section to prevent the reformation of disulfide bonds. The magnetic nanoparticles were separated and the reduced/alkylated protein was further subjected to tryptic digestion. The tryptic peptides were run through C18 spin column (Pierce, Rockford, IL) and the solvent was removed under vacuum. The acquired LC-MS/MS raw data were processed by PEAKS (Bioinformatics Solutions Inc, Ontario, Canada) and the search parameters employed for database search were as follows: differential mass increase of 57.07 Da for carbamidomethylated cysteine residues, and 15.99 Da for oxidation of methionine residues. Bovine insulin consists of 51 amino acids in two polypeptide chains, the amino terminal B chain containing 30 amino acids and the carboxyl-terminal A chain with 21 amino acids. Insulin contains six cysteine residues which form two interchain disulfide bonds and one intrachain bond within the A polypeptide. The results of the ESI-MS/MS analysis of reduced/alkylated bovine insulin are summarized in Table 4.2. The successful cleavage and alkylation of two insulin interchain disulfide bonds (A7-B7 and B19-A20) was proved by carbamidomethylation of the A7, B7, B19 and A20 residues. The alkylation of A6 and A11 residues (Table 4.2) also confirmed the reduction/alkylation of the intrachain (A6-A11) disulfide bond. Figure 4.4 shows the MS/MS spectrum of a reduced/alkylated peptide

in the A chain of insulin (A8-A21, table 1). The sequence of the peptide was confirmed by matching the b and y ions with the detected m/z values.

Reduced/alkylated peptides	Peptide sequence	- log p
A8- A21	(C)ASVC(+57.02)SLYQLENYC(+57.02)N	106.94
B6- B22	(H)LC(+57.02)GSHLVEALYLVC(+57.02)GER(G)	87.19
A3-A13	(I)VEQC(+57.02)C(+57.02)ASVC(+57.02)SL(Y)	71.85
A9- A21	(A)SVC(+57.02)SLYQLENYC(+57.02)N	62.19
B10-B22	(S)HLVEALYLVC(+57.02)GER	56.95
A7- A21	C(+57.02)ASVC(+57.02)SLYQLENYC(+57.02)N	45.64

Table 4.2: List of peptides in A and B chains of bovine insulin obtained by LC-MS/MS analysis of reduced/alkylated bovine insulin. All cysteine residues in A and B chains of insulin were modified with carbamidomethyl group.

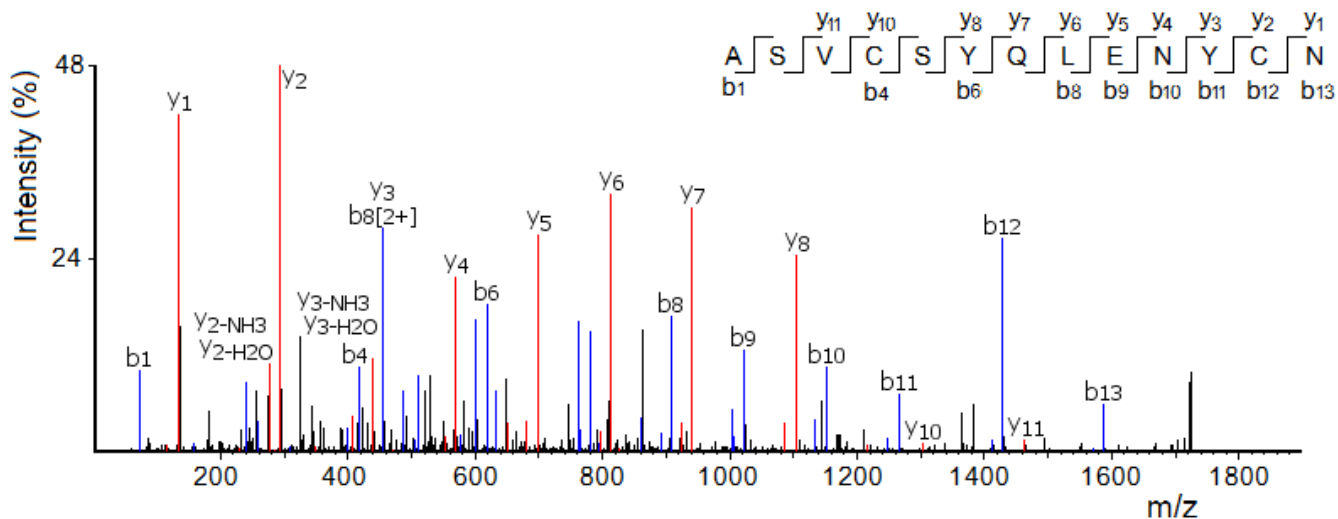


Figure 4.4: MS/MS spectrum of the reduced/alkylated peptide "ASVCSLYQLENYCN" of  $m/z$  860.85 (molecular mass of 1719.72 Da)

#### 4.4 Conclusion

TCEP coated MNPs have been fabricated as novel solid supported reducing agents to cleave disulfide linkages in peptides and proteins. Amine groups on the surface of  $\text{Fe}_3\text{O}_4@SiO_2$  MNPs were covalently conjugated to carboxylic acid groups of TCEP via EDC coupling reaction. The surface functionalization of nanoparticles with amine and TCEP groups was confirmed by zeta potential measurements using DLS. The reduction reaction by TCEP immobilized MNPs was performed in water for protein samples and water /ethanol mixtures for peptides samples.

The results from LC-MS/MS analysis of cyclic peptides and protein samples treated with TCEP coated  $\text{Fe}_3\text{O}_4@SiO_2$  MNPs, clearly indicated the ability of our reducing agent immobilized MNPs to efficiently cleave disulfide bonds in both organic and aqueous solvents at

room temperature. The TCEP-immobilized magnetic nanoparticles can be easily separated from the reaction mixture using an external magnet, which eliminates the need to use time-consuming separation methods such as gel filtration and dialysis. This minimizes the sample loss and enhances the sensitivity of sample analysis. Easy and fast reduction procedure, mild reaction condition, less sample processing step, and easy separation makes TCEP-immobilized MNPs an efficient tool for reduction of portions. Future studies include the determination of TCEP loading capacity of the MNPs as well as the reusability of our TCEP-coated MNPs for reduction of disulfide bonds.

## References

1. Stark GR., Stern. K., Atala. A., Yoo J., *Methods Enzymol*, 1977, 47 (2): 129–32.
2. Chakravarthi S., Jessop C. E., Bulleid N. J., *EMBO Reports*, 2006, 7(3), 271–275.
3. Cabisco E., Tamarit J., Ros J., *Int Microbiol*, 2000 Mar;3(1):3-8.
4. Nakamoto H., Bardwell J.C., *Biochim Biophys Acta*, 2004, Nov 11;1694(1-3):111-9.
5. M. Scigelova P., Green A., Giannakopoulos A., Rodger D. Crout, and P. Derrick, *Eur. J. Mass Spectrom.*, 2001, 7, 29–34.
6. N. J. Hauser and F. Basile, *J. Proteome Res.*, 2008, 7, 1012–1026.
7. Getz E.B., Xiao M., Chakrabarty T., Cooke R., Selvin P.R., *Anal Biochem*, 1999, 273(1):73-80.
8. Visser C. C., Heleen Voorwinden, *J. Drug Targeting*, 2004, 12, 569–573.
9. Schumacher F. F., Nobles M., *Ryan Bioconjugate Chem.*, 2011, 22, 132–136.
10. P. D. Tzanavaras, C. Mitani, A. Anthemidis and D. G. Themelis, *Talanta*, 2012, 96, 21–25.
11. M. E. Levison, A. S. Josephson, D. M. Kirschenbaum, *Experientia* 1969, 25, 126-127.
12. U. T. Rüegg, J. Rudinger, Academic Press, San Diego, 1977.
13. J. A. Burns, J. C. Butler, J. Moran, G. M. Whitesides, *J. Org. Chem*, 1991, 56, 2648-2650.
14. Shriver-Lake L.C., North S.H., Rowe Taitt C., *Biotechniques*, 2013, 55(6):292-4
15. Shafer D.E., J.K. Inman, and A. Lees, 2000, *Biochem*, 282:161-164.
16. G. Miralles, P. Verdíe, G. Subra, *ACS Comb. Sci.*, 2013, 15, 169–173.

17. Alzahrani E. and K. Welham, *Analytical Methods*, 2014, 6(2): p. 558-568.
18. Wu. W., He Q., and Jiang C., 2008, *Nanoscale Research Letters*, 3(11), 397–415.
19. Laurent S., Forge D., Port M., Roch A., Robic C., Vander Elst. L., and Muller R. N., 2008, *Chem. Rev.*, 108 (6), 2064–2110.
20. M. Etienne and A. Walcarius, *Talanta*, 2003, 59, 1173–1188.
21. Hakami O., Zhang Y., Banks C.J., *Water Res.*, 2012, 46(12):3913-22
22. Schiestel T., Brunner H., Tovar G.E., *J. Nanosci Nanotechnol*, 2004 May;4(5):504-11.
23. S. Ravindran, S. Chaudhary, B. Colburn, M. Ozkan and C. S. Ozkan, *Nano Lett.*, 2003, 3, 447–453.
24. N. O. Dhoot, C. A. Tobias, I. Fischer and M. A. Wheatley, *J. Biomed. Mater. Res., Part A*, 2004, 71, 191–200.
25. Lioe H., O. Hair R.A., *J. Am. Soc. Mass Spectrom.*, 2007 Jun;18(6):1109-23.

## Chapter 5

### Conclusions

Qualitative and quantitative characterization of NHS ester groups immobilized on the surface of  $\text{Fe}_3\text{O}_4@\text{SiO}_2$  MNPs was performed by fluorescence based methods. The presence of NHS ester groups on the surface of nanoparticles was confirmed by green fluorescence of dansylcadaverine fluorophore conjugated to MNPs using fluorescence microscopy. The accurate quantification of NHS ester groups was carried out by reductive cleavage of disulfide bond in the linker between the fluorophore and MNPs followed by fluorometric detection of the released fluorophore. The labeling efficiency of native protein with NHS ester functionalized MNPs was also investigated. Maintaining the concentration of fresh NHS ester coated MNPs during the conjugation reaction plays a critical role in maximizing the number of MNPs conjugated per protein molecule or maximizing the number of proteins being labeled in a complex mixture such as cell surface proteome. The methods presented in this study provide better estimation of active functional groups on the surface of nanoparticles that are available for further conjugation with chemical or biomolecules.

NHS ester modified  $\text{Fe}_3\text{O}_4@\text{SiO}_2$  MNPs were utilized to label amine groups in surface exposed segments of apoB-100 in intact human LDL under physiological condition (aqueous medium, ambient temperature, neutral pH). Easy, efficient and quick delipidation of apoB-100 was achieved using SDS treatment and magnetic separation. Magnetic separation also provided fast and efficient removal of the detergent which is essential for maintaining the activity of proteolytic enzymes and preventing signal suppression in LC-MS/MS analysis. The apoB-100

tryptic peptides were released from MNPs by cleaving the disulfide bond linker under mild condition (aqueous solution, ambient temperature).

The labeled lysine residues (with distinct mass shift) and their position in the full length of apoB-100 sequence were identified by LC-MS/MS. The MS/MS analysis revealed 30 labeled peptides which are believed to present on the surface of intact LDL particles since the lysine residues embedded inside the lipid core of LDL are not reachable by our bulky labeling reagent. High efficiency and specificity of NHS ester reaction with amine groups makes our labeling reagent a useful tool to identify surface exposed segments of large hydrophobic proteins. Results from in vitro studies provided us some useful structural information about apoB-100. LDL oxidation causes structural changes in protein. Therefore, we would like to map apoB-100 on the surface of LDL samples acquired from patients with different clinical stages of atherosclerosis using NHS ester functionalized nanoparticles and compare the results with our in vitro studies.

Reduction and alkylation of cyclic peptides and proteins was performed successfully using TCEP-immobilized  $\text{Fe}_3\text{O}_4@\text{SiO}_2$  MNPs. The surface of silica coated MNPs was first functionalized with amine groups followed by TCEP immobilization in presence of EDC and sulfo-NHS. DLS studies confirmed amine and TCEP surface functionalization of MNPs. The reduction and alkylation of disulfide linkages in peptides and proteins using TCEP-Coated MNPs was achieved in one step at room temperature in both organic and aqueous solvents that was confirmed by LC-MS/MS analysis. The reducing agent was easily separated from protein solution by magnetic separation. Compare to the conventional methods, utilizing TCEP-immobilized MNPs provides the chance to perform fast and one step reduction/ alkylation of proteins and peptides at room temperature with minimal sample loss. Future work involves accurate quantification of TCEP groups on the surface of MNPs. We would also like to evaluate

the reusability of the reducing agent immobilized MNPs as well as their ability to reduce disulfide bonds in complex proteins such as apoB-100.

## VITA

Parisa Pirani was born in Abdanan, Iran. She graduated with a B.Sc. in Chemistry from University of Tehran. She obtained her master degree in Organic Chemistry from Sharif University of Technology. She continued her graduate education with the Department of Chemistry at the University of New Orleans in August 2009. Further, she joined Professor Matthew Tarr's group in September 2011.